

Electronic Thesis and Dissertation Repository

7-22-2021 10:45 AM

Investigation of Small Remotely Piloted Aircraft System (sRPAS) to Human Head Impact

Yuhu Weng, *The University of Western Ontario*

Supervisor: Mao, Haojie, *The University of Western Ontario*

A thesis submitted in partial fulfillment of the requirements for the Master of Engineering
Science degree in Mechanical and Materials Engineering

© Yuhu Weng 2021

Follow this and additional works at: <https://ir.lib.uwo.ca/etd>



Part of the [Biomechanical Engineering Commons](#)

Recommended Citation

Weng, Yuhu, "Investigation of Small Remotely Piloted Aircraft System (sRPAS) to Human Head Impact" (2021). *Electronic Thesis and Dissertation Repository*. 7978.
<https://ir.lib.uwo.ca/etd/7978>

This Dissertation/Thesis is brought to you for free and open access by Scholarship@Western. It has been accepted for inclusion in Electronic Thesis and Dissertation Repository by an authorized administrator of Scholarship@Western. For more information, please contact wlsadmin@uwo.ca.

Abstract

Small remotely piloted aircraft system (sRPAS) to ground human head impact could cause injuries to the public. Skull fractures and brain injuries have been observed in sRPAS-related impacts, which varied in angles, locations and velocities. This study developed a representative quadcopter sRPAS finite element model and incorporated it with THUMS ver 4.02 50th percentile male and 5th percentile small female models to simulate sRPAS to human head impacts. The simulations were validated with cadaver experiments. The common injury metrics such as head injury criteria (HIC) and brain injury criterion (BrIC) were correlated with head injury-related responses such as skull von Mises stress, brain strain, and strain-based cumulative strain damage measure (CSDM). HIC showed moderate to strong correlations with skull stress. BrIC correlated with brain strains but at weaker correlations compared to the correlations in other impact scenarios such as sports- or auto-related collisions, demanding further investigation. The most damaging impact directions were identified as rear 0 degree for inducing high skull von Mises stress and frontal 58 degree and rear 58 degree for inducing high brain strain. Lastly, this study compared the head and brain responses between different sexes under sRPAS impacts and highlighted the higher risks for small female compared to average male.

Keywords

Small remotely piloted aircraft system, finite element analysis, impact biomechanics, skull von Mises stress, brain strain, head injury metrics, head kinematics

Summary for Lay Audience

With the increasing usage of small remotely piloted aircraft system (sRPAS), development of a new method to investigate the sRPAS related injury mechanism and assessment of the injury risks are needed. This study mainly focused on using computational techniques (finite element methods) to simulate the impact processes, collected the head kinematics, and calculated injury metrics and parameters. The finite element analysis being applied to sRPAS is a new approach, which systematically considered the objects' geometries, material properties, contact conditions and impact conditions such as initial positions and velocities.

This thesis study started with the development of a representative quadcopter finite element model and incorporated it with a high biofidelity human model which had complex head and brain structures and detailed meshes. The head center gravity kinematics data were collected and then compared with the data of cadaveric experiments. With validated sRPAS finite element model, the work then progressed to searching injury metrics, which could be used to regulate sRPAS safety for the public. Furthermore, our study identified the most vulnerable impact locations. Finally, our research incorporated developed sRPAS model with small female human model. The head injury responses and risks between different sexes were compared with small female potentially subjecting to higher brain injury risks under the same impact conditions as an average male, hence demanding better protection.

Co-Authorship Statement

Chapter 2 (Small Remotely Piloted Aircraft System to Head Impact – Computational Model Development and Head Response Analysis) was co-authored by Dr. Haojie Mao, Kewei Bian, Kalish Gunasekaran, Ruella Carlos, Matthew Spanos, Javad Gholipour Baradari, and Charles Vidal

Chapter 3 (Investigation of the Correlation between Head Kinematics, Injury Metrics and Injury-Related Head Responses under Small Remotely Piloted Aircraft System (sRPAS) to Human Head Impact) was co-authored by Dr. Haojie Mao, Kewei Bian and Kalish Gunasekaran

Chapter 4 (Investigation of Difference between Small Female and Average male under Small Remotely Piloted Aircraft System (sRPAS) to Head Impact) was co-authored by Dr. Haojie Mao and Kewei Bian

All manuscripts were drafted by Yuhu Weng and reviewed by Dr. Haojie Mao.

Acknowledgments

I would like to thank my supervisor Dr. Haojie Mao for his consistent support of my research. I specially acknowledge Dr. Mike Shkrum for not only helping jumpstart the project but also being my committee member and providing valuable suggestions along the way. I acknowledge Kewei Bian and Kalish Gunasekaran for their assistances in my research with computational modeling. I acknowledge Transport Canada and National Research Council for their support on this thesis research.

Table of Contents

Abstract.....	ii
Summary for Lay Audience.....	iii
Co-Authorship Statement.....	iv
Acknowledgments.....	v
Table of Contents.....	vi
List of Tables.....	ix
List of Figures.....	x
List of Acronyms.....	xi
Chapter 1.....	1
1 Introduction and background.....	1
1.1 Brief Research Rationale.....	1
1.2 Brain and Head anatomy.....	1
1.2.1 Brain anatomy.....	1
1.2.2 Skull anatomy.....	3
1.3 sRPAS to human head impact studies.....	3
1.3.1 Anthropomorphic test device (ATD).....	4
1.3.2 Post mortem human surrogate (PMHS).....	5
1.3.3 Finite element analysis.....	6
1.4 Research objectives.....	8
1.5 Thesis structure.....	9
Chapter 2.....	10
2 Small remotely piloted aircraft system (sRPAS) to head impact – computational model development and head response analysis.....	10
Abstract.....	10
2.1 Introduction.....	11
2.2 Methods.....	13
2.2.1 Available cadaver data for validation.....	13
2.2.2 sRPAS model development.....	13
2.2.3 sRPAS to head impact.....	17
2.2.4 Skull stress.....	22

2.2.5 Brain strain and cumulative strain damage measure (CSDM)	22
2.2.6 Sensitivity analysis – Impact location, angle, and arm first	23
2.3 Results	24
2.3.1 Resultant linear acceleration validation.....	24
2.3.2 Resultant rotational velocity validation.....	26
2.3.3 Skull stress.....	28
2.3.4 Brain strain	29
2.3.5 Sensitivity analysis	30
2.4 Discussion	35
2.5 Conclusions	37
Chapter 3.....	38
3 Investigation of the correlation between head kinematics, injury metrics and injury-related head responses under small remotely piloted aircraft system (sRPAS) to human head collision.....	38
Abstract	38
3.1 Introduction	38
3.2 Methods.....	40
3.2.1 Impact setting	40
3.2.2 Injury metric and head response.....	42
3.3 Results	45
3.3.1 Linear acceleration, HIC, and skull stress	45
3.3.2 BrIC, rotational velocity and brain strain	51
3.3.3 Scalability	55
3.4 Discussion	58
3.5 Conclusions	59
Chapter 4.....	60
4 Investigation of difference between small female and average male under small remotely piloted aircraft system (sRPAS) to head impact.....	60
Abstract	60
4.1 Introduction	60
4.2 Methods.....	61
4.2.1 THUMS version 4.02 female model.....	61
4.2.2 Impact setting	62
4.2.3 Mass-based scaling method.....	64

4.3 Results	65
4.3.1 Resultant head linear acceleration verification.....	65
4.3.2 Resultant head rotational velocity verification.....	67
4.3.3 Female vs. male head kinematics and injury metrics	69
4.3.4 Male vs. small female in terms average values	71
4.4 Discussion	73
4.5 Conclusions	74
Chapter 5.....	76
5 Conclusions and future work.....	76
5.1 summary and conclusions	76
5.2 Limitations	77
5.3 Future study.....	78
5.3.1 Injury metrics.....	78
5.3.2 Vulnerable population	79
5.3.3 Protection method.....	79
5.4 Novelty, significance and impact of work	79
References.....	81
Curriculum Vitae	86

List of Tables

Table 2-1 Material properties.....	17
Table 2-2 Human head model material properties.....	19
Table 2-3 sRPAS to head impact setups.....	21
Table 3-1 sRPAS to head impact setups.....	40
Table 4-1 sRPAS to female head setups.....	62
Table 4-2 PMHS subjects.....	64
Table 4-3 the summarized head kinematics, injury metrics, skull von Mises stress and brain strain value of female cases.....	70
Table 4-4 the summarized head kinematics, injury metrics, skull von Mises stress and brain strain of male cases.....	70

List of Figures

Figure 1-1 Human brain anatomy (sagittal section)	2
Figure 1-2 Human skull	3
Figure 1-3 FAA Hybrid III 50th percentile male dummy (ATD).....	5
Figure 1-4 PMHS (Cadaver) experiments conducted by OSU.....	6
Figure 1-5 Different finite element head models' cross-section view.	8
Figure 2-1 sRPAS finite element model details.....	15
Figure 2-2 THUMS version 4.02 50 th percentile male model.	22
Figure 2-3 sensitivity studies.	24
Figure 2-4 Head resultant linear acceleration validation.	26
Figure 2-5 Head resultant rotational velocity validation.	28
Figure 2-6 Skull stress distributions for 17 validated cases.....	29
Figure 2-7 Brain strain contours and CSDM15 for 17 validated cases.	30
Figure 2-8 Sensitivity analysis of impact angle.....	31
Figure 2-9 Sensitivity analysis of impact location.....	32
Figure 2-10 Skull stress and brain strain contour comparisons in arm-first impacts and their comparisons to corresponding body shell-first impact.	34
Figure 3-1 Maximum skull stress collection.....	44
Figure 3-2 the correlation of HIC and peak linear acceleration.....	45
Figure 3-3 the correlation of HIC and maximum skull stress.....	46
Figure 3-4 the correlation of HIC and skull stress under different impact directions.	46
Figure 3-5 Analysis of frontal 58 degree impacts.....	47
Figure 3-6 Analysis of lateral 58 degree impacts	48
Figure 3-7 Abnormal frontal 58 degree impact case investigation.....	49
Figure 3-8 Abnormal lateral 58 degree impact case investigation.	50
Figure 3-9 Average HIC and skull stress comparisons of different impact directions	51
Figure 3-10 Correlation between rotational velocity and BrIC	52
Figure 3-11 Correlation between rotational velocity and CSDM; BrIC and CSDM.....	53
Figure 3-12 Rotational velocity profiles of different cases.	54
Figure 3-13 Average CSDM10, CSDM15 and BrIC.....	55
Figure 3-14 Scalability study of linear responses.....	56
Figure 3-15 Scalability study of rotational responses.....	57
Figure 4-1 THUMS male and female model comparison.....	62
Figure 4-2 Typical impact directions.....	63
Figure 4-3 Head resultant linear acceleration of female.....	67
Figure 4-4 Head resultant rotational velocity of female.	69
Figure 4-5 Average peak linear acceleration, HIC and skull stress comparisons of male and female model.....	72
Figure 4-6 Average peak rotational velocity, BrIC and CSDM comparisons of male and female model.....	73

List of Acronyms

ATD: Anthropomorphic test device

BrIC: Brain injury criterion

CSDM: Cumulative strain damage measure

FAA: Federal Aviation Administration

FE: Finite element

GHBMC: Global Human Body Models Consortium

HIC: Head injury criteria

NIAR: National Institute for Aviation Research

OSU: Ohio State University

PMHS: Post mortem human surrogate

THUMS: Total Human Model for safety

Chapter 1

1 Introduction and background

1.1 Brief Research Rationale

Small remotely piloted aircraft system (sRPAS), or referred to as small unmanned aircraft system (sUAS), are being increasingly used [1]. The sRPAS market was worth \$609 million in 2014 and increased to \$4.8 billion in 2021 [2]. Operation of sRPAS near human induced collisions [3]. For example, Chung et al. reported a case that a 13-year-old male experienced a brief loss of consciousness and had lower extremity numbness and weakness after a racing sRPAS impact. In the later imaging examination of this case, the skull fracture was observed [1]. In April 2014, a triathlete was impacted by a filming sRPAS during the race and sustained head injury [4]. Though sRPAS emerges only in recent years and lacks epidemiology data so far, these accidents showed the potential risks of operating sRPAS in public area due to sRPAS's high velocities and altitudes, especially if the impacts happen to human head. However, there is no appropriate safety regulation to protect people from sRPAS ground collision due to the lack of sRPAS to head impact analysis. A systematic sRPAS-to-human collision analysis is immediately needed in finding appropriate head injury metrics and establishing sRPAS safety regulations.

1.2 Brain and Head anatomy

1.2.1 Brain anatomy

The structure of human brain is extremely complicated. The human brain consists of different parts and each part can process, integrate and coordinate the information coming from different organs and send the instructions back to ensure them function normally. Figure 1-1 shows the sagittal section of human brain anatomy. In general, the brain consists of two major soft tissues, grey matter and white matter. The grey matter constructs the central nervous system of human body. It consists nerve cells, glial cells, capillaries and neuropil [5]. The white matter is made up by myelinated axons which connect the grey matter areas (neurons) with each other. There are three

major parts of human brain, including the cerebrum, cerebellum and brainstem. The cerebrum is the largest part which consists of different components such as the cortex, hippocampus, thalamus, basal ganglia and corpus callosum. The brainstem consists of the midbrain, pons and medulla, which connect the cerebrum with spinal cord. The cerebellum is a separate part at the bottom of the brain and is connected with the brainstem. Generally, the brain parts are protected by the skull and there is a layer called cerebrospinal fluid (CSF) between the skull and the brain. However, the human brain is more fragile than other soft tissues and organs such as muscles and the heart, which can deform without damage [5].

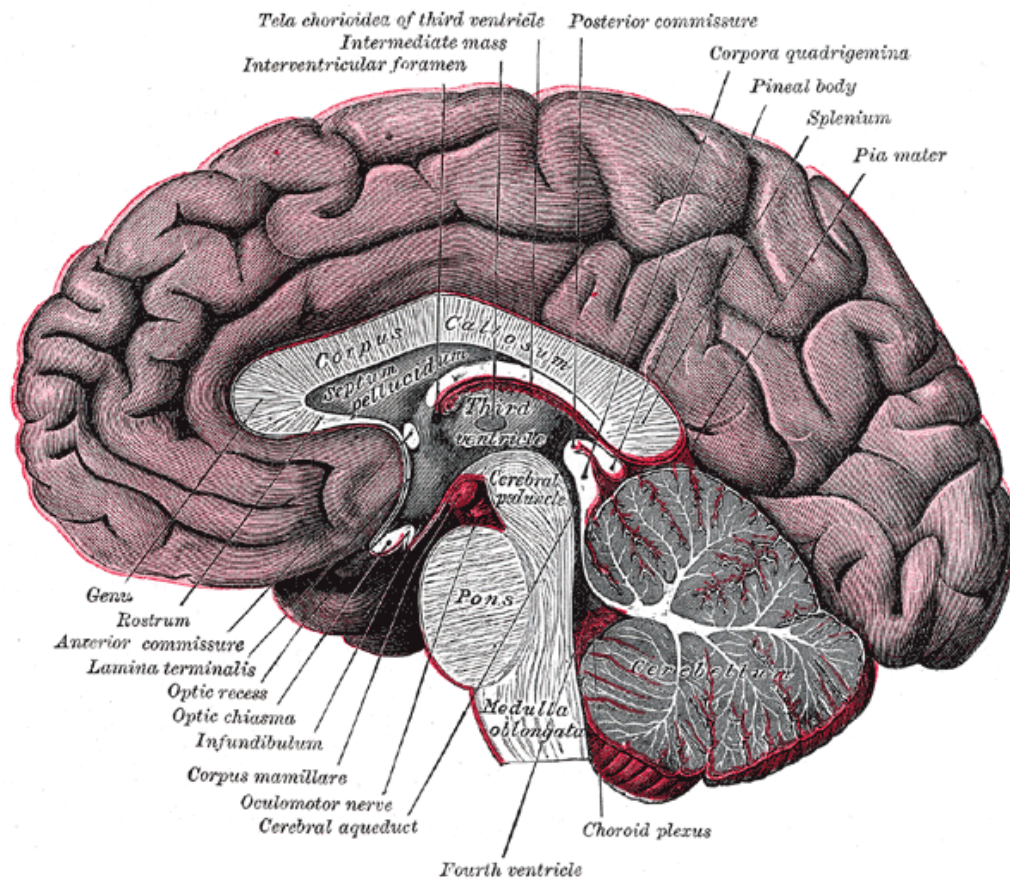


Figure 1-1 Human brain anatomy (sagittal section) (Adapted from Wikimedia Commons).

1.2.2 Skull anatomy

The skull is formed by bone structure and it has a cranial cavity to protect the brain [6]. The human skull consists of three major parts, including neurocranium, sutures and facial skeleton. Figure 1-2 shows the human skull anatomy with landmarks. The neurocranium has 8 cranium bones, which include 2 temporal bones, 2 parietal bones, 1 occipital bone, 1 sphenoid bone, 1 ethmoid bone and 1 frontal bone. The sutures are the major fibrous joints between the bones of cranium. The facial skeleton consists 14 facial bones. Although the skull has hard characteristic and can provide excellent protection to the brain, the skull fractures still commonly show in impact cases.

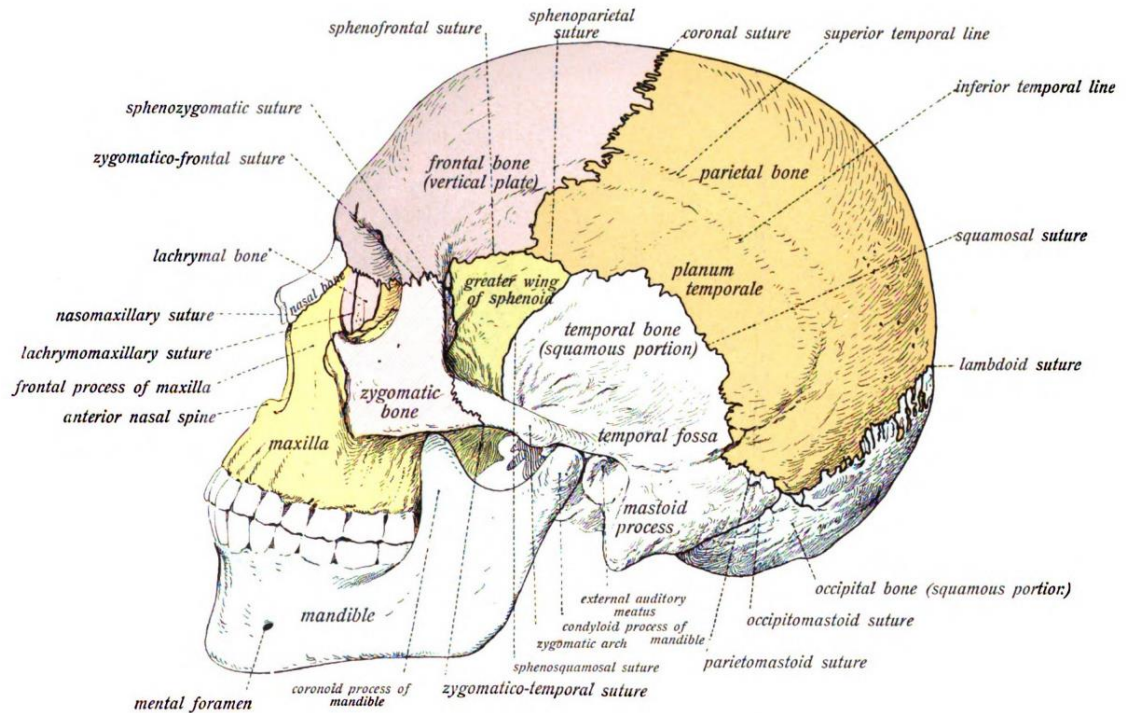


Figure 1-2 Human skull (Adapted from Wikimedia Commons).

1.3 sRPAS to human head impact studies

Recently, the U.S Federal Aviation Administration (FAA) supported a large consortium to investigate sRPAS-to-human collisions. Most of their results were reported in the Alliance for System Safety of SRPAS through Research Excellence (ASSURE) report

[4]. Since the sRPAS-related injury is relatively novel, the cadaveric experiment data collected in ASSURE report are invaluable. Meanwhile, the sRPAS-related impacts are complicated, because the impact energy and construction stiffness, which is the combination effect of structure and material [4], vary. Different type sRPAS can work at different velocity ranges. The masses of the sRPAS are quite different. In addition, sRPAS can collide with human at different impact orientations of sRPAS malfunctions. The sRPAS failure modes were recorded in the University of Alabama in Huntsville (UAH) flight test reports, in which the vertical and downward angled impacts are reported to be most likely to happen.

1.3.1 Anthropomorphic test device (ATD)

Anthropomorphic test device (ATD), also known as dummy, was used as a method to investigate the damage sRPAS could bring. National Institute for Aviation Research (NIAR) used FAA Hybrid III 50th percentile male representative ATDs (Figure 1-3) installed with 6 linear accelerometer and 3 angular rate sensor to collect impact kinematics under sRPAS impacts [4]. The ATD can represent the full size of an average male and it has improved head and neck biofidelity [7]. The ATD also has high degree of repeatability which makes it easy to collect data compared to using cadavers [8]. However, the ATD test also has limitations. The first limitation for investigating sRPAS to head impact is that the ATD can only accurately measure the kinematics and force responses through installed sensors [9]. For skull and brain responses such as skull stress and brain strain during the impact, those responses could not be measured using the HIII ATD. The other limitation is that, compared to computational method, ATD test still takes more time and higher cost to conduct, because sRPAS collisions would destroy the sRPAS and the position of ATD and sRPAS need to be accurately placed after for experiment. Still, ATD remains a good tool to help understand the head responses during impacts and is commonly used in safety regulation tests.

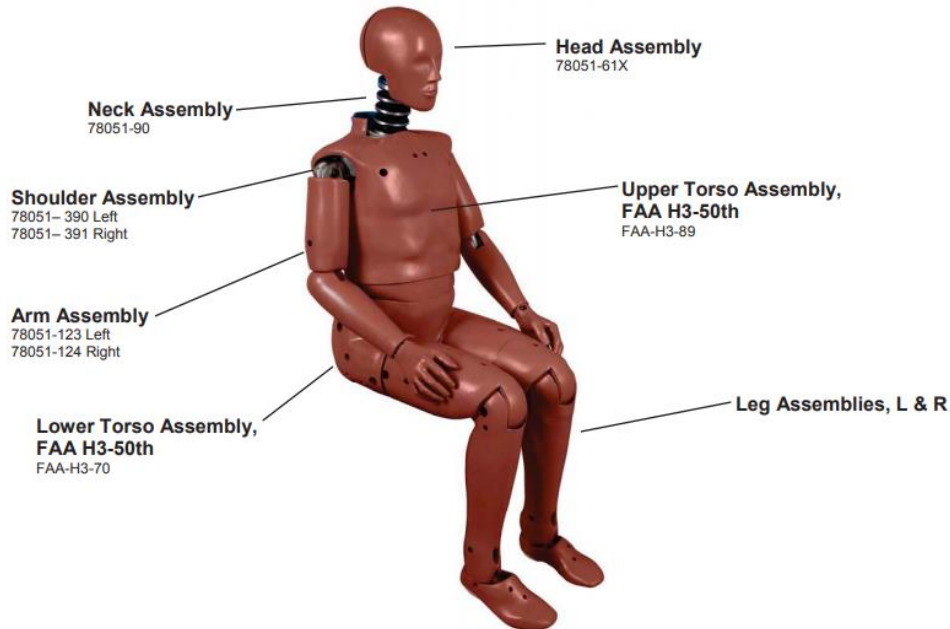


Figure 1-3 FAA Hybrid III 50th percentile male dummy (ATD) (Adapted from HUMANTICS website).

1.3.2 Post mortem human surrogate (PMHS)

Post mortem human surrogate (PMHS) subjects have been used to estimate the risk of injury related to sRPAS impact [4]. In automotive safe field, the responses of the human body to vehicle collision have been investigated using PMHS tests, supporting finite element (FE) model development[10, 11]. Many skull fracture studies and safety criteria were based on PMHS tests [12, 13]. Different from the ATD test, the PMHS test has its advantage of using human body to study responses. Many injury characteristics such as skull fracture can be represented. Regarding sRPAS to head impacts, the Ohio State University (OSU) conducted multiple PMHS experiments (Figure 1-4). The subjects were all male. Strain gauge sensors and accelerometer were instrumented on the PMHS skull to collect skull strain and head kinetics data. It was observed that sRPAS-related collision could induce skull fracture [4]. Although PMHS test provided valuable data, it still has its limitations. One limitation is the high cost when involving the entire cadaveric body. Another limitation is that the cadaver subjects lack of neck muscle tension, which could affect head kinematics under impacts [14, 15].

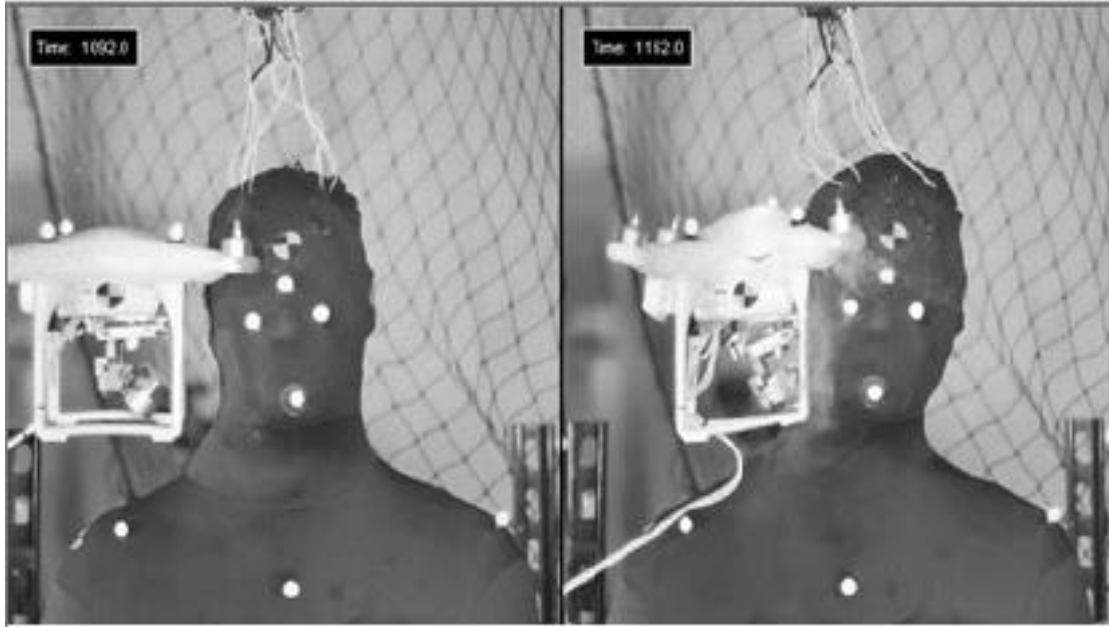


Figure 1-4 PMHS (Cadaver) experiments conducted by OSU (Adapted from ASSURE A14 report [4]).

1.3.3 Finite element analysis

Finite element analysis is a computational method to solve differential equations arising in engineering and mathematical modeling. The basic concept of this method is to divide a complicated or large system into finite number of simple and smaller subsystems (element) and solve the simplified subsystem by partial differential equations to obtain the critical engineering measures for solving reality problems. This method has been considered as an important tool in studying the injury biomechanics of the human head, because it is capable to report the internal biomechanical response of the brain such as the transient stress pattern [16]. In addition, the FE method can help to address concerns such as the non-standardized experimental procedures, biased data caused by lack of subjects, or high expenses, among other experimental limitations [17]. There are several FE studies related to sRPAS impact cases. The Mississippi State University developed an FE head model and a quadcopter sRPAS model to determine the damage level of impact [18]. Dori conducted the simulations to investigate the thoracic injury response caused by

impact of sRPAS [19]. However, none of these FE sRPAS models has been validated against cadaveric data.

1.3.3.1 Review of FE human model

Currently, the human body model was developed based on computed tomography (CT) and magnetic resonance imaging (MRI) of the volunteers. The material properties of each parts were assigned based on literature [20]. Most of head models were validated with cadaver experimental data. The earliest 3D FE head model was developed a by Ruan et.al from Wayne State University (WSU) in 1992 [21]. Later, the model was refined and more details were added such as grey matter and white matter by Zhou et al [22, 23]. After that many institutions started to develop their own model. For example, in 2011, Mao et al. applied multi-block approach to develop high-quality hexahedral brain meshes and eventually used 270,552 elements to represent different brain parts [24, 25]. The model responses were validated according to data collected from thirty five experimental cases, including brain pressure, skull-brain relative motion, skull responses and facial responses [24]. Besides the GHBMC model (Figure 1-5a), another head model that is also commonly used by industry and academic users is the Total Human Model for safety (THUMS) model (Figure 1-5b), which was developed by Toyota Central R&D Lab. In addition, there are other FE head and brain models, including Kungliga Tekniska Högskolan (KTH) [26], University of Dublin Brain Trauma Model (UCDBTM) [27], Simulated injury Monitor (SIMon) FEHM [28], University Louis Pasteur of Strasbourg (ULP) finite element head model [29] and Dartmouth Head Injury Model (DHIM) or WPI model [30].

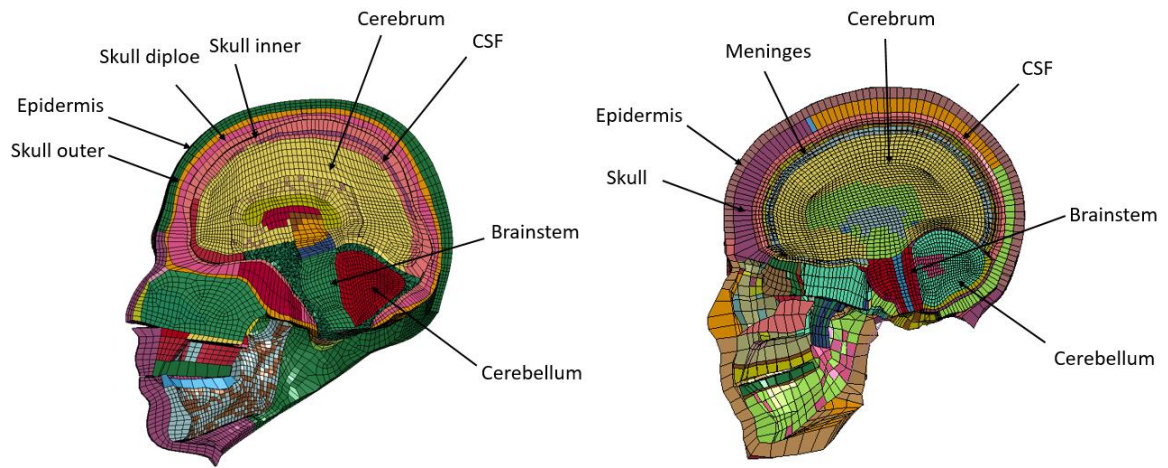


Figure 1-5 Different finite element head models' cross-section view. (a) GHBMC model; (b) THUMS model.

1.4 Research objectives

In order to better understand head responses and injury risks induced by sRPAS to human head impact and hence support safety regulation development, the thesis focused on the below objectives.

#1 developing a high quality quadcopter sRPAS FE model and combining it with high biofidelity human model (THUMS) to understand sRPAS to head impacts

#2 validating the models according to PMHS experimental data

#3 conducting the sensitivity studies regarding sRPAS impact locations and angles for better understanding the tolerances and effects of slightly varying impact postures

#4 investigating how several mainstream injury metrics such as HIC and BrIC could be applied to sRPAS collision related head injuries and providing data to support sRPAS safety regulation development

#5 investigating the differences between average male and small female to support the protection of vulnerable population.

1.5 Thesis structure

Chapter 1 introduces the background of head injuries and sRPAS to human head impacts. Also, in this chapter the major investigating methods such as PMHS test, dummy test and FE models are introduced.

Chapter 2 describes the methods of development of a representative quadcopter sRPAS FE model. The sRPAS model was combined with THUMS model to simulate PMHS (Cadaver) experiments conducted by OSU. The linear acceleration and rotation velocity curves from PMHS tests were used to validate the FE models. Based on validated simulations, skull stress and brain strain were analyzed. In addition, sensitivity study was conducted to investigate the effects of small shifts of location, angle during the collision.

Chapter 3 describes the current mainstream head injury metrics (HIC and BrIC). The correlations of head kinematics, injury metrics and head injury-related parameters were analyzed.

Chapter 4 compares the head responses of 50th percentile male and 5th percentile small female. The developed sRPAS model was combined with small THUMS female model. Based on the scaled OSU PMHS male experiments data, the verification of simulation was conducted. Then, the head kinematics and injury metrics predicted by both the average male and small female models were compared.

Chapter 5 summarizes the thesis research and discusses the limitation in current study. Besides, future study, significance, and novelty are also discussed.

Chapter 2

2 Small remotely piloted aircraft system (sRPAS) to head impact – computational model development and head response analysis

Abstract

Understanding small remotely piloted aircraft system (sRPAS) to human head impacts is needed to better protect human head during ground collision accidents. Recent literature reported invaluable cadaveric data on sRPAS to human head impacts, which provided a unique opportunity for developing validated computational models. Meanwhile, complexities and variances in sRPAS to human impacts and the lack of understanding of brain strain during these impacts require systematic investigation using a computational approach. Hence, a representative quadcopter style sRPAS finite element (FE) model was developed and applied the model to THUMS human body model to simulate a total of 45 impacts. Among these 45 simulations, 17 were defined according to cadaveric setting for model validation and the others were conducted to understand the sensitivity of impact angle, impact location, and impacted sRPAS components. Results demonstrated that FE-model-predicted head linear acceleration and rotational velocity generally agreed with cadaveric data with average predicted linear acceleration 4.5% lower than experimental average and average predicted of rotational velocity 2% lower than experimental average. From validated simulations, high skull stresses and moderate level of brain strains were observed for several cases. Also, sensitivity study demonstrated significant effect of impact angle and impact location with 3-degree variation inducing 30% changes in linear acceleration and 29% changes in rotational velocity, further highlighting the need to accurately defining and documenting impact conditions in the future. Also, arm-first impact was found to generate more than two times higher skull stresses and brain strains compared to regular body-shell-first impact.

2.1 Introduction

With the technological innovations in small remotely piloted aircraft system (sRPAS), or referred to as small unmanned aircraft system (sUAS), various applications including commercial and recreational usages have been observed [1]. The sRPAS industry was worth \$609 million in 2014 and it has been continuously growing with up to \$4.8 billion expected in 2021 [2]. The growth of sRPASs usage may also bring the risk to public safety because the light weighted types of these machines are operated over people with the risk of impact human heads at speeds that can reach over 20 m/s [4].

In recent years, the Federal Aviation Administration (FAA) supported a large project to understand sRPAS to human head impacts. The most recent results have been summarized in Alliance for System Safety of UAS through Research Excellence (ASSURE) report 14, including Anthropomorphic Test Device (ATD) test and cadaveric test [4]. Various impact directions including frontal, lateral, and top impacts and various velocities of sRPAS-to-head impacts have been studied. The PMHS experiments provided an invaluable opportunity to develop and validate sRPAS to human head impact finite element (FE) simulations. Prior to the ASSURE cadaveric data, while FE simulations of sRPAS to head impacts have been studied [31], the validations against cadaveric data have yet to be conducted. To predict injury risks, the Civil Aviation Safety Authority and Monash University investigated an injury prediction model for sRPAS-to-ground person collision, which could estimate the injury severity by the function of drone mass and impact velocity [32]. A mathematical model was proposed by Xin to predict injury level of drone to human impact [33]. Magister proposed a modelling method to assess the sRPAS-related injury based on blunt ballistic impact [34].

Both cadaveric experiments and FE models provided useful information in understanding head injuries. An AIS2 skull linear fracture was observed from one quadcopter-type sRPAS to head impact among various impacts [35]. While subject-specific bone structure, quality, and thickness could affect the risk of skull fracture, understanding skull stress distributions under various impacts can provide more insights into the injury mechanisms, for which FE head model has been helpful. Position and Personalize

Advanced Human Body Models for Injury Prediction (PIPER) scalable child model was used to investigate the relationship between skull stress and skull fracture [36] for children. From the study, it was noticed that the model predicted stress responses, such as von Mises stress, can better predict skull fracture than kinematic-based injury measures [37]. Another important topic that the existing cadaveric testing hasn't addressed yet is to understand brain strains, partially because either brain-skull relative motion or brain strains need to be evaluated with meticulous setting through either using high-speed X-ray [38, 39] or sonomicrometry crystals [40]. To this, validated 3D human head FE models can provide unique information on detailed brain strains during sRPAS to head impacts.

There are various human full-body models that include the head and neck for conducting sRPAS to human impact simulations, including the GHBMC (Global Human Body Model Consortium) with validated head & neck components [41, 42] and THUMS (Total Human Model for Safety) full-body model [43]. Especially, the THUMS v4.02 has been improved with a detailed brain model that has been used for brain injury analysis [44-48]. These full-body FE models provide an opportunity to not only investigate head linear and rotational kinematics during sRPAS to human impacts, but also investigate skull stresses and brain strains directly related to head injuries.

The main objective of this study was to understand sRPAS to human head impact dynamics and head responses from these impacts. A representative quadcopter style FE model was developed and validated against cadaveric data under a total of 17 impact scenarios including frontal, lateral and top impacts. Based on validated impact simulations and validated human head model, both skull von Mises stress and brain maximum principal strain (MPS) were analyzed. Moreover, the sensitivity studies on impact angles and impact directions, which are difficult and expensive to conduct on cadaveric subjects, were further investigated using validated models. Lastly, arm-first impacts were compared to body-shell first impacts.

2.2 Methods

2.2.1 Available cadaver data for validation

The sRPAS to human collision cadaveric test data are available through the detailed ASSURE report [4]. The PMHS experiments were conducted by the Ohio State University. From the report, 17 quadcopter style sRPAS related experimental data could be used for FE model validation with detailed head kinematics time histories under impacts. In the 17 experiments, 3 different cadaver subjects were involved, and all the subjects were males with body masses of 170 lb (77.1 kg), 164 lb (74.4 kg) and 143 lb (64.9 kg), respectively. The experiments were conducted at different angles and impact locations, including 4 typical location settings as frontal 58 degree, lateral 0 degree, lateral 58 degree and top 90 degree. All PMHS subjects were instrumented with head kinematics sensors to measure head linear acceleration, head rotational velocity and head rotational acceleration at head center gravity during impacts.

2.2.2 sRPAS model development

A representative 1.2 kg quadcopter style sRPAS FE model (Figure 2-1a) was developed by using HyperMesh (Altair, Troy, MI USA). The FE model was consisted of various parts, including body shell upper portion, body shell lower portion, motor casing, motor, camera assembly fixture, camera, circuit board, battery support and battery. Totally, the FE quadcopter style sRPAS model was made of 43,863 elements, including 14,673 3D hexahedral elements, 45 3D prism elements, 29,055 2D quads elements, 82 2D triangular elements and 8 1D beam element. The mesh quality for the FE model was meticulously improved to a high level. For 3D solid elements, only 1.0% of elements had warpage greater than 5 with the maximum value of 13.39. All 3D elements had aspect ratio below 5 with maximum aspect ratio of 3.38. 2.6% of elements had Jacobian less than 0.7 with the minimum value of 0.56. 1.6% of elements had element length less than 1 mm with the minimum value of 0.7 mm. 3.8% of elements had element length greater than 3.5 mm with the maximum value of 4 mm. For 2D shell elements, 4% of elements had warpage value greater than 5 with the maximum value of 15.01. All 2D elements had aspect ratio below 5 with the maximum value of 4.16. 1.8% of 2D elements had Jacobian value

smaller than 0.7 with the minimum value of 0.44. All 2D elements had element length greater than 1 mm and 6.5% elements had length greater than 3.5 mm with maximum length of 4.98 mm. Besides ensuring mesh qualities, the dimensions of the FE model were verified based on the sRPAS specifications (Figure 2-1b).

The sRPAS FE model was defined with the upper and lower portions being separated. For a physical sRPAS, the upper and lower body shells were connected by clips located at the shell edge. During the collision, these weakly connected clips would break, and the upper and lower body shells would separate due to shell deformation. While for the arm portion, screws were used to reinforce the connection between two shells, preventing separation. To better represent these features in the FE model, the node connections between upper and bottom shell were implemented at four drone arms while there was no node connection in the rest of edge space (Figure 2-1c). Due to deformation, force would transfer between the upper and bottom shells through the edge between them. Therefore, edge-to-edge contact was added in the FE model.

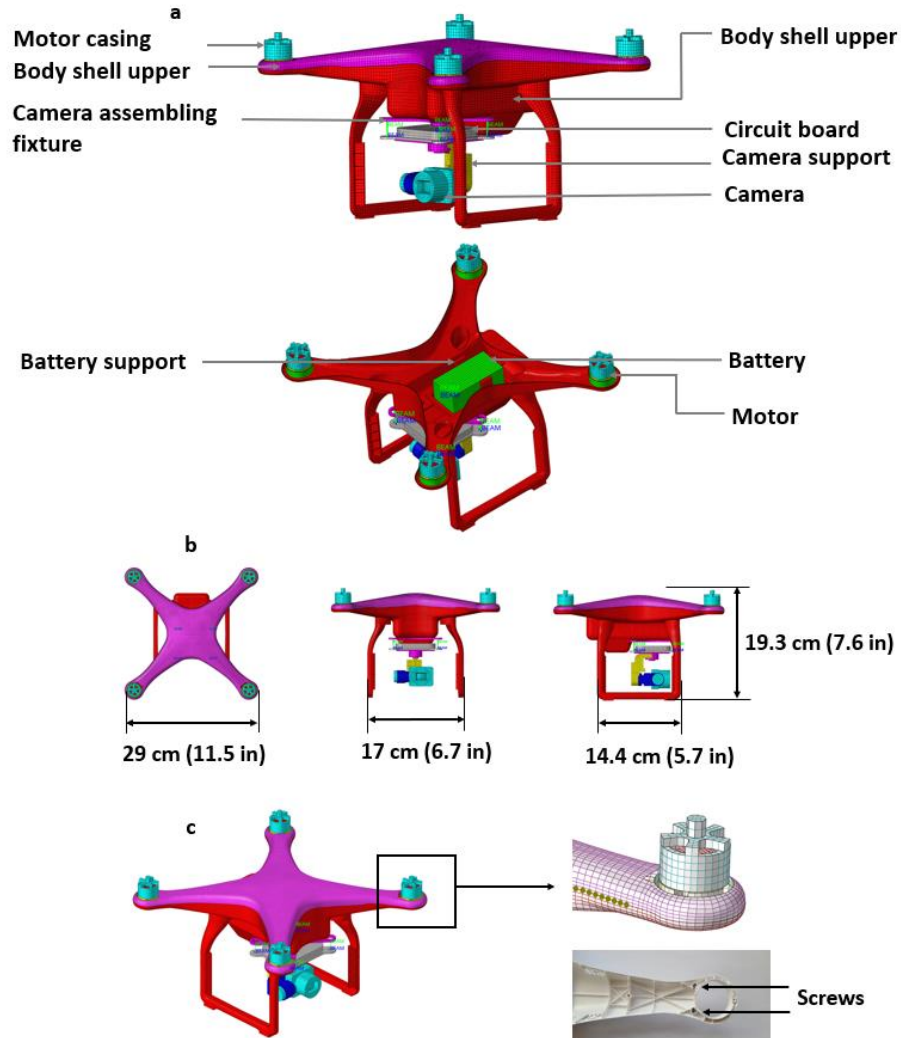


Figure 2-1 sRPAS finite element model details. (a) was sRPAS finite element model. The model included detail components, (b) was verified in terms of overall dimensions, and (c) was defined with an edge contact between upper and lower body shell except the arm region.

The body shell thickness was one major factor affecting the overall sRPAS stiffness. To determine the thickness of body shell in modelling, 10 different locations were selected and measured by a Vernier caliper on both upper and bottom drone shell. The measurements yielded an average of 1.34 mm with a standard deviation of 0.094 mm. In addition, on body shell, there were strengthened bars which would increase stiffness. By both measuring the average drone body shell thickness and considering the effect of widely distributed strengthening bars, the final thickness of body shell was defined as 1.5 mm.

The material properties of various parts of the sRPAS FE model were referred to published data in ASSURE report, which are summarized in Table 2-1. Polycarbonate material was assigned to the body shell and camera support (Table 2-1a). The camera assembly fixture, camera, and motor casing were modeled using Cast Aluminum 520F. Motor was modeled using Steel 4030. The circuit board was modeled using G10 Fiber glass. The battery and battery support were simplified as elastic materials. The FE model has a total weight of 1.207 kilograms, which is consistent with the physical model. Table 2-1b shows the drone material parameters.

The body shells were postulated as the most critical parts during collisions because the shells would directly contact with human head. The energy of a moving sRPAS would first transfer from body shells to head. Therefore, the material properties of drone body shell was estimated to play an important role in the collision of a sRPAS to human head. In general, the shell was made from polycarbonate plastic which was a strong and tough material used in engineering structures. According to ASSURE report, the Johnson-Cook model was found appropriate to simulate shells. Table 2-1c summarizes the material properties of polycarbonate based on the ASSURE report.

Table 2-1 Material properties

(a) Parts and material types

Drone Part	Material
Drone body shell	Polycarbonate
Camera assembly fixture	Cast Aluminum 520 F
Camera	Cast Aluminum 520 F
Motor casing	Cast Aluminum 520 F
Motor	Steel 4030
Circuit board	G10 Fiber glass
Camera support	Polycarbonate
Battery support	Elastic
Battery	Elastic

(b) General material properties

Material	Young's modulus (MPa)	Poisson's ratio	Density (ton/mm³)
Cast Aluminum 520F	66,600	0.33	2.87E-09
Steel 4030	200,500	0.29	8.65E-09
G10 Fiber glass	13,790	0.12	1.98E-09
Battery	500	0.33	5.477E-09

(c) Detailed material properties of polycarbonate

Density (kg/m³)	Young's Modulus (GPa)	Shear Modulus (GPa)	A (MPa)	B (MPa)	C	m	n	Cv (KJ/kgK)	Tmelt (K)
1197.8	2.59	0.93	80	75	0.0052	0.548	2	1.3	562

2.2.3 sRPAS to head impact

2.2.3.1 THUMS human body model

The THUMS Version 4.02 corresponding to 50th percentile male adult model was used to investigate drone-to-human collision head responses. This model was developed and released by Toyota Motor Corporation. For the version 4.02, the model can simulate internal organ injuries at tissue level. The head model of this version has very detailed head parts, including the skin, skull, facial bones, eyeballs, meninges, cerebrum, cerebellum, brainstem, and cerebrospinal fluid (CSF). Especially, Version 4.02 models

have very detailed brain meshes and the element length of the brain part was around 1.2 to 5 mm. The version 4.02 for the 50th percentile male model contains 772,156 nodes and 1,975,599 elements with a total mass of 77.6 kilograms. THUMS model has three layers for the skull. The outer and inner tables are defined as shell and an elastic-plastic material model with optional damage was used to define the property. The middle spongy bone (diploe) is defined as solid and the material is defined by an elastic viscoplastic material. The brain part includes the white matter and grey matter which are defined by nearly incompressible and viscoelastic material. The skin and flesh parts are represented as hyperelastic material. The skull inner nodes and arachnoid nodes were defined as tied contact and a low shear modulus cerebrospinal fluid (CSF) layer was created to allow some brain surface motion. The detailed human head components' material properties are shown in Table 2-2. The neck model was developed based on the anatomy with vertebral bodies, discs, ligaments, muscles defined providing a human-like response. The inferior part of head is attached to the neck model and the merging position is located at occipital condyle. The muscles are modeled as 1D element and the attachment points to bony part are referred to actual insertion points. However, in THUMS model version 4.02, the contract forces at neck was not included. The head model was validated by several experiments, including translational impact conducted by Nahum et al. (1977) to validate brain pressures; translational impact conducted by Yoganandan et al. (1995) to validate skull impact forces; translational and rotational impact conducted by Hardy et al. (2001) and Kleiven and Hardy (2002) to validate brain-skull relative motion. The neck parts of THUMS model was validated by dynamic axial loading by Nightingale et al. (1997) [43].

Table 2-2 Human head model material properties

Viscoelastic material model					
Human head components	Density (kg/m³)	Bulk density (GPa)	Short-term shear modulus (MPa)	Long-term shear modulus (MPa)	Decay Constant (Beta s⁻¹)
Cerebrum	1060	2.16	0.006	0.0012	80
Cerebellum	1060	2.16	0.006	0.0012	80
Brainstem	1060	2.16	0.006	0.0012	80
CSF	1000	2.00	0.0004	0.0001	80
Elastic/ Elastic-plastic material model					
Head Component	Density (kg/m³)	Young's modulus (MPa)	Poisson's ratio		
Scalp	1000	22	0.42		
Cortical bone	1920	14900	0.22		
Spongy bone	1000	1090	0.22		

2.2.3.2 Simulation of 1.2 Kg representative sRPAS to human head impact

Both HyperMesh and LS-PrePost version 4.3 (LSTC/ANSYS, Livermore, CA) were used for the sRPAS model and THUMS model integration during the preprocessing stage. Initial boundary/loading conditions included placing sRPAS model relative to human head, setting sRPAS flying velocities, and defining contact condition between sRPAS and human head. The initial position, angles and velocities were referred to Ohio State University (OSU) PMHS experiments settings (Table 2-3). Figure 2-2 shows the 50th percentile THUMS model (Figure 2-2a) and four typical sRPAS to head impact directions, including lateral 0-degree (Figure 2-2b), frontal 58-degree (Figure 2-2c), lateral 58-degree (Figure 2-2d) and top 90-degree impacts (Figure 2-2e). The *INITIAL_VELOCITY in LS-DYNA (LSTC/ANSYS, Livermore CA) was used to assign the flying velocity. The *AUTOMATIC_SURFACE_TO_SURFACE was used to define the contact between sRPAS model and human head model. The friction coefficient was set as 0.3 between the drone and the head. The numerical accelerometers were

defined on the human head model to collect linear acceleration and rotational velocity at head center of gravity following local coordinates. Both head linear acceleration and rotational velocity were plotted every 0.01 ms (100 kHz). It was observed that direct resultant acceleration output from LS-PrePost would induce artificial numbers at the middle to later stage. Hence, linear acceleration of x, y, and z directions were first filtered with low-pass CFC (channel frequency class) 1000 Hz filter and then resultant acceleration calculated from filtered x, y, and z data. Rotational velocities were filtered with CFC 180 Hz filter.

Table 2-3 sRPAS to head impact setups. FPS: foot per second. OSU: Ohio State University.

Case #	Impact Direction	Impact Angle degree)	Sex	Impact Velocity m/s (FPS)	Cadaver Subject
1	Lateral	0	Male	16.8 (55.1)	1
2	Lateral	0	Male	18.3 (60.1)	1
3	Lateral	0	Male	21.1 (69.2)	1
4	Front	58	Male	17.5 (57.3)	1
5	Front	58	Male	18.0 (59.2)	2
6	Front	58	Male	18.3 (59.9)	2
7	Front	58	Male	21.4 (70.1)	2
8	Lateral	58	Male	18.7 (61.2)	2
9	Lateral	58	Male	21.9 (71.9)	2
10	Top	90	Male	16.8 (55.2)	2
11	Top	90	Male	19.5 (63.9)	2
12	Top	90	Male	21.5 (70.5)	2
13	Lateral	58	Male	18.6 (60.9)	3
14	Lateral	58	Male	21.9 (71.9)	3
15	Front	58	Male	21.9 (71.8)	3
16	Top	90	Male	19.7 (64.5)	3
17	Top	90	Male	21.5 (70.5)	3

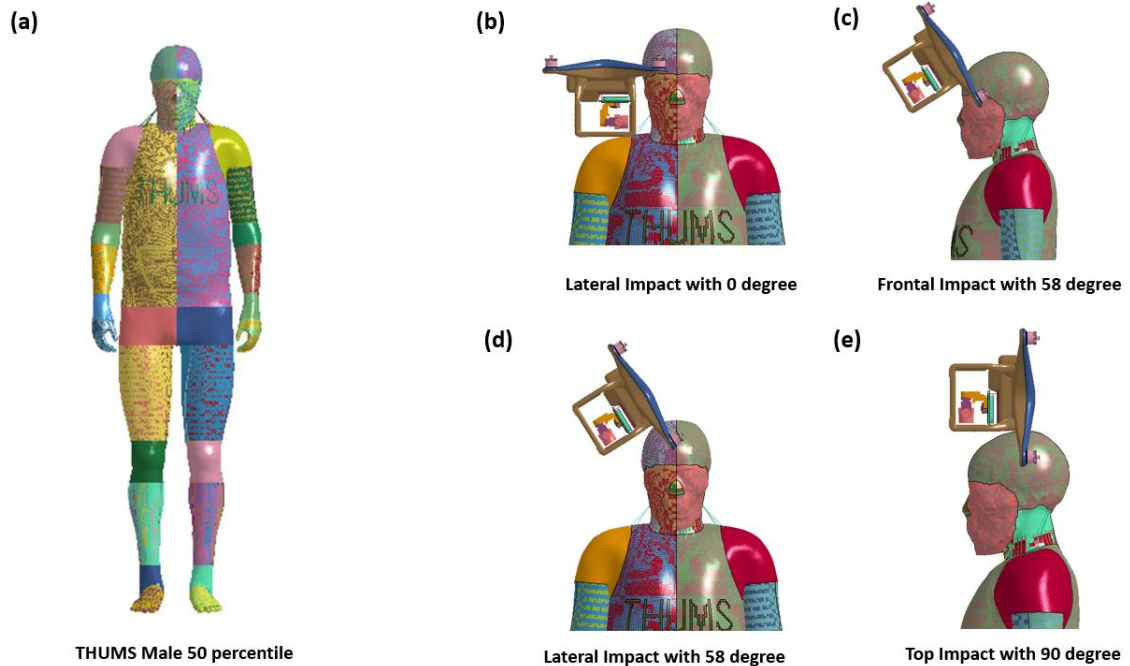


Figure 2-2 THUMS version 4.02 50th percentile male model. (a) full model, (b-e) typical impact directions.

2.2.4 Skull stress

The maximum skull stress was obtained from LS-PrePost. Normally, the maximum skull stress happened at the very beginning of collision. In Ls-PrePost, highest von Mises stresses from skull shells were visually determined and their time histories were plotted. Then, the time histories of nine elements with highest stresses, which were visually selected based on stress contours, were plotted and the averaged curve was obtained. The maximum value on the averaged curve represented as the maximum skull stress.

2.2.5 Brain strain and cumulative strain damage measure (CSDM)

The entire brain maximum principal strain distribution over the 40 milliseconds impact durations were analyzed. The CSDM is a method to evaluate the deformation-related brain strains caused by head impact. It calculates the volume fraction of brain experiencing strains greater than a critical level. In this study, the volume of all the elements which experienced a strain level over specified threshold values was recorded and the fraction of recorded volume to the total brain volume resulted in the CSDM value. For CSDM15, the volume of brain elements experiencing strains above 0.15 would

be calculated. The calculated CSDM values were further verified with brain strain contour to confirm a visual agreement between high CSDM and large high-strain areas. The in-house CSDM code was used and its accuracy has also been verified in our previous human and animal brain strain analysis.

2.2.6 Sensitivity analysis – Impact location, angle, and arm first

2.2.6.1 Impact location and angle

It could be reasonably postulated that the three cadaver heads used in experiments possessed different shapes that could affect the definition of impact location and angle relative to the human head. Hence, despite the FE model has been meticulously exercised to best match with experimental settings, a sensitivity analysis on the impact location and angle could help to understand the changes of head kinematics if small impact angle and impact direction changes occurred. Four typical direction cases (Figure 2-3) were used as original cases for sensitivity study. For angle sensitivity of all directions, the impact angles were increased and decreased at ± 3 degrees (Figure 2-3a). For impact position sensitivity, the initial positions were change at ± 5 mm and ± 10 mm (Figure 2-3b) perpendicular to the moving direction of sRPAS. All other variables were kept the same.

2.2.6.2 Arm-first impacts

Arm-first scenario was considered as a possible impact scenario as one of the four arms of a quadcopter style sRPAS could contact the head first. Compared to body-shell-first scenario, arm-first scenario has smaller contact area during drone collision. Thus, investigating the arm-first scenarios was also conducted in this study. Figure 2-3c shows the four typical directions for simulations of arm-first cases.

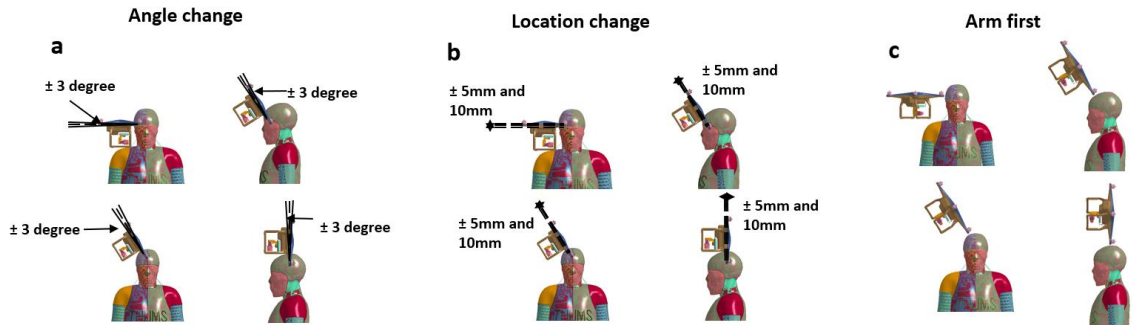


Figure 2-3 sensitivity studies. (a) Simulation settings of sensitivity study on impact angle, (b) impact location, and (c) arm-first impact.

2.3 Results

A total of 45 simulations including cases #1 to #17 for validation, 8 cases for impact degree sensitivity study, 16 cases for impact location sensitivity study, and 4 cases for arm-first impacts were calculated using LS-DYNA. Computers with Intel Xeon 8-core CPUs and 24-core CPUs were used to solve simulations. When using 2 CPUs, it took approximately 20 hours to solve 40-millisecond impact cases.

2.3.1 Resultant linear acceleration validation

In the lateral 0 degree impact cases (1, 2 and 3 shown in Figure 2-4), typically one peak linear acceleration appeared during the impact. The durations of the impact were approximately 2 milliseconds. The curve shape and impact duration matched well with experimental data for all three cases. The simulated peak linear acceleration also matched with cadaver experiments, except for case 3 in which a high initial velocity (21.1 m/s – 69.2 FPS) was defined. For case 3, the peak linear acceleration of simulation was about 20% smaller than that of experiment.

In the frontal 58 degree impact cases in which the drone was placed close to the face (4, 5, 6 and 7 shown in Figure 2-4), the linear acceleration curves typically had 2 peaks and the second peak was generally similar to or lower than the first peak. The impact duration was around 3 milliseconds. Except for case 5, the curve shape and peak linear acceleration matched well with cadaver experiments. In case 5, the simulation curve did not match with experiment curve. However, the cadaver experiment curve of case 5 was

not consistent with other three frontal 58-degree cases, showing three peaks with the last peak being the largest.

In the lateral 58 degree impact cases (8, 9, 13 and 14 shown in Figure 2-4), generally, the simulation impact duration and curve shape matched well with cadaver experiments. However, in some cases the peak values were over predicted. In case 9 and 13, the peak linear accelerations were 17% and 35% higher than those measured cadaver experiments, respectively. In case 14, the simulated peak value and curve shape were close to the cadaver experiments.

Case 15 was a typical case in which the initial position of drone was close to coronal suture instead of the face. Under this case, the simulation and cadaver had similar peak linear accelerations, which were 370.9 g's and 378.2 g's, respectively. The impact durations were perfectly matched, which were around 2 milliseconds.

In the top 90 degree impact cases (10, 11, 12, 16, and 17 shown in Figure 2-4), the impact durations of cadaver experiments were roughly 1 millisecond longer than those of simulations. Generally, the peak linear accelerations of cadaver experiments were larger than those of simulations, especially for the cases using cadaver subject 2 (case 10, 11 and 12). Under these three cases, the cadaver experiments had two peaks which was different from simulations where only one peak appeared. Under cases using cadaver subject 3 (case 16 and 17), the model-predicted peak linear accelerations were close to cadaver results and the curve shapes were very similar.

From average linear acceleration bar charts of all 17 cases, we can observe that average peak linear accelerations of simulation was 4.5% lower than that of experiment. Through calculation of root-mean-square error (RSME), the simulation result had 95.2 g root-mean-square deviation with PMHS result and the normalized root-mean-square deviation (NRMSD) was 0.3.

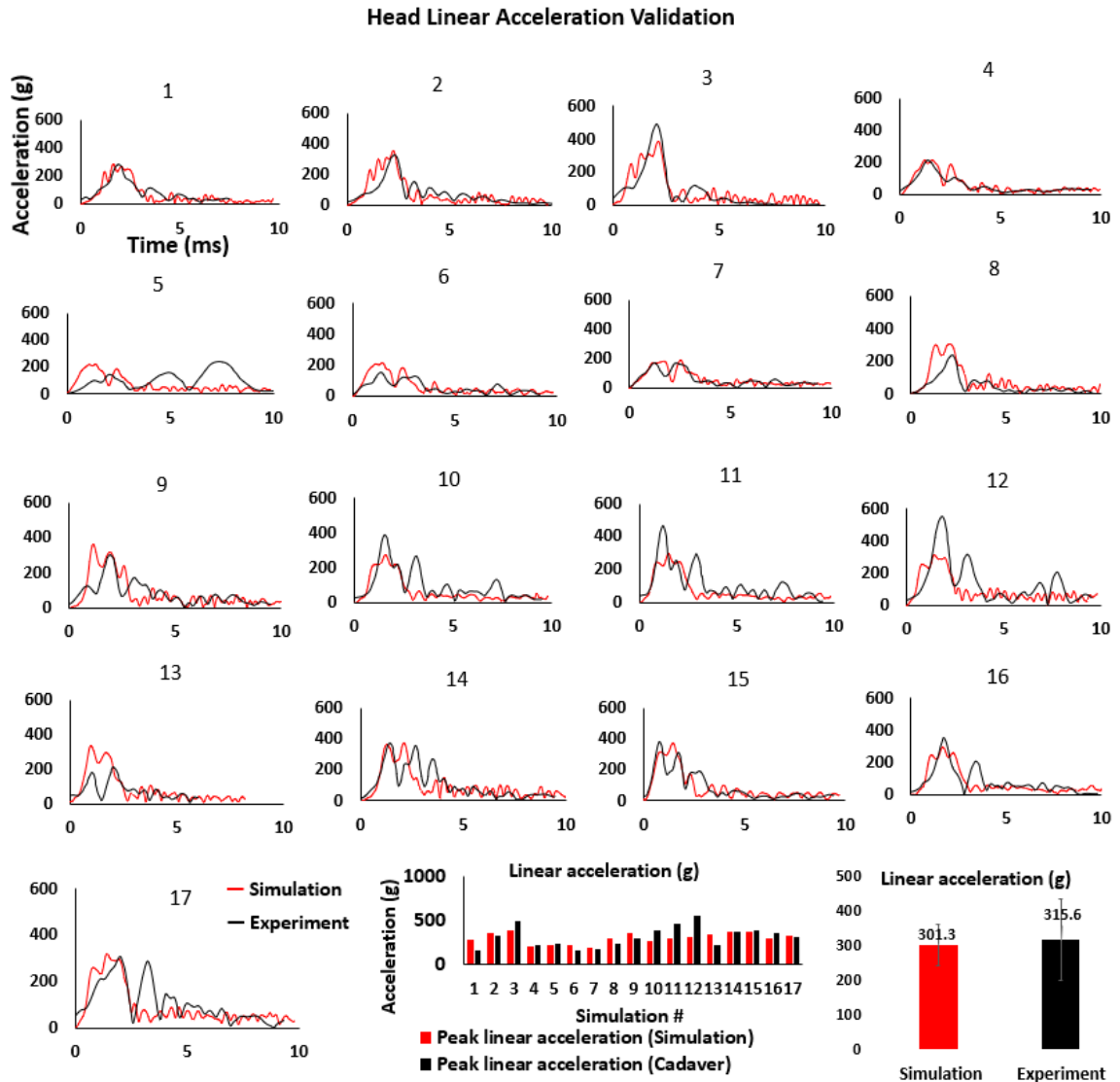


Figure 2-4 Head resultant linear acceleration validation. Experimental data were digitized based on ASSURE report.

2.3.2 Resultant rotational velocity validation

In lateral 0 degree cases (1, 2 and 3 shown in Figure 2-5), the rotational velocity curves were well validated. The curves of simulations and cadaver experiments matched well, and the peak rotational velocity values were generally close.

In frontal 58 degree cases (4, 5, 6, and 7 shown in Figure 2-5), the curve shapes and trends matched well. However, under low initial velocity (case 4, 5 and 6 which had initial velocity of 17.5 m/s - 57.3 FPS, 18.0 m/s - 59.2 FPS and 18.3 m/s - 59.9 FPS, respectively), the simulated peak rotational velocity values were underpredicted by approximately 50%. However, under high velocity (case 7 with initial velocity of 21.4 m/s - 70.1 FPS), the peak value and curve shape were well matched.

In lateral 58 degree cases (8, 9, 13 and 14 shown in Figure 2-5), generally the peak rotational velocities were overestimated. In case 8 and case 13, the peak rotational velocity values were overpredicted by 29% and 14%, respectively. In case 13 and 14, the curve shape and trend were matched. However, the peak values were 29% and 24% higher than those of experiments.

In frontal 58 degree with initial drone position being close to the coronal suture (case 15 shown in Figure 2-5), the simulation and experiments curves had different shapes. However, the peak rotational velocity values were close, which were 1410 degree/second and 1443 degree/second, respectively.

In top 90 degree cases (10, 11, 12, 16 and 17 shown in Figure 2-5), the curve shapes were similar. Generally, the peak rotational velocity of simulation were underpredicted. In cases 10 and 11, the simulated peak rotational velocities were 17% and 18% lower than experimental results, respectively. In case 12, the predicted peak value was 11 % higher than that of experiment. In case 16 and 17, the peak rotational velocity values were 19% and 29% lower than experimental results, respectively.

From average bar charts of rotational velocity, the average peak rotational velocity was 2% lower than that of experiment. In root-mean-square deviation analysis, the simulation was 280 deg/s different from PMHS experiment and the normalized root-mean-square deviation was 0.22.

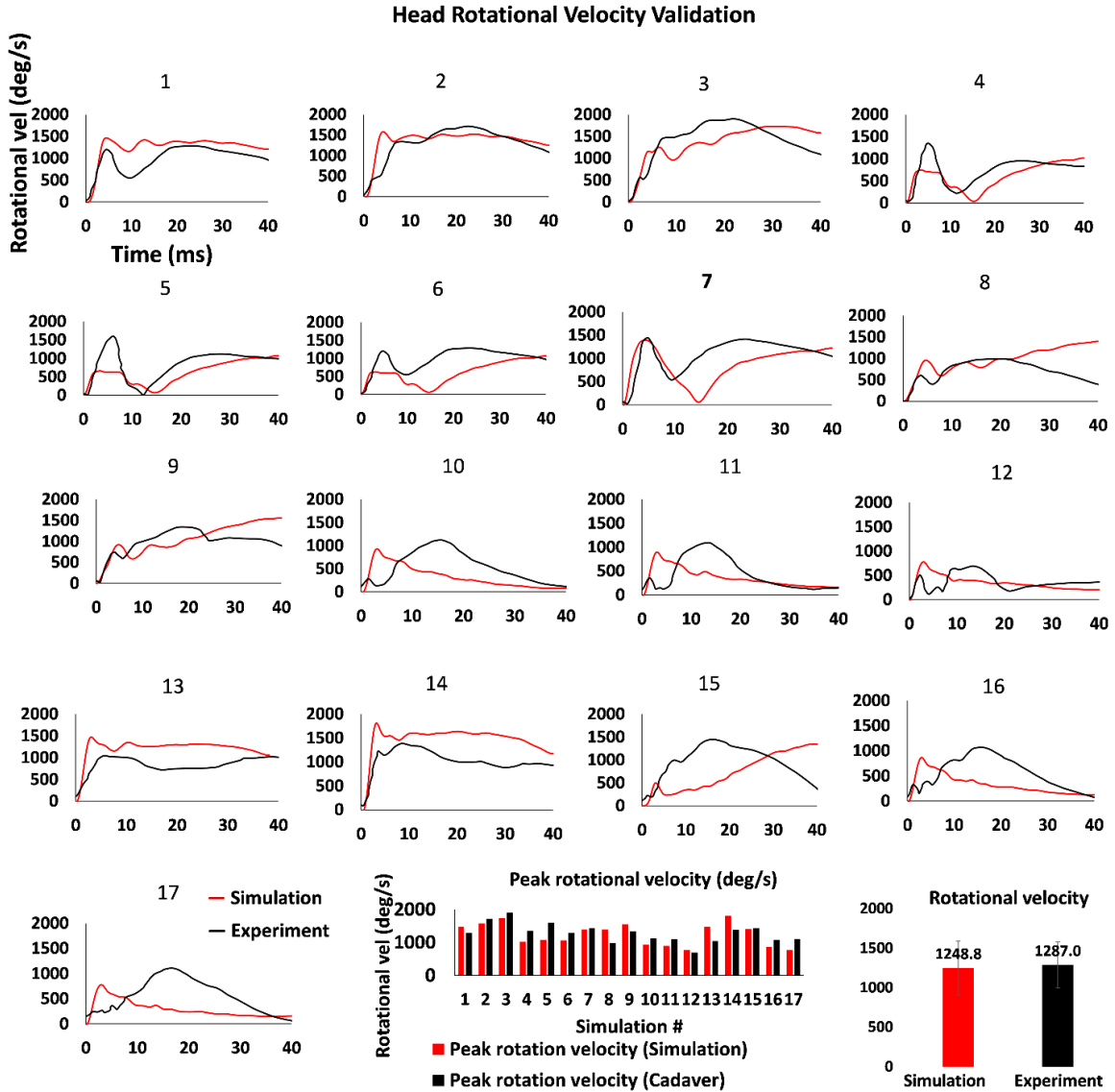


Figure 2-5 Head resultant rotational velocity validation. Experimental data were digitized based on ASSURE report.

2.3.3 Skull stress

Variances in skull von Mises stresses (Figure 2-6) further demonstrate the effect of sRPAS structures. For example, while top 90 degree impacts have similar impact velocities as other impacts, the skull stresses were much lower than those in other cases due to relatively larger contact areas.

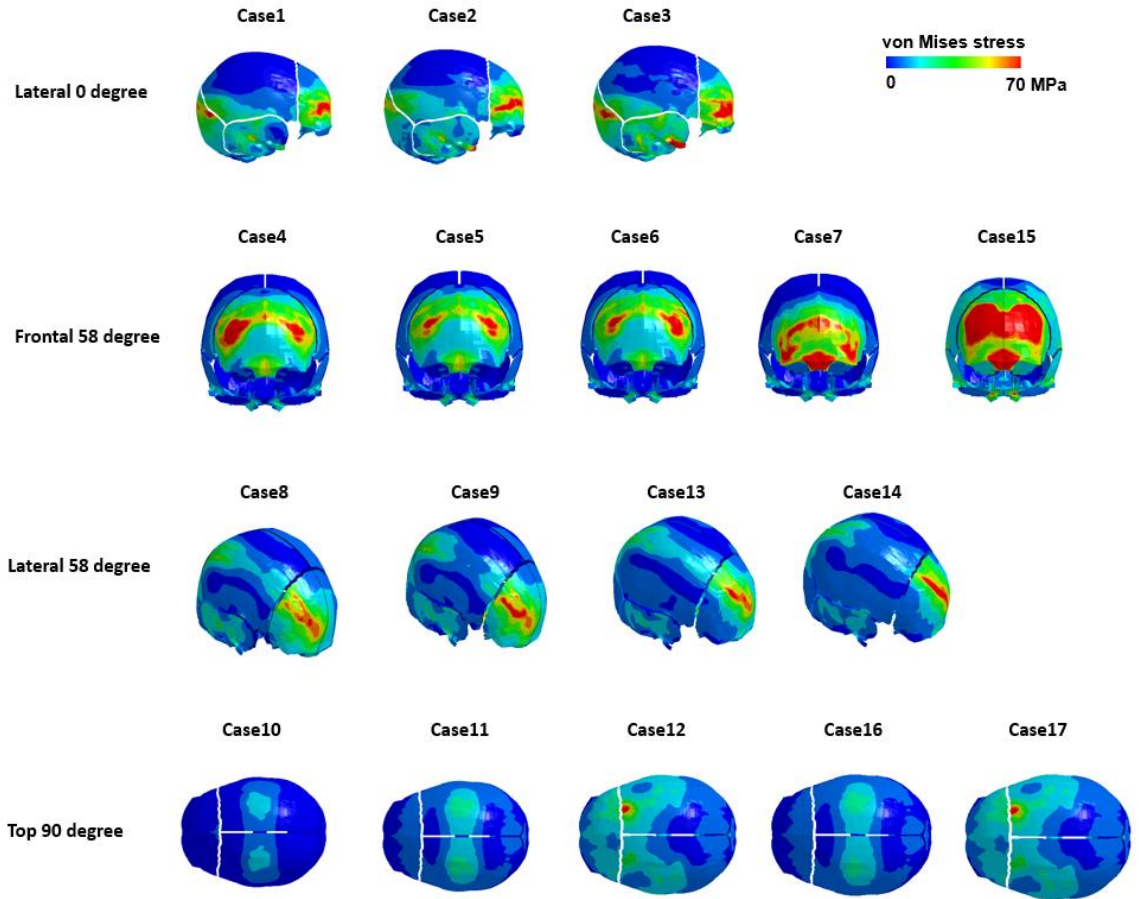


Figure 2-6 Skull stress distributions for 17 validated cases.

2.3.4 Brain strain

Brain contour (Figure 2-7) demonstrates that relatively high brain strains were produced for several situations (such as cases 1, 2, 3, 7, 13, and 14), while in other cases especially top 90 degree impacts the strains were small. Large variances across impact cases were demonstrated with smallest CSDM15 close to 0 to 0.02 while largest CSDM of 0.49.

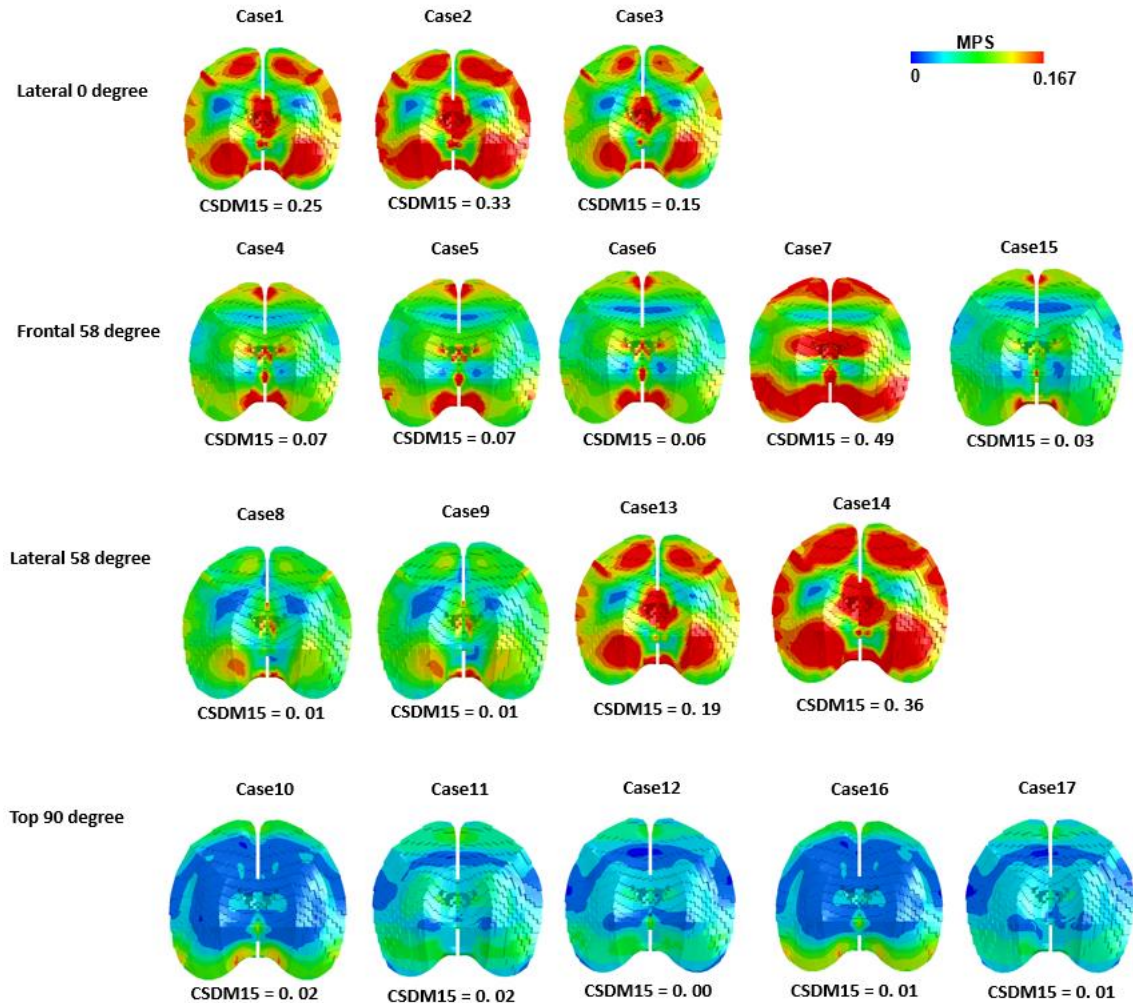


Figure 2-7 Brain strain contours and CSDM15 for 17 validated cases.

2.3.5 Sensitivity analysis

2.3.5.1 The effect of impact angle change

Figure 2-3a illustrates the changes in the peak linear acceleration and rotational velocity with changing the impact angle by ± 3 degrees. From the peak linear acceleration bar chart, in general, it can be observed that with the increase of angle, the head linear acceleration increased and the changes depended on the impact directions (Figure 2-8a). In minus 3 degree cases, under lateral impact cases (0 degree and 58 degree), the peak linear acceleration increased. For frontal and top cases, the peak value decreased. Under top 90 degree impacts, with 3 degree angle change cases, the peak linear acceleration had around 30% of variation (Figure 2-8a). In peak rotational velocity chart, in general the

variation was relatively small (Figure 2-8b). However, it can be observed the largest variance also happened in top 90 degree cases which had 29% of variations (Figure 2-8b).

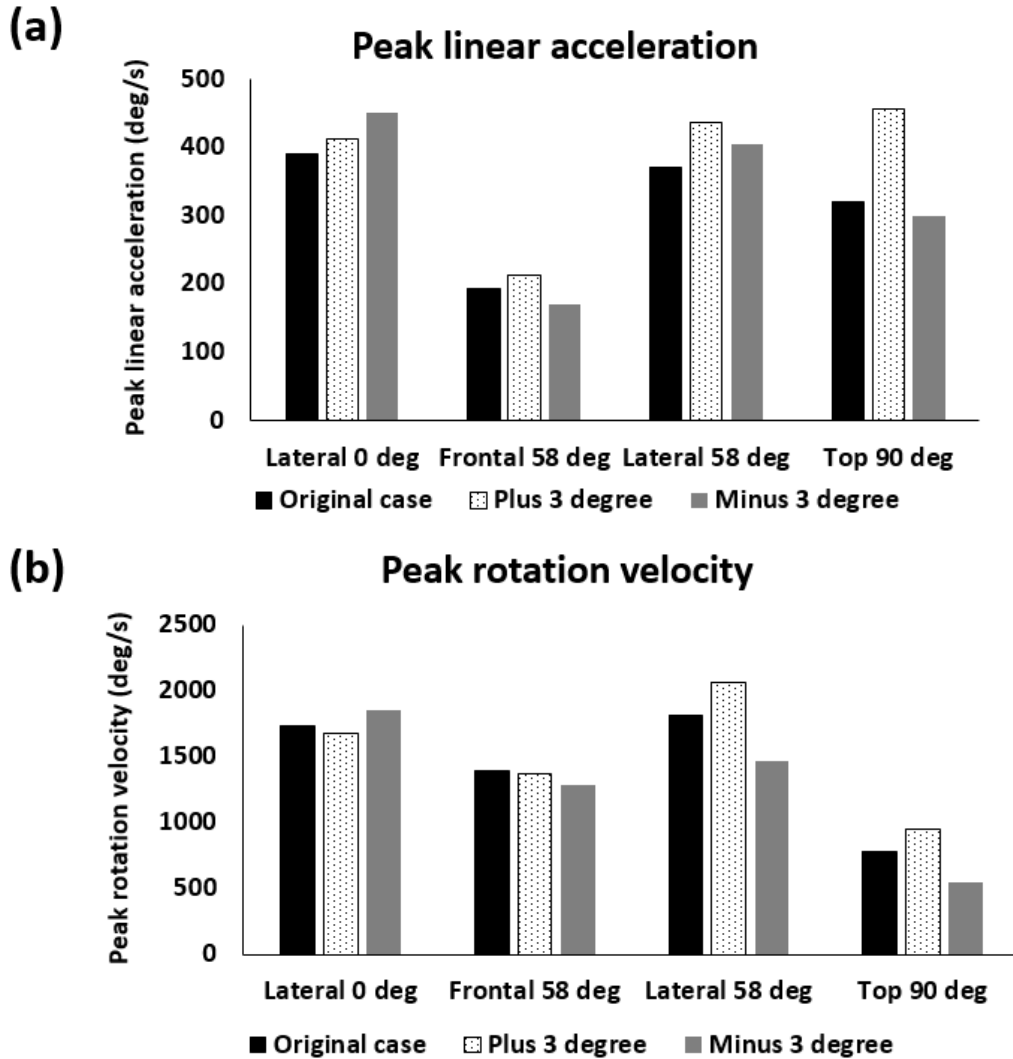


Figure 2-8 Sensitivity analysis of impact angle. (a) Peak linear acceleration and (b) peak rotational velocity changes for ± 3 degrees impact angle changes.

2.3.5.2 The effect of impact location

Previous Figure 2-3b illustrates the changes in peak linear acceleration and rotational velocity with ± 5 mm and ± 10 mm impact location changes. Under lateral 0 degree and

frontal 58 degree impacts, the linear acceleration was not very sensitive to location changes with maximum variation of 19.5% (Figure 2-9a). However, under lateral 58 degree and top 90 degree impacts, the location change had larger effect on head peak linear acceleration. Under those directions, 10-mm location change induced around 27.0% of variation.

The effect of impact location change on peak rotational velocity was generally similar as it had on peak linear acceleration (Figure 2-9b). In lateral 0 degree and frontal 58 degree impacts, the head rotations did not change much due to impact location changes. In lateral 58 degree and top 90 degree impacts, head rotational velocities were more sensitive to location shift and showed a maximum variation of 21.9%.

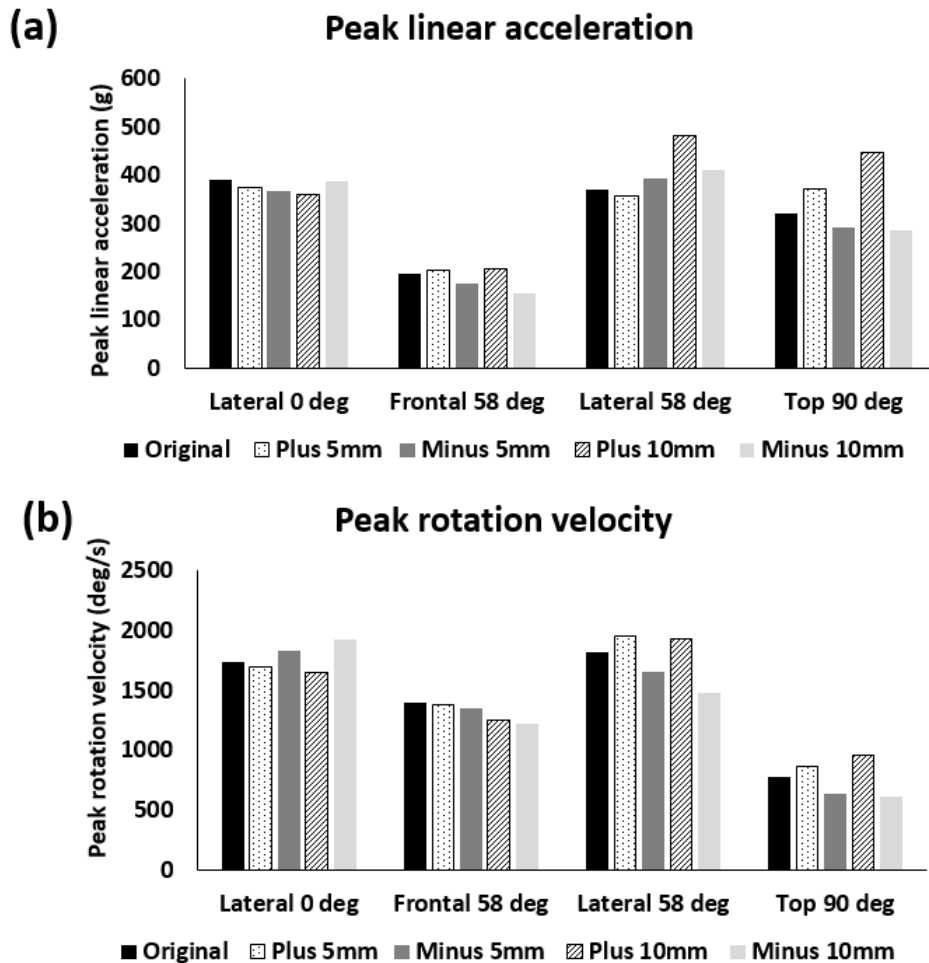


Figure 2-9 Sensitivity analysis of impact location. (a) Peak linear accelerations and (b) peak rotational velocity changes under various impact locations.

2.3.5.3 The effect of arm-first impact

Previous Figure 2-3c illustrates the von Mises skull stress as well as the brain strain in arm-first impacts, in which the arm-first impacts the head. All arm-first impact cases demonstrated concentrated high stresses directly under the impact site (Figure 2-10a). Arm-first impact induced much larger skull stresses and higher brain strains than the corresponding body impacts, in which the shell first impacts the head. On average, peak stresses for four arm-first cases were 125.0% larger than the values from corresponding “regular” cases. Brain strain estimated as CSDM15 were 54.3% larger than the values from corresponding “regular” cases (Figure 2-10b).

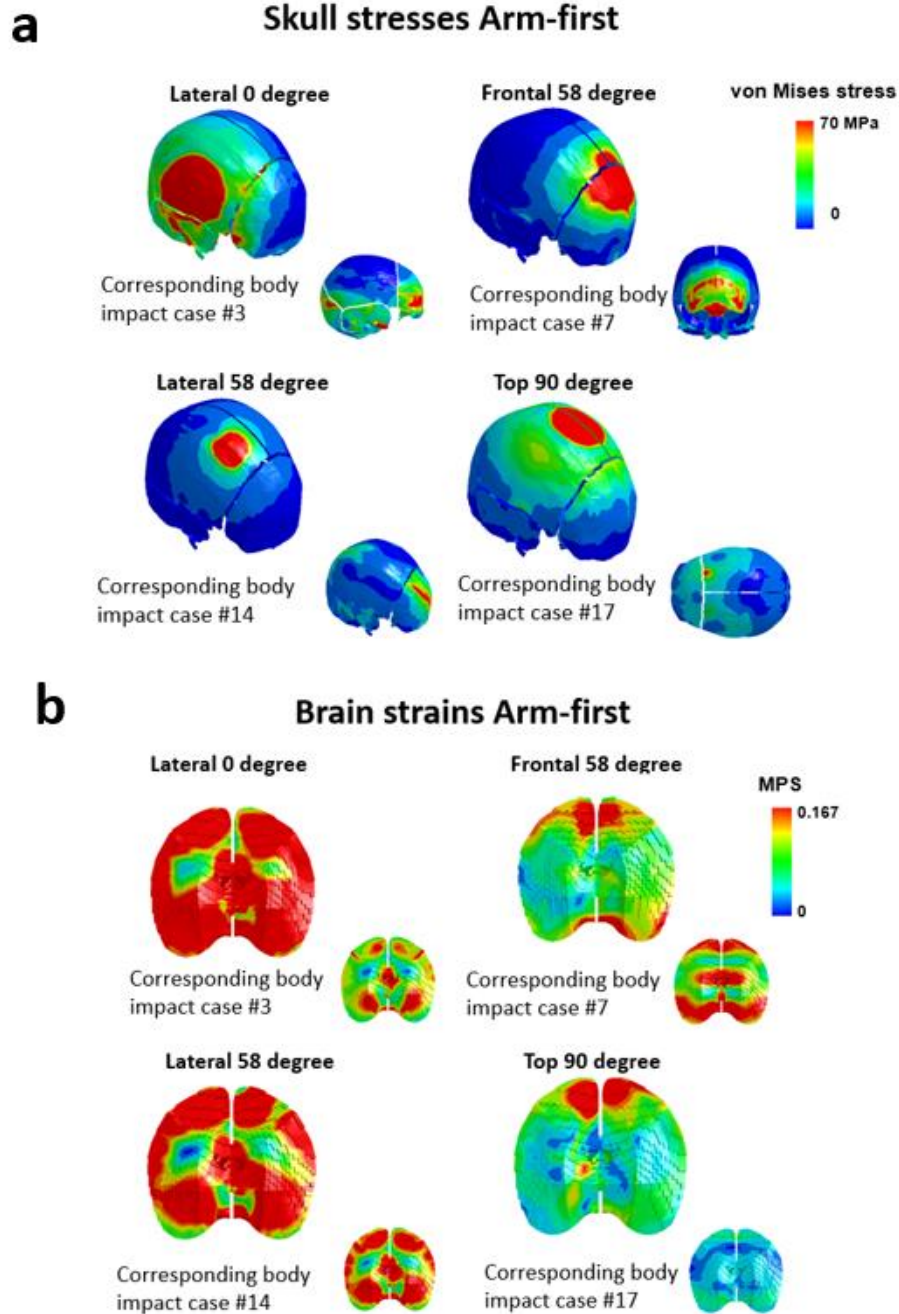


Figure 2-10 Skull stress and brain strain contour comparisons in arm-first impacts and their comparisons to corresponding body shell-first impact. (a) Skull stress (b) Brain strain. The contours from arm-first cases are presented with relatively larger sizes while the contours from corresponding body impact cases are presented with relatively smaller sizes.

2.4 Discussion

To investigate human head responses during sRPAS to human impacts, we developed a detailed FE model of a representative quadcopter style sRPAS and validated the model with 17 sRPAS-to-human-head impact settings. Model-predicted head linear acceleration and head rotational velocity agreed with data collected from cadaveric heads. Based on validated FE models, the von Mises skull stress and brain maximum principal strain were analyzed. It was shown that during impacts, the human head experienced very different stress and brain responses that were greatly affected by impact settings. To the best of our knowledge, our study served as the first computational study with validated sRPAS-to-human-head models and to provide data on brain strains as well as skull stresses under these validated simulations.

Highest von Mises skull stress was observed in the frontal 58-degree impact simulation (case 15, Figure 2-6). Interestingly, an AIS 2 level, 13 cm linear skull fracture was observed in cadaveric study during the frontal 58-degree impact at 21.5 m/s speed [35]. In the literature, the von Mises stress was used as injury predictor under skull loading conditions [37]. It was found that von Mises stress value of 110.9 MPa was compatible with skull fracture level [36]. Roth et al. proposed a 3-year-old head model and considered that von Mises stress was the most predictive parameter [49]. The von Mises stress was also used as a predictor to assess the femur and pelvis fracture risk during vehicle crashes [50].

The 17 validated cases showed a mild level of brain strains with most of strains below 0.15. However, for two lateral 0 degree (#1, #2), one frontal 58 degree (#7), and two lateral 58 degree cases (#13, #14), a large portions of brain strains exceeding 0.15 with an average CSDM15 of 0.12 calculated from 121,074 brain elements. For all top impacts, the risk of brain injury is limited as brain strains are almost all below 0.1. Our data demonstrated that further experimental investigation of potential brain injury due to sRPAS-to-human impacts is warranted, and such an investigation could be geared toward certain frontal and lateral impact settings. Compared to extensive brain injury data associated with head kinematics being reported for automotive accidents or sports

collisions, to the best of the authors' knowledge, brain injury data for sRPAS-to-human impacts have yet to be collected.

Slight impact angle and direction changes across experiments could be expected for cadaveric setting, partially due to complexity in posing cadavers without muscle tone as well as the need to release restrains before sRPAS impacts. Hence, it is reasonably postulated that investigating the effects of small angle and direction changes using cadaveric subjects could be challenging. Our validated computational models provided an ideal setting to investigate these effects as impact parameters could be conveniently and accurately controlled in FE modelling. The data demonstrated that a minor 3-degree change could induce large changes in head kinematics especially for top impacts with variances up to 29%. For the position effect, the lateral 58-degree and top impacts seemed to be most sensitive with variances up to 22%.

It is possible that the arm of a quadcopter could impact the head before the body shell. The arm-first impact simulations demonstrated a much higher risk of skull fracture as stresses were more concentrated in these impacts for which the contact areas were small. For brain strains, it is interesting that arm-first impacts especially generated high strains under lateral 0-degree and lateral 58-degree impacts but low strains under frontal 58-degree and top impacts. It also needs to be highlighted that the high strains generated during arm-first impacts were higher than those generated by "regular" impacts. With both skull stress and brain strain data, this study highlights the need to address potentially higher risk induced by the arm of quadcopter.

There are several limitations of this study. First, although extensive validation on head kinematics has been conducted, there is no direct validation on head responses such as brain strain during sRPAS-to-human impacts. Nevertheless, the THUMS head model used in this study has been validated against brain-skull relative motion data and been extensively used in automotive and sports collision fields. Hence, the head model was justified to be appropriate for brain strain as the strain level predicted in this study was in the range comparable to mild head impacts. The second limitation of this study is that the battery component was defined as a simplified block with a simple elastic material.

Though for a physical battery, the material is much complex. Generally, Lithium-ion (Li-ion) battery was used to power sRPAS, and typically has several coating layers and polymer layer separators with different material model and properties assigned [51]. This geometry combination directly determine the overall mechanical properties and deformation situations during collisions. Lastly, a no-fracture version of the human body model was used and hence the stress values predicted by the model should be referred as a comparative purpose as once fracture was allowed and happened then the stresses would maintain or decrease. Despite aforementioned limitations, we justify that by developing a sRPAS model with extensive validation of head kinematics under sRPAS-to-human impacts, we provided novel data to better understand head responses during these impacts. Also, further experimental and computer investigation is strongly recommended given the expected rapid growth of sRPAS usage.

2.5 Conclusions

A representative quadcopter type sRPAS finite element model was developed and applied to conduct a total of 17 impact simulations, with different settings from lateral 0-degree, frontal 58-degree, lateral 58-degree, to top 90 degree. Overall, model-predicted head linear accelerations and rotational velocities agreed well with measured data from the cadaveric experiments. High skull stresses and mild to moderate level of brains strains were observed from these impacts, while these stress/strain values varied greatly among different impact scenarios. Additional sensitivity analysis demonstrated that head dynamics could be sensitive to slight changes of impact angle (± 3 degrees) and impact locations (± 5 mm and ± 10 mm) with variances up to 30%. In the impact cases where the sRPAS arm contacted the head first, skull stresses and brain strains were higher compared to corresponding body-shell-contacting cases.

Chapter 3

3 Investigation of the correlation between head kinematics, injury metrics and injury-related head responses under small remotely piloted aircraft system (sRPAS) to human head collision

Abstract

With the increasing usage of small remotely piloted aircraft system (sRPAS), preventing sRPAS-induced head injuries is critical. The correlations between head kinematics, injury metrics and injury-related head responses such as skull stresses and brain strains are important for guiding sRPAS safety regulation development to minimize injury risks. The previously developed sRPAS finite element (FE) model and the THUMS ver 4.02 male human body model were combined for investigating a total of 68 impacts involving 6 different impact directions and 12 impact velocities. For injury metrics, HIC (head injury criteria) values correlated with skull stresses, supporting the effectiveness of using HIC. Interestingly, brain injury criteria (BrIC) values were only moderately correlated to brain strains, weaker than the correlations in other blunt impact scenarios, suggesting a unique, diminishing effectiveness of BrIC under sRPAS to head impacts. For skull stress, rear 0 degree setting was considered as the most dangerous. Regarding brain strain, frontal 58 degree and rear 58 degree settings induced the largest brain strain. Top 90 degree setting generated both the least skull stress and least brain strain compared to other impact settings.

3.1 Introduction

With the innovation of small remotely piloted aircraft system (sRPAS), more sRPASs are being used and hence regulating sRPAS to human impact injury risk is needed.

Especially, the safety of the head during sRPAS-related impacts is of the biggest concern [4]. Traditional head safety injury criteria include head injury criterion (HIC), which is calculated using the magnitude and duration of resultant linear acceleration based on Wayne State University cadaveric experiments [5]. HIC has been widely adopted as a primary head injury metric in automotive safety [52, 53]. Besides HIC, peak resultant

linear acceleration was also regulated. For example, based on the European standardization commission guidelines for helmet standard, the peak resultant linear acceleration of 200 to 250 g could result the AIS (abbreviated injury scale) 4 head injuries [44]. Also, an upper limit of 80g's for a 3 milliseconds continuous time clip is commonly used in automotive safety regulations.

Besides linear acceleration, head rotation could cause brain injuries such as diffuse axon injury (DAI) and subdural hematoma [54, 55], and hence rotation-related injury metrics are also needed. As early as in 1992, Margulies and Thibault proposed DAI tolerances with a rotational velocity of 46.5 rad/s and an angular acceleration of 16,000 rad/s² [56]. Recently, Takhounts et al. proposed an injury metric named as brain injury criteria (BrIC) that takes account of impact direction effect for rotation-induced brain injuries [57]. However, whether these injury metrics could apply to the sRPAS-related impacts remains unknown.

Tissue-level head responses such as stresses and strains, rather than linear or rotational kinematics, are the direct cause of damage. Using finite element (FE) methods, the investigation of tissue-level head responses under high-rate impacts became possible. The skull stress was found to be related to the risk of skull fracture [36, 37]. The brain maximum principal strain (MPS) was proposed as a predictor of concussion and DAI [58, 59]. Especially, the MPS was widely used in evaluating the performance of head protection gear such as a helmet [60]. Based on MPS, the CSDM concept was introduced as this method counts the volume of total affected brain tissues rather than peak values [28]. How these tissue level responses correlate to linear and rotational head kinematics during sRPAS to human impacts needs to be investigated. Then, kinematics-based injury metrics could be evaluated in terms of their effectiveness in predicting head injuries.

The purpose of this study was to investigate head kinematics, injury metrics, and tissue-level head responses such as skull stress and brain strain in sRPAS to head impacts. A total of 68 simulations with 6 different impact directions and 12 velocities were involved. The relationships between head kinematics, injury metrics, and injury-related head

responses were analyzed. In addition, the results of each impact direction were analyzed to help define prioritized impact settings when developing sRPAS safety regulations.

3.2 Methods

3.2.1 Impact setting

A total of 68 sRPAS to human head impacts were simulated. These impact cases involved 6 different impact directions, including lateral 0 degree, frontal 58 degree, lateral 58 degree, top 90 degree, rear 0 degree and rear 58 degree. In each direction, three typical velocities 17.1 m/s (56 foot per second, FPS), 18.6 m/s (61 FPS) and 21.6 m/s (71 FPS) were applied. In order to investigate the effect of velocity in a larger range, the lateral 0 degree setting was selected based on the stability of impact in this direction. 12 different initial velocities from 4.9 m/s (16 FPS) to 21.6 m/s (71 FPS) were applied. Lastly, sensitivity studies involving small angle and impact position changes were included. All the detailed impact settings are summarized in Table 3-1.

Table 3-1 sRPAS to head impact setups. FPS: foot per second. OSU: Ohio State University.

Case #	Impact Direction	Impact Angle (Degree)	Sex	Impact Velocity (m/s - FPS)
1	Lateral	0	Male	16.8 - 55.1
2	Lateral	0	Male	18.3 - 60.1
3	Lateral	0	Male	21.1 - 69.2
4	Front	58	Male	17.5 - 57.3
5	Front	58	Male	18.0 - 59.2
6	Front	58	Male	18.3 - 59.9
7	Front	58	Male	21.4 - 70.1
8	Lateral	58	Male	18.7 - 61.2
9	Lateral	58	Male	21.9 - 71.9
10	Top	90	Male	16.8 - 55.2
11	Top	90	Male	19.5 - 63.9

12	Top	90	Male	21.5 - 70.5
13	Lateral	58	Male	18.6 - 60.9
14	Lateral	58	Male	21.9 - 72
15	Front	58	Male	21.9 - 71.8
16	Top	90	Male	19.7 - 64.5
17	Top	90	Male	21.5 - 70.5
18	Lateral	3	Male	21.1 - 69.2
19	Frontal	61	Male	21.4 - 70.1
20	Lateral	61	Male	21.9 - 72
21	Top	93	Male	21.5 - 70.5
22	Lateral	-3	Male	21.1 - 69.2
23	Frontal	55	Male	21.4 - 70.1
24	Lateral	55	Male	21.9 - 72
25	Top	87	Male	21.5 - 70.5
26	Lateral	0	Male	21.1 - 69.2
27	Frontal	58	Male	21.4 - 70.1
28	Lateral	58	Male	21.9 - 72
29	Top	90	Male	21.5 - 70.5
30	Lateral	0	Male	21.1 - 69.2
31	Frontal	58	Male	21.4 - 70.1
32	Lateral	58	Male	21.9 - 72
33	Top	90	Male	21.5 - 70.5
34	Lateral	0	Male	21.1 - 69.2
35	Frontal	58	Male	21.4 - 70.1
36	Lateral	58	Male	21.9 - 72
37	Top	90	Male	21.5 - 70.5
38	Lateral	0	Male	21.1 - 69.2
39	Frontal	58	Male	21.4 - 70.1
40	Lateral	58	Male	21.9 - 72
41	Top	90	Male	21.5 - 70.5
42	Rear	0	Male	21.6 - 71
43	Rear	0	Male	18.6 - 61

44	Rear	0	Male	17.1 - 56
45	Rear	58	Male	21.6 - 71
46	Rear	58	Male	18.6 - 61
47	Rear	58	Male	17.1 - 56
48	Rear	3	Male	21.6 - 71
49	Rear	-3	Male	21.6 - 71
50	Rear	61	Male	21.6 - 71
51	Rear	55	Male	21.6 - 71
52	Rear	0	Male	21.6 - 71
53	Rear	58	Male	21.6 - 71
54	Rear	0	Male	21.6 - 71
55	Rear	58	Male	21.6 - 71
56	Rear	0	Male	21.6 - 71
57	Rear	58	Male	21.6 - 71
58	Rear	0	Male	21.6 - 71
59	Rear	58	Male	21.6 - 71
60	Lateral	0	Male	20.1 - 66
61	Lateral	0	Male	15.5 - 51
62	Lateral	0	Male	14 - 46
63	Lateral	0	Male	12.5 - 41
64	Lateral	0	Male	11 - 36
65	Lateral	0	Male	9.4 - 31
66	Lateral	0	Male	7.9 - 26
67	Lateral	0	Male	6.4 - 21
68	Lateral	0	Male	4.9 - 16

3.2.2 Injury metric and head response

Head injury criterion (HIC)

The equation of HIC is expressed below [5].

$$HIC = \max_{t_1, t_2} \left\{ (t_2 - t_1) \left[\frac{1}{t_2 - t_1} \int_{t_1}^{t_2} a(t) dt \right]^{2.5} \right\}$$

where t_1 and t_2 are the initial and final times of the maximum HIC interval and $a(t)$ is the measured acceleration of head center gravity.

To calculate HIC of each impact case, a numerical accelerometer was defined at the location of head center of gravity to collect linear acceleration data. The linear accelerations at x, y, and z directions were outputted at every 0.01 millisecond, reaching a sampling rate of 100K frequency. The original data were then filtered by low-pass filter using CFC 1000 HZ. MATLAB 2019 (MathWorks, Massachusetts, USA) was then applied to calculate the resultant linear acceleration using the filtered x, y, and z data. An in-house code was written to calculate HIC15.

Brain injury criteria (BrIC)

Brain injury criteria is a relatively new injury metric to assess brain injury caused by the rotational motion of head. The mathematical formulation is expressed below.

$$BrIC = \sqrt{\left(\frac{\omega_x}{\omega_{xC}}\right)^2 + \left(\frac{\omega_y}{\omega_{yC}}\right)^2 + \left(\frac{\omega_z}{\omega_{zC}}\right)^2}$$

Where ω_x , ω_y , and ω_z are maximum angular velocities in x, y, and z axes, respectively. ω_{xC} , ω_{yC} , and ω_{zC} are the critical angular velocities in their respective directions.

The maximum angular velocities at x, y, z direction were collected from head center of gravity. The rotational velocity data were filtered by CFC 180 HZ. According to the literature, the critical angular velocity applied at x, y and z directions were 66.25, 56.45 and 42.87 rad/s, respectively [57].

Maximum skull stress

The maximum skull stress was obtained from LS-PrePost version 4.03 during post-processing, where the skull elements were examined (Figure 3-1a). The von Mises (VM) stress was checked at the contact location between sRPAS and human head (Figure 3-1b). To better represent the maximum skull stress value of the contact area, an average strategy was applied. The time histories of VM stress of nine different elements, which were visually selected based on stress contours, were plotted and the averaged curve was

obtained (Figure 3-1c & d). The maximum value on the averaged curve represented as the maximum skull stress.

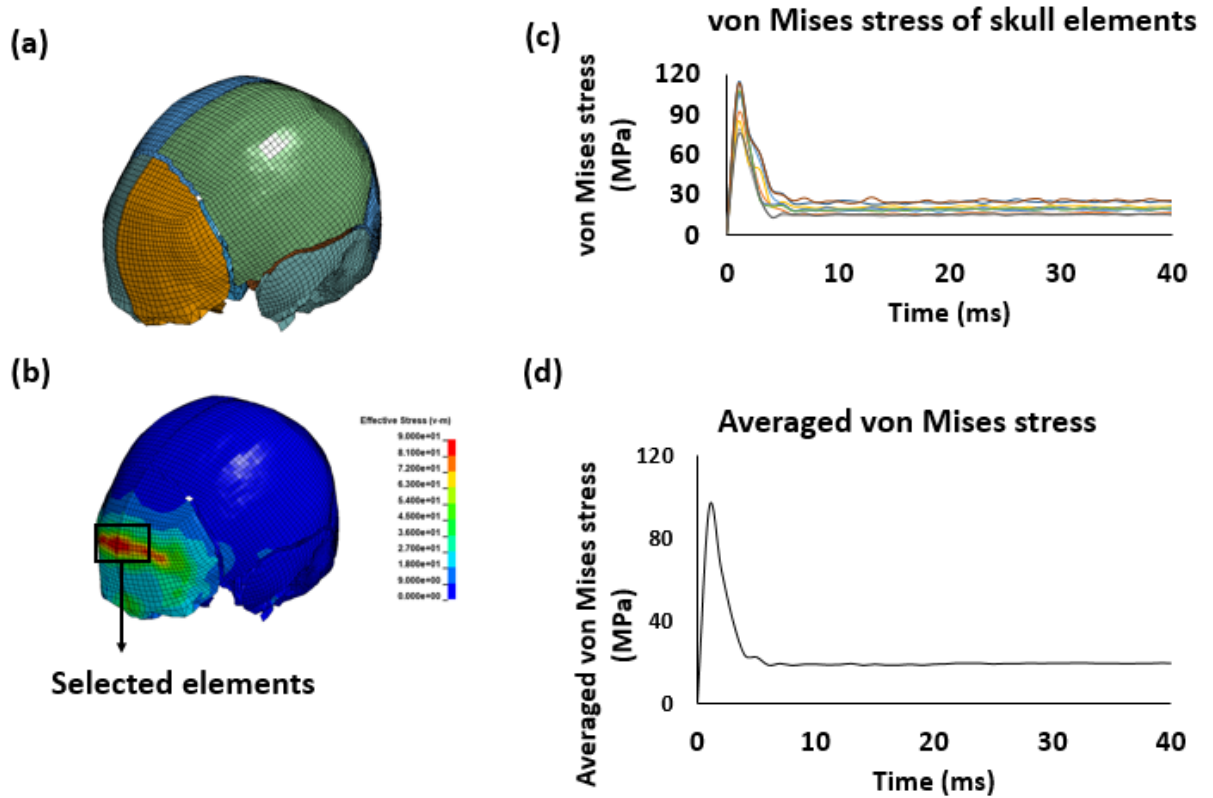


Figure 3-1 Maximum skull stress collection

Cumulative strain damage measure (CSDM)

The CSDM is a method to evaluate the deformation-related brain injuries caused by head impact. It can be calculated by the fraction of the brain experiencing strain level greater than specified level. In this study, the volume of all the elements which experienced a strain level over specified threshold values was recorded. For CSDM10 and CSDM15, the volumes of brain elements experiencing strains above 0.1 and 0.15 were calculated. The calculated CSDM values were further verified with brain strain contour to confirm a visual agreement between high CSDM and large strain areas.

3.3 Results

3.3.1 Linear acceleration, HIC, and skull stress

There was a strong correlation between HIC and peak linear acceleration with R squared value of 0.9495 and probability value (P value) less than 0.001 (Figure 3-2). Meanwhile, the impact durations, calculated as the time span of the main acceleration shape, were around 3 milliseconds.

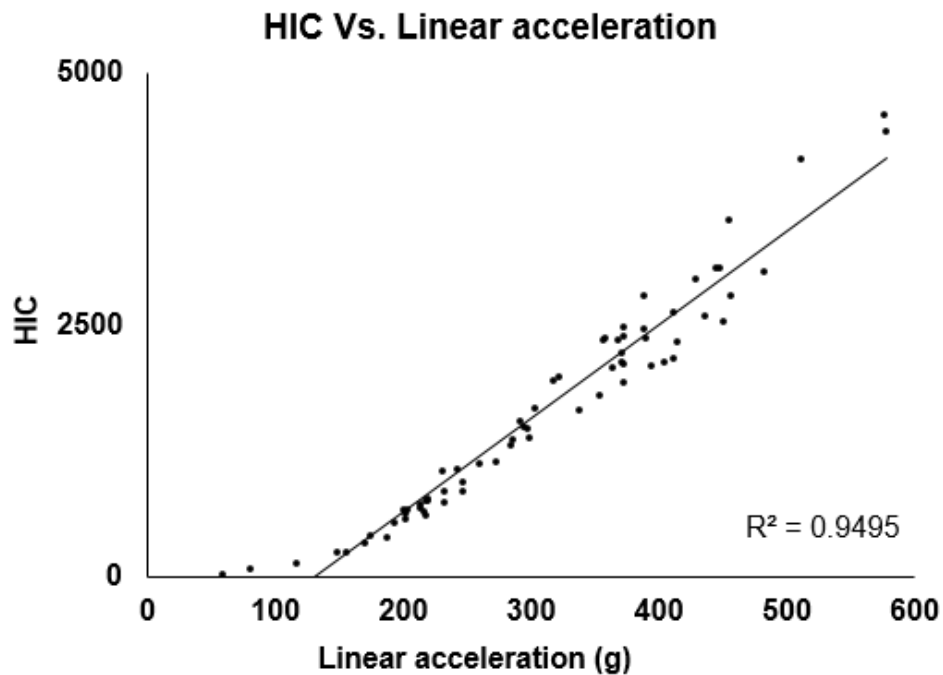


Figure 3-2 the correlation of HIC and peak linear acceleration ($P < .001$)

There was a moderate correlation between HIC and skull stress, with R squared value of 0.4113 with P value less than 0.001 (Figure 3-3). However, when the impacts were analyzed for each direction, skull stress and HIC showed improved level of correlation, especially for lateral 0 degree (Figure 3-4a) and top 90 degree (Figure 3-4d), which had R squared values of 0.8543 and 0.8949, respectively. The P values of these two correlations were both less than 0.001. In frontal 58 degree (Figure 3-4b) and lateral 58 degree (Figure 3-4c), the correlations were not that strong with R squared values of 0.5268 and 0.4034, respectively. The P values of these two correlations were both less than 0.005.

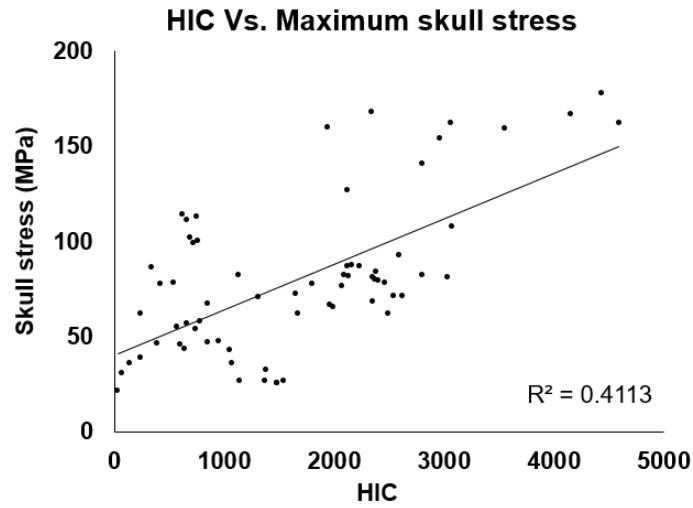


Figure 3-3 the correlation of HIC and maximum skull stress ($P < .001$)

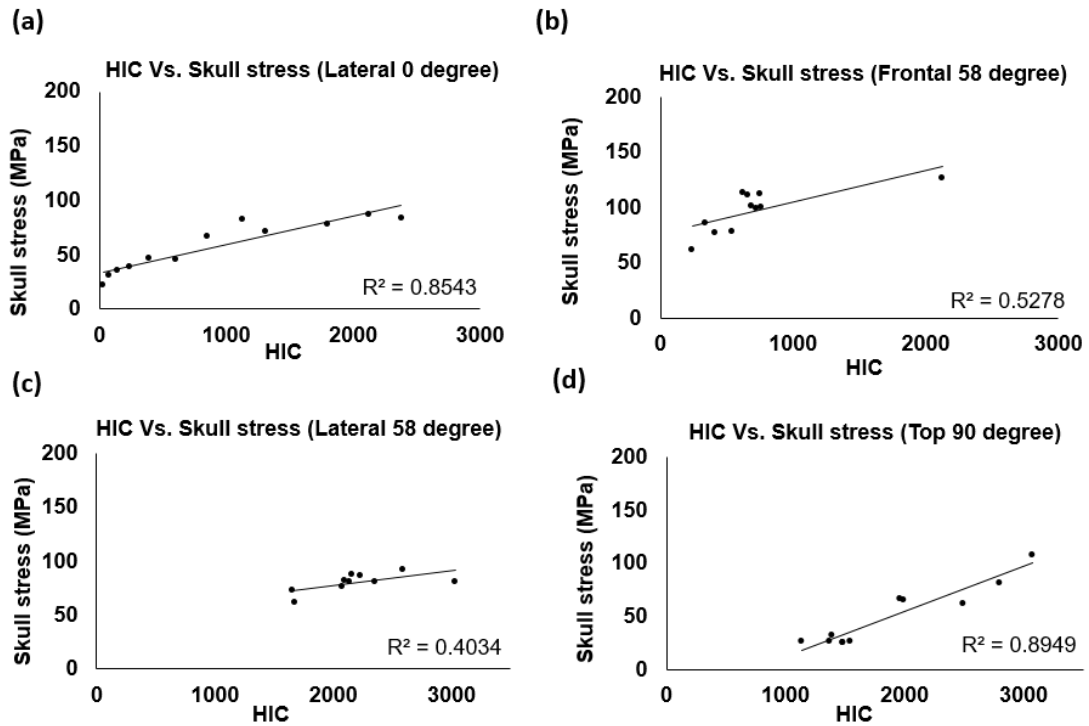


Figure 3-4 the correlation of HIC and skull stress under different impact directions. (a) Lateral 0 degree ($P < .001$); (b) frontal 58 degree ($P < .005$); (c) lateral 58 degree ($P < .005$); (d) top 90 degree ($P < .001$).

3.3.1.1 Analysis of the correlation between HIC and maximum skull stress

The direction of impact had large effects on HIC and skull stress. The frontal 58 degree cases had relatively lower HIC values, while their skull stress values were high (Figure 3-5a). Under most of the frontal 58 degree impacts, the arm of sRPAS first contacted with the head skin (Figure 3-5b). The sRPAS continued to compress the head during impacts and as a result, the force transferred from sRPAS concentrated at the region where sRPAS arms contacted with human head (Figure 3-5b & c). Through the contour of skull stress (Figure 3-5d), the stress concentration regions could be observed at the locations beneath the sRPAS arm.

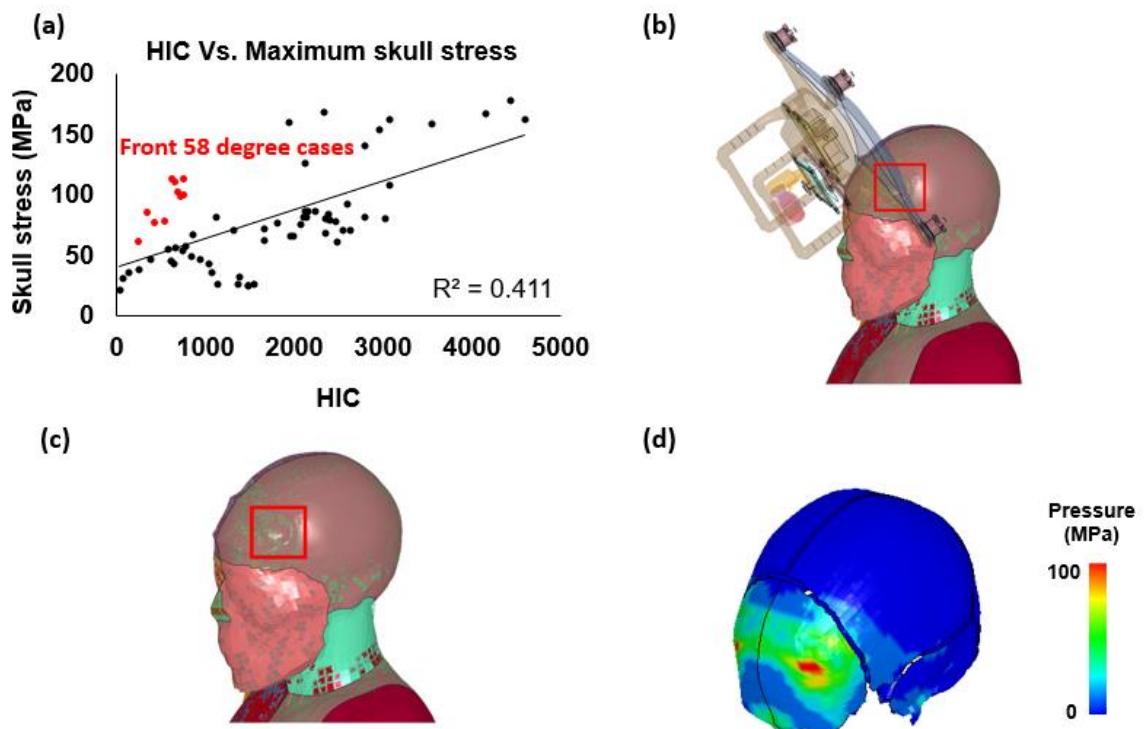


Figure 3-5 Analysis of frontal 58 degree impacts. (a) the correlation of HIC and maximum skull stress with low HIC and high skull stress cases highlighted; (b) the contact location of highlighted the cases; (c) the location of head deformation; (d) the skull stress contour with fringe level of 100MPa.

Compared to frontal 58 degree cases, top 90 degree cases had higher HIC but lower skull stresses (Figure 3-6a). It was observed that the contact areas between sRPAS and human head were relatively larger (Figure 3-6b & c). The force transferred from the sRPAS was distributed in a large contact area, which made the skull experience lower stress during the impacts. From the skull stress contour (Figure 3-6d), the maximum skull stress distributed through the contact region rather than concentrated on small contact areas, producing smaller stresses.

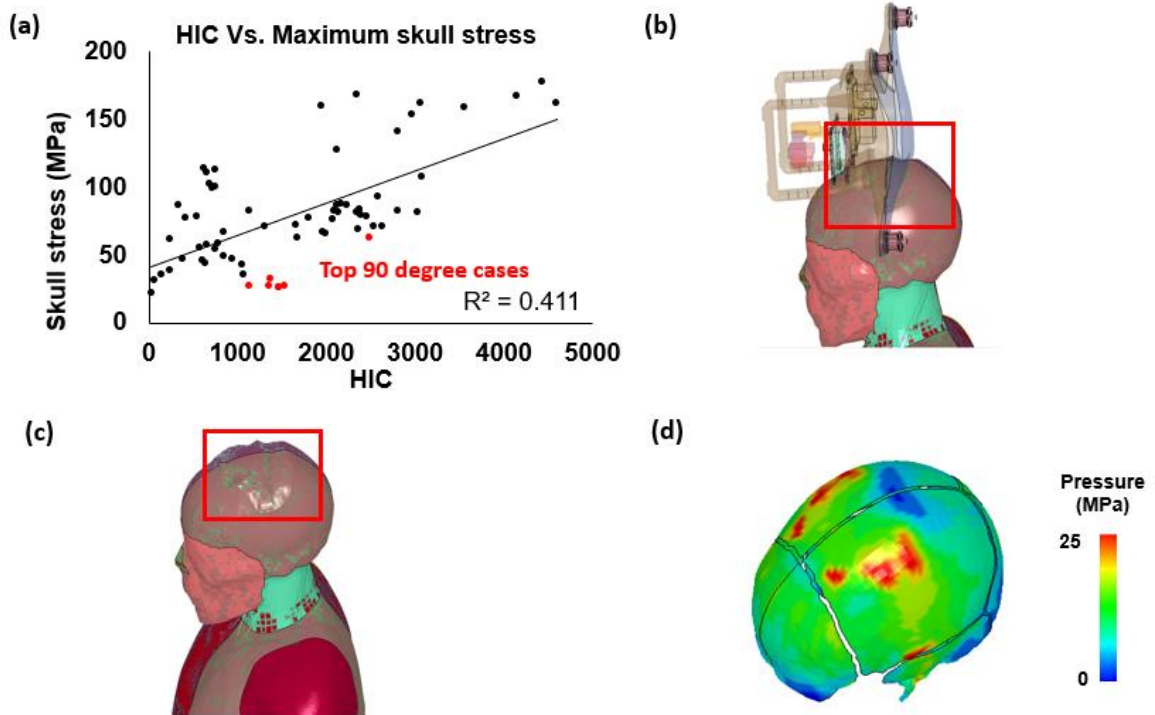


Figure 3-6 Analysis of lateral 58 degree impacts (a) the correlation between HIC and maximum skull stress with low HIC and low skull stress cases highlighted; (b) the contact location of highlighted cases; (c) the location of head deformation; (d) the skull stress contour with fringe level of 25 MPa.

3.3.1.2 Investigation of abnormal cases

In frontal 58 degree and lateral 58 degree cases, there were no strong correlations between the HIC and skull stress. It was observed that there was one case that had extremely large HIC, but had the same level of skull stress as other cases (Figure 3-7a). At the beginning of impact, the camera assembly fixture and the sRPAS body shell

simultaneously contacted the human head, which caused HIC value to be extremely high (Figure 3-7c). The contact of camera assembly with human head contributed to the largest skull stress during the impact (Figure 3-7d). Therefore, after excluding this case from the correlation analysis, the R squared value increased to 0.6945 and the P value of new correlation was less than 0.005 (Figure 3-7b).

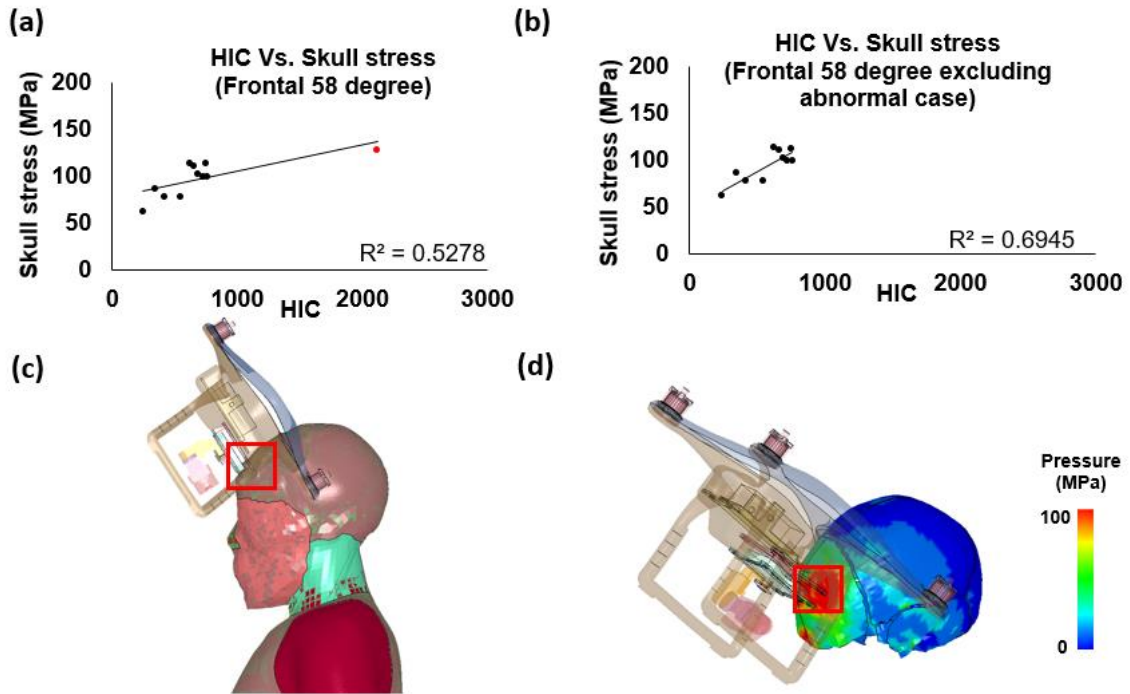


Figure 3-7 Abnormal frontal 58 degree impact case investigation. (a) the original correlation of HIC and skull stress under frontal 58 degree impacts (abnormal case in red color) ($P < .005$); (b) the correlation of HIC and skull stress with the abnormal case excluded ($P < .005$); (c) contact between camera assembly fixture and human head; (d) skull stress contour

In lateral 58 degree cases, there was also one case that had extremely large HIC value than other cases while the skull stress of that case was comparable to others, which affected the general correlation of HIC and skull stress (Figure 3-8a). The camera assembly fixture of sRPAS contacted with the human head at the beginning of collision (Figure 3-8c), which caused higher HIC. From skull stress contour, the camera assembly fixture (Figure 3-8d) resulted in peak skull stress on human skull. After excluding this case, the R squared value increased to 0.7734 with P value less than 0.005 (Figure 3-8b).

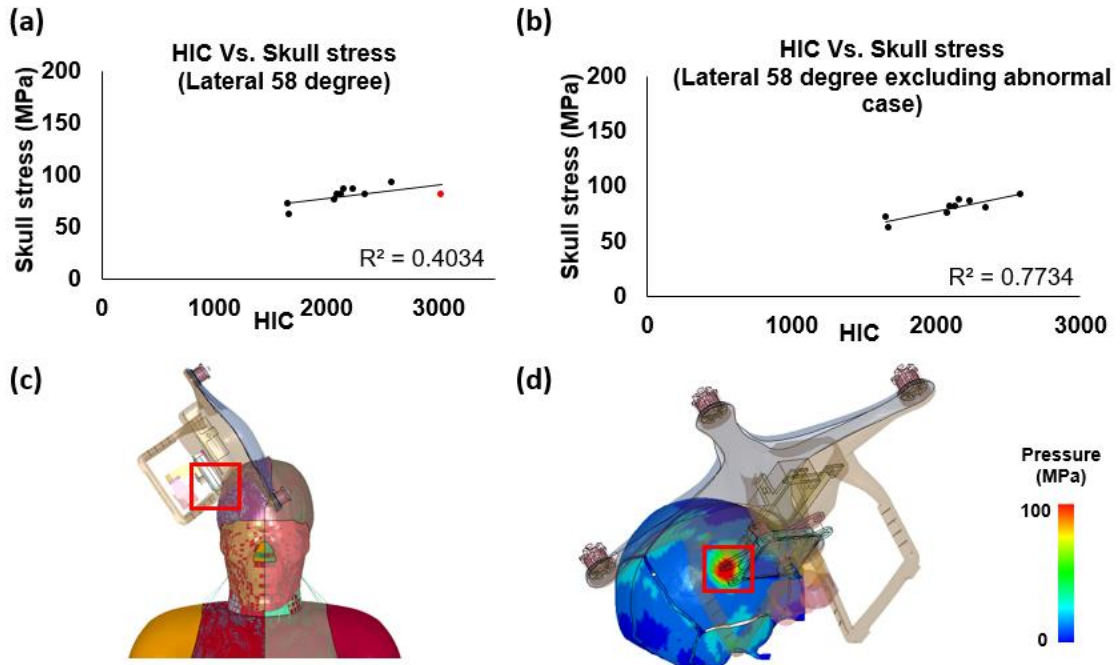


Figure 3-8 Abnormal lateral 58 degree impact case investigation. (a) Correlation between HIC and skull stress under lateral 58 degree impacts (abnormal case in red color) ($P < .005$); (b) Correlation between HIC and skull stress with abnormal case excluded ($P < .005$); (c) Contact between camera assembly fixture and human head; (d) Skull stress contour.

3.3.1.3 Average HIC and skull stress under each impact direction

HIC and skull stress values showed variances under each impact direction. To quantitatively analyze the effects of each impact direction, the cases with the impact velocity of 21.6 m/s (71 FPS) were selected. Under each impact direction, the results of all the cases were averaged for comparison. Under lateral 0 degree, lateral 58 degree, top 90 degree and rear 0 degree directions, the HIC values were extremely large (Figure 3-9a). Under frontal 58 degree and rear 58 degree cases, the HIC values were relatively small (Figure 3-9a). Interestingly, in small-HIC-value cases of frontal 58 degree and rear 58 degree impacts, the sRPAS not only had the movement pointing to the head center of gravity, but also had the movement tangent to the face. Hence, the sRPAS slid down along the face. However, in other cases with large HIC values, this sliding situation did not happen, in which the initial energy of sRPAS directly transferred to the head through

the direction normal to head surface. For skull stress (Figure 3-9b), the rear 0 degree was the most dangerous case which produced the largest stress. The top 90 degree was considered as the safest case in terms of the skull stress, which produced the skull stress level of 50 MPa. The variances of skull stress were due to the effects of sRPAS structures.

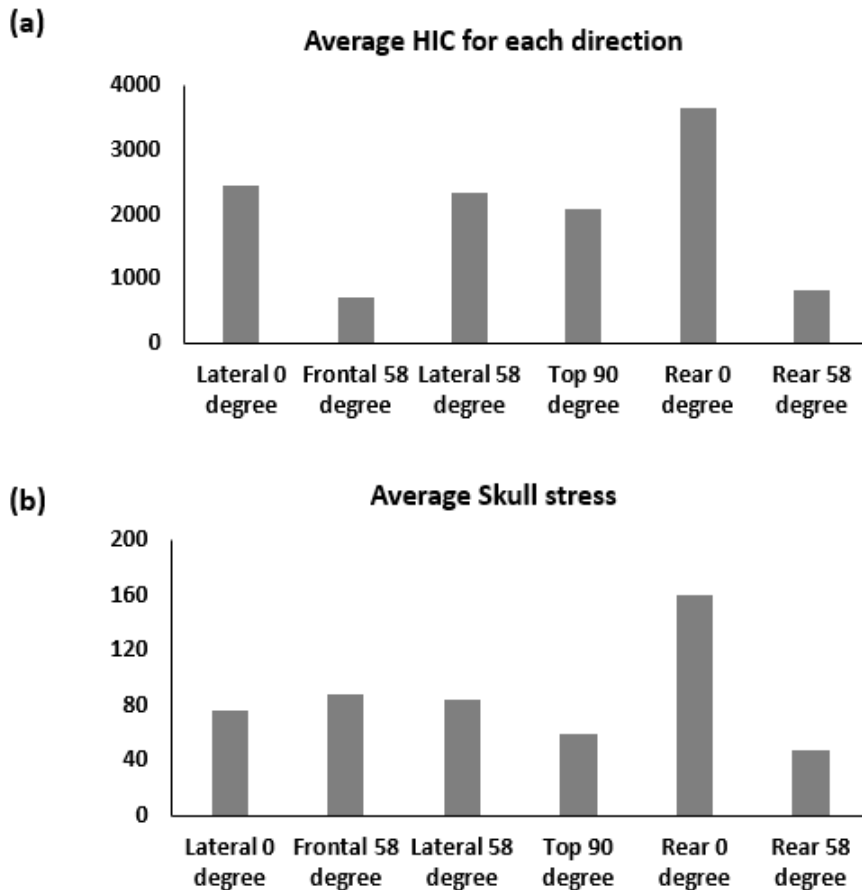


Figure 3-9 Average HIC and skull stress comparisons of different impact directions (a) Average HIC; (b) average skull stress.

3.3.2 BrIC, rotational velocity and brain strain

The BrIC and peak rotational velocity had strong correlation with R squared value of 0.9732 (Figure 3-10) and the P value was less than 0.001. From all 68 cases, it was observed that CSDM10 and CSDM15 had some correlation with peak rotational velocity with R squared values of 0.5742 ($P < .001$) and 0.3809 ($P < .001$) (Figure 3-11a & b). The BrIC had certain level correlation with CSDM10, with R squared value of 0.6634 (P

<.001) (Figure 3-11c). The BrIC had lower correlation with CSDM15 than CSDM10, with squared value of 0.4335 ($P < .001$) (Figure 3-11d).

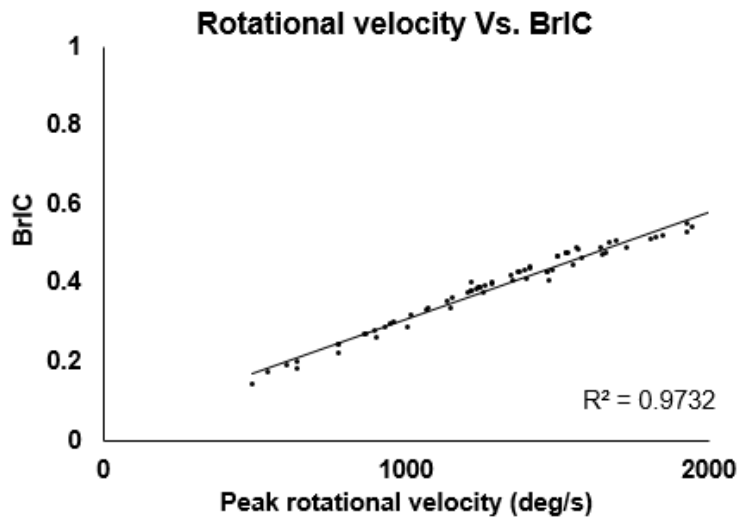


Figure 3-10 Correlation between rotational velocity and BrIC ($P < .001$)

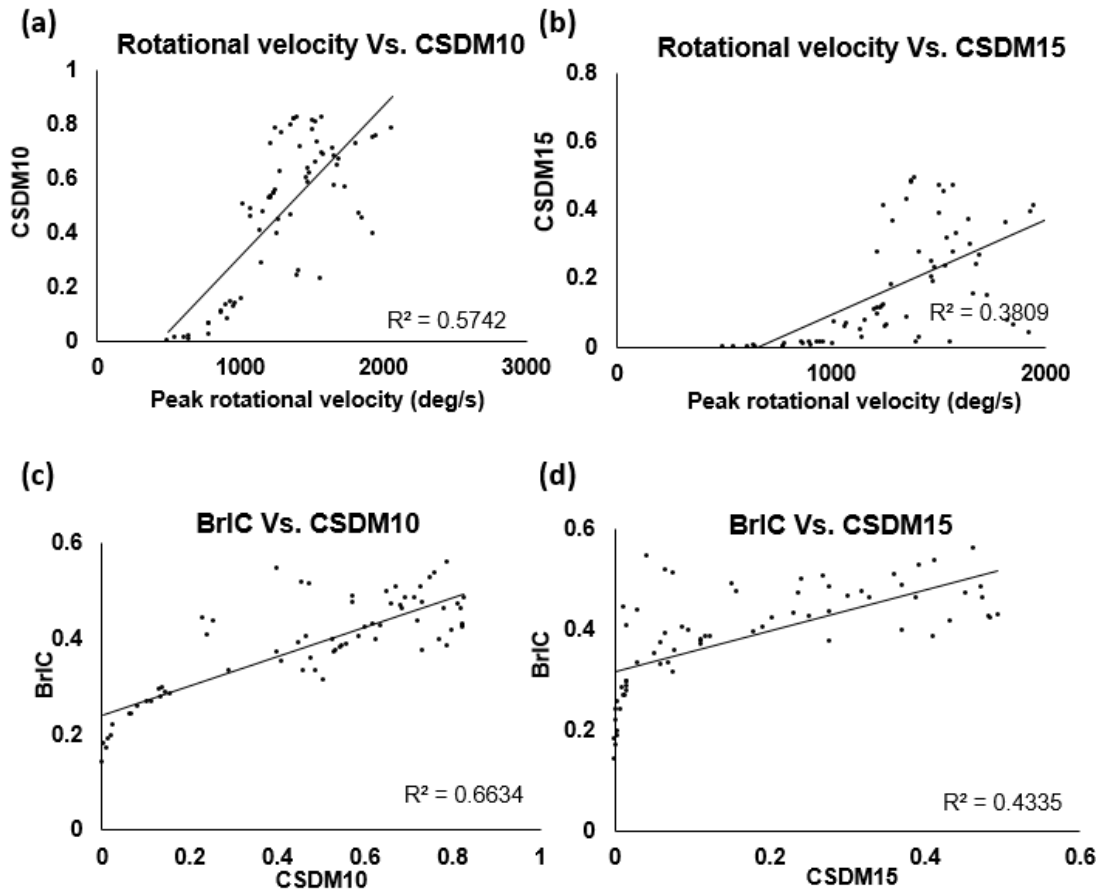


Figure 3-11 Correlation between rotational velocity and CSDM; BrIC and CSDM
(a) The correlation between rotational velocity and CSDM10 ($P < .001$); (b) the correlation between rotational velocity and CSDM15 ($P < .001$); (c) the correlation between BrIC and CSDM10 ($P < .001$); (d) the correlation between BrIC and CSDM15 ($P < .001$).

3.3.2.1 Analysis of the correlation between rotational velocity and CSDM15

The correlation rotational velocity and CSDM15 was not that strong. There were several cases that showed mild peak rotational velocities, but showed large CSDM15 values (Figure 3-12). To better understanding this phenomenon, the rotational velocities at x, y and z directions were collected. In Figure 3-12, one case with low peak rotational velocity but high CSDM (red point) was selected as an example. By looking into its rotational velocity components, the rotational velocity (in Y direction) changed to opposite direction (from -1500 deg/s to 1000 deg/s) during the impact (Figure 3-12, top right). The large brain strain (CSDM15) was due to the sudden direction change of head rotational direction. Interestingly, different rotational velocity profiles were observed, with the aforementioned case changing rotational velocity, one case peaking at the later stage (Figure 3-12, bottom left) and one case peaking at early time (Figure 3-12, bottom right).

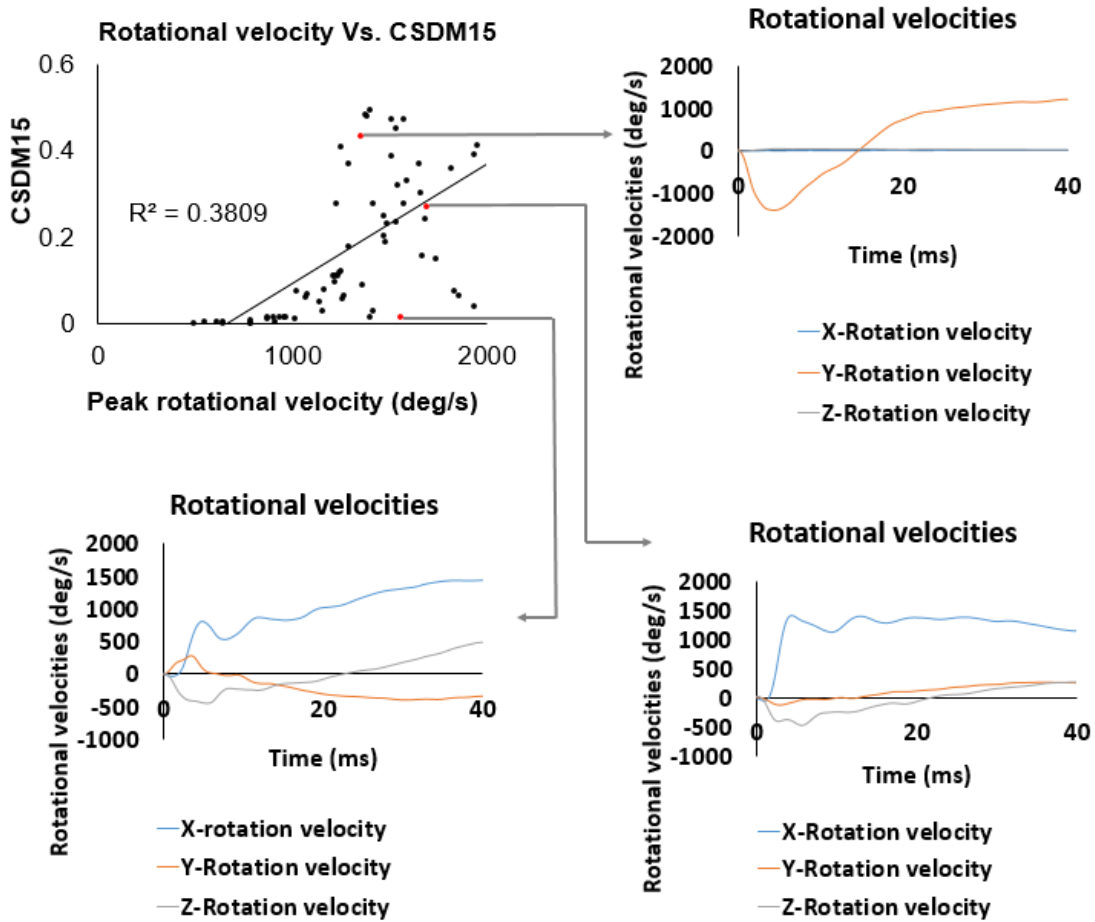


Figure 3-12 Rotational velocity profiles of different cases. The figure analyzes the case with extremely high CSDM15 value and its angular velocity curves in XYZ directions; the case with low CSDM15 value and its angular velocity curve in XYZ directions; Normal case and the XYZ angular velocity curve pattern.

3.3.2.2 Average CSDM10, CSDM15 and BrIC

To quantitatively analyze the variances of impact directions, the average values of CSDM10, CSDM15 and BrIC were collected. From the bar chart (Figure 3-13a & b), top 90 degree case was the safest case regarding brain strain during the collision. The frontal 58 degree and rear 58 degree induced the largest brain strain. For frontal 58 degree direction, CSDM10 and CSDM15 were 0.75 and 0.37, respectively. For rear 58 degree direction, CSDM10 and CSDM15 were 0.8 and 0.39, respectively. The top 90 degree

cases had the smallest average BrIC value (Figure 3-13c). The impact from lateral side had the largest average BrIC values.

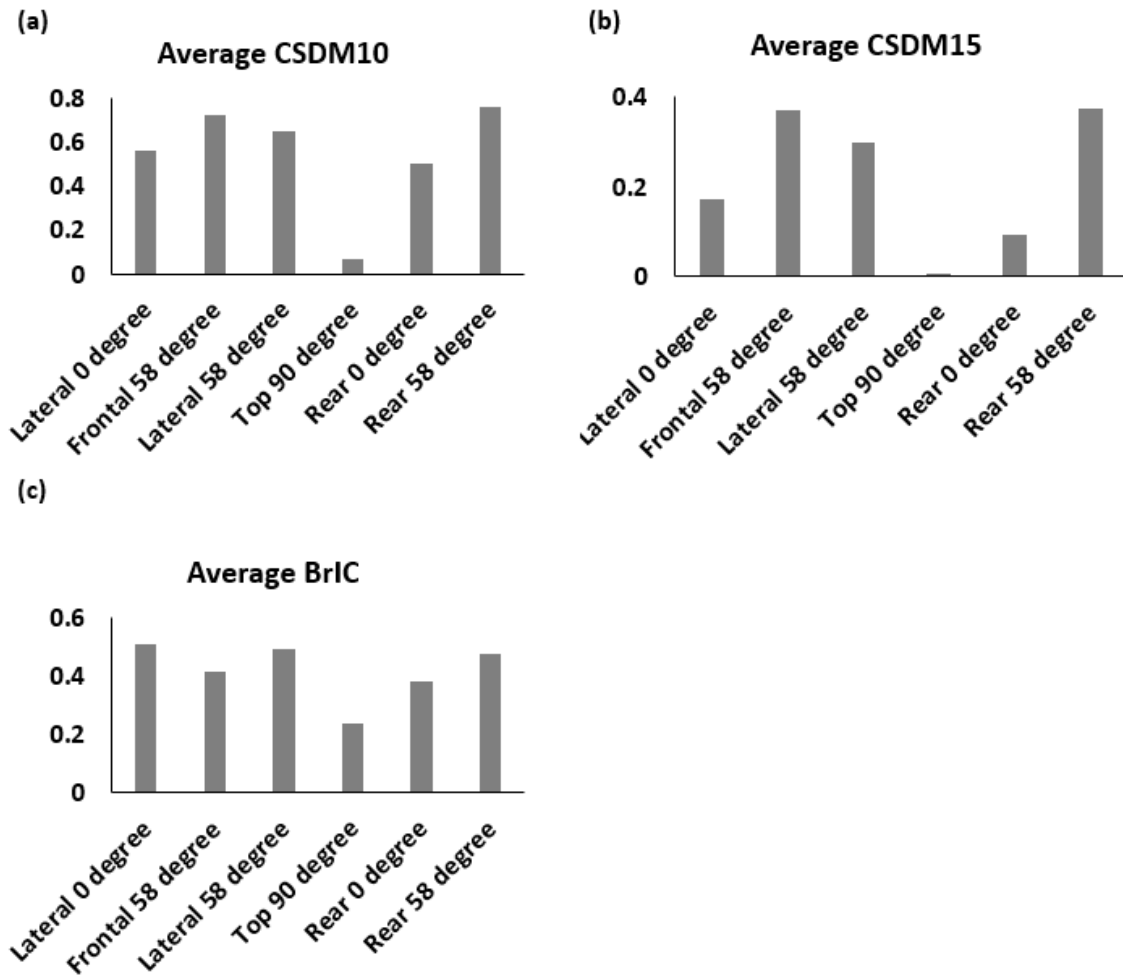


Figure 3-13 Average CSDM10, CSDM15 and BrIC. (a) the comparison of average CSDM10 value between different impact directions; (b) comparison of average CSDM15 value between different impact directions; (c) comparison of average BrIC value between different impact directions.

3.3.3 Scalability

Linear acceleration had a strong correlation with kinetic energy with an R squared value of 0.9673 (Figure 3-14a). The correlation between HIC and kinetic energy was also strong with an R squared value of 0.9929 (Figure 3-14b). Although the correlation between skull stress and kinetic energy was not as high as HIC or linear acceleration, it was still a very strong correlation with R squared value of 0.8853 (Figure 3-14c).

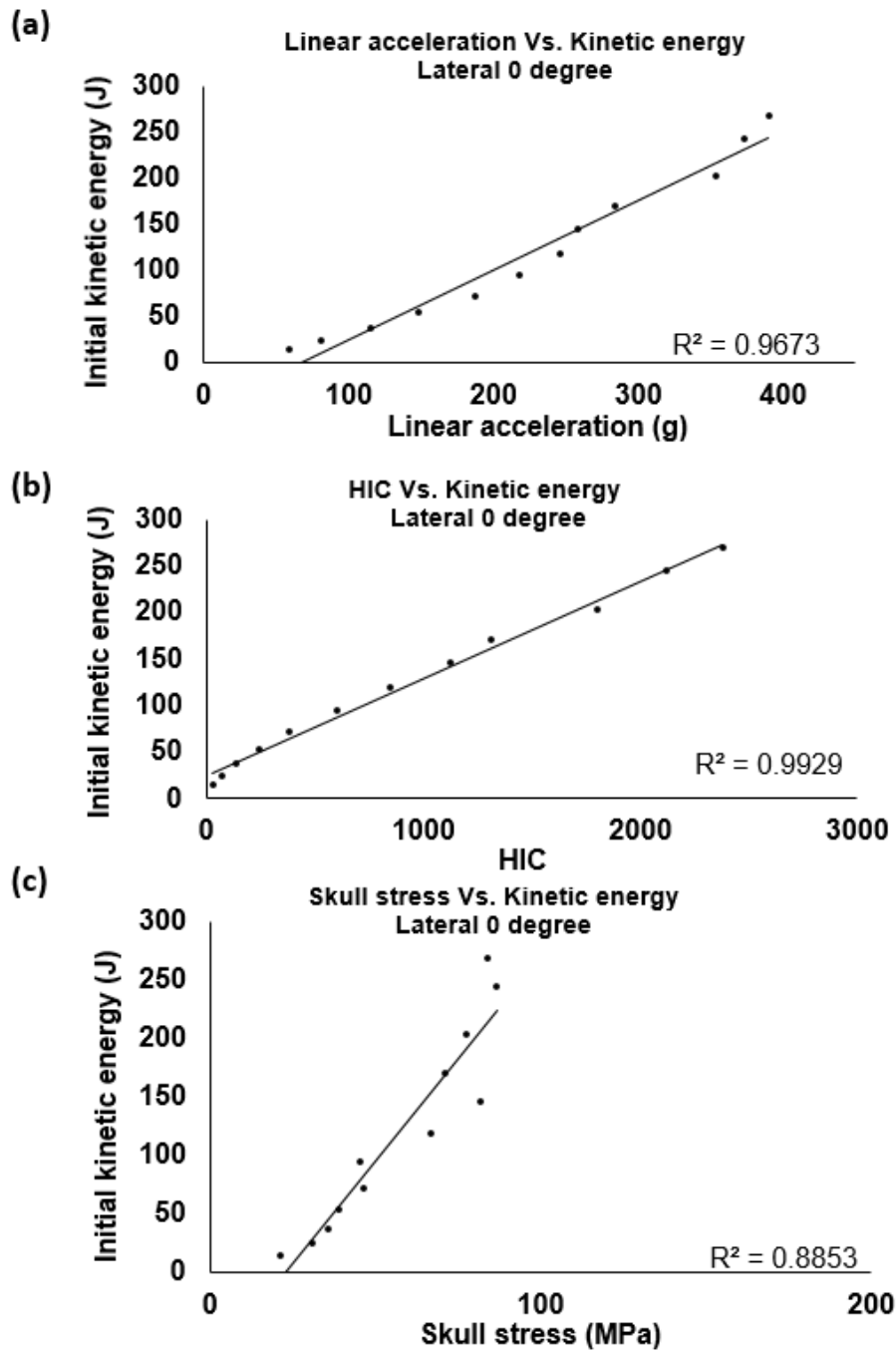


Figure 3-14 Scalability study of linear responses. (a) the correlation between linear acceleration and kinetic energy under lateral 0 degree impact; (b) the correlation between HIC and kinetic energy under lateral 0 degree impact; (c) the correlation between skull stress and kinetic energy under lateral impact.

For rotational velocity, there was a strong correlation between rotational velocity and kinetic energy, which had an R squared value of 0.9464 (Figure 3-15a). The BrIC also had a good correlation with kinetic energy with an R squared value of 0.9299 (Figure 3-15b). Comparing CSDM10 and CSDM15, CSDM10 showed stronger correlation with kinetic energy than CSDM15 did, with R squared values of 0.8549 and 0.6079, respectively (Figure 3-15c and Figure 3-15d).

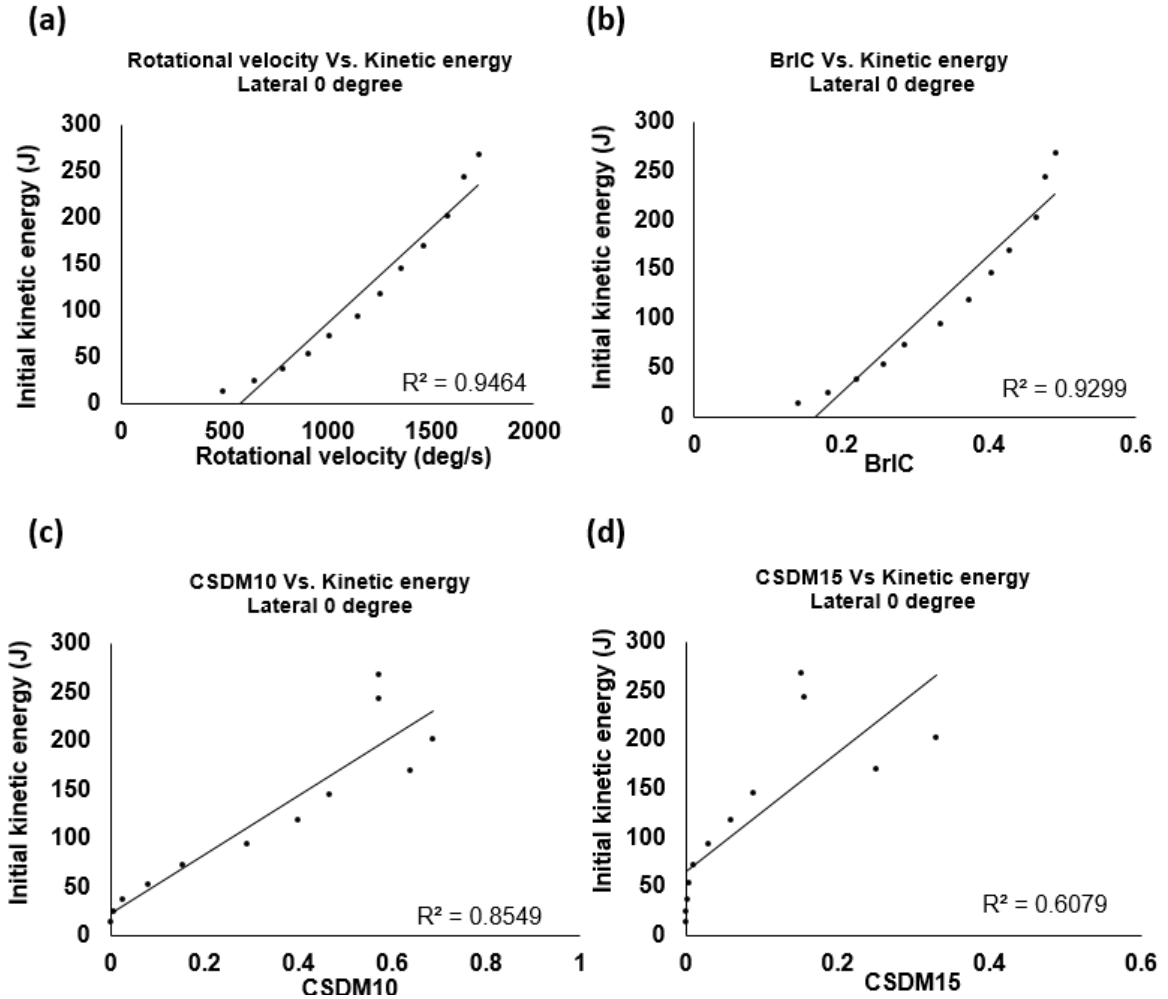


Figure 3-15 Scalability study of rotational responses. (a) Correlation between rotational velocity and kinetic energy under lateral 0 degree impact; (b) Correlation between BrIC and kinetic energy under lateral 0 degree impact; (c) Correlation between CSDM10 and kinetic energy under lateral 0 degree impact; (d) Correlation between CSDM15 and kinetic energy under lateral 0 degree impact.

3.4 Discussion

A validated quadcopter sRPAS FE model was used to investigate head kinematics, injury metrics, and head injury-related responses under sRPAS to head impact scenarios. A total of 68 cases were involved for analysis, including 6 different impact directions and 12 impact velocities. High skull stresses were observed and strong correlations between HIC and skull stress were demonstrated, supporting using HIC as an injury metric. Mild to moderate level brain strains were observed under these sRPAS to head impacts and these brain strains only moderately corrected with BrIC, suggesting further investigation of BrIC before putting it into regulation. Given the very limited PMHS studies involving only three cadaveric heads being impacted with a quadcopter sRPAS, this computational study using validated FE sRPAS and human body model provided an opportunity of systematic investigation of sRPAS to head impacts.

sRPAS structure could greatly affect skull stress. Under different impact directions, various parts of sRPAS contacted the head, bringing large variances in skull stress response. For example, for frontal 58 degree cases, the head only contacted a small portions through the arm shell which induced higher skull stresses due to such a concentrated contact. For top 90 degree case, the whole bottom surface of sRPAS contacted the head which resulted less skull stress. To reduce structure effects, simplified testing approach like using a block to represent a sRPAS could be helpful. Excluding the structure effect, HIC was recommended for helping mitigate stress-related skull fractures.

Top 90 and rear 58 degree cases were considered as the safest cases. More investigation should focus on other directions, especially rear 0 degree, for which the skull stress value was the highest among all cases. The von Mises stress of 110.9 MPa was linked to skull fracture [36]. In our simulation results, all the rear 0 degree impacts had von Mises stresses over 110.9 MPa . Therefore, more PMHS studies could focus on this direction. The average skull stress of other directions such as frontal 58 degree, lateral 0 degree and lateral 58 degree were generally lower than 110.9 MPa. However, some high skull von Misses stresses (over 100 MPa) were still observed from a few cases under those directions. During the PMHS experiments, there was also an AIS 2 level, 13 cm linear

skull fracture observed in the case of frontal 58 degree impact with the 21.5 m/s speed [4].

Rotational velocity did not have very strong correlation with CSDM10 and CSDM15, in which the R squared values were 0.5742 and 0.3809, respectively. Similarly, BrIC had moderate correlation with CSDM10 and CSDM15 with R squared values of 0.6634 and 0.4335, respectively. On the other hand, literature studies reported strong correlations between rotational velocity and CSDM, with R squared value larger than 0.8 [61]. In evaluating hockey helmet study, the strong correlation between BrIC and CSDM was also observed [62]. In analyzing the cases in this study with low strain but high BrIC, it was observed that rotational velocity reached the peak value late close to the end of the impact. The application of BrIC to sRPAS safety regulation needs to be further investigated.

In terms of brain strain responses, the top 90 degree impact direction was considered as the safest setting which only induced CSDM15 of less than 0.1. The frontal 58 degree and rear 58 degree directions were considered as the most dangerous cases regarding on the brain strain, producing CSDM15 of 0.370 and 0.375, respectively. Future investigation of brain strain-related injuries could focus more on these two directions.

3.5 Conclusions

This study investigated head kinematics, injury metrics, and injury-related head responses in sRPAS to head impact simulations. A total of 68 simulations were conducted. The HIC and skull stress had a moderate level of correlations with the confounding sRPAS structural effect. Such a correlation became strong when considering specific impact direction. A simple block representing a sRPAS could be used to minimize such a impact-direction-associated structural effect. The BrIC and brain strain did not show very strong correlations. Beside of peak value, the shape of rotational velocity curves also had large effect of brain strain. Hence, the peak rotational velocity and BrIC need to be further investigated for their efficacy in sRPAS to head safety. Lastly, the most damaging impact directions were identified, including rear 0 degree for inducing high skull stress and frontal 58 degree and rear 58 degree for inducing high brain strains.

Chapter 4

4 Investigation of difference between small female and average male under small remotely piloted aircraft system (sRPAS) to head impact

Abstract

Understanding head responses between small female and average male under small remotely piloted aircraft system (sRPAS) to head impact is important to better protect vulnerable people. The literature did not provide data of female under sRPAS impact, which limited the capability to regulate sRPAS to small female collision safety. Hence, we used the validated sRAPS finite element (FE) model and a small female human body FE model to simulate various sRPAS to small female head impacts. We verified the simulations by scaling available 17 male cadaveric data using established scaling laws. Results demonstrated that FE-model-predicted head linear acceleration and rotational velocity agreed with scaled cadaveric data, with average prediction of linear acceleration 2.3% higher than the experimental measurement and average prediction of rotational velocity 12.5% higher than the experimental average. Small female experienced 24.7% higher peak linear acceleration and 81.5% higher head injury criteria (HIC) compared to average male. However, skull von Mises stress was similar between small female and average male. Small female experienced 31% higher peak rotation velocity and 41.7% higher brain injury criteria (BrIC). Small female also experienced 43% and 113.5% higher cumulative strain damage measure (CSDM)₁₀ and CSDM₁₅, respectively.

4.1 Introduction

Different populations can suffer different head injury severities even under the same impact condition due to differences in body mass, shape and stiffness. It was found that concussion risks were higher among the female athletes in sports such as baseball, basketball, ice hockey and soccer [63-65]. In ice hockey, the rate of concussion for females was around 1.1 to 2.2 times higher than the rate for males [63, 66-68].

There are several explanations regarding sex differences. Female's smaller head and neck, and lower body mass could play a role [63]. In addition, compared to male, female had lower neck strength [69]. Female shows smaller extension force and shorter neck length compared to male [70]. The strength of the neck could affect head kinematics (velocity and acceleration) during impacts [71].

Currently, there are no sRPAS-to-female impact studies available in the literature. Without cadaveric data, the direct validation of finite element (FE) model was limited. On the other hand, the mass-based scaling law could be applied for scaling cadaveric male data to calculate biomechanical data that could be relevant to female. Yoganandan and Pintar used scaling laws to develop acceleration, deflection and force-time responses for small female [72]. The scaling methods have also been used for calculating head responses between different species [73].

The objective of this study was to investigate the differences between average male and small female under the same sRPAS to head impact scenarios. The sRPAS to small female impact simulations were verified according to scaled PMHS data. The head kinematics, head injury metrics, skull stress and brain strain were summarized and compared between the average male and small female.

4.2 Methods

4.2.1 THUMS version 4.02 female model

The Total Human Model for Safety (THUMS) version 4.02 5th percentile small female model was used. Figure 4-1 shows the comparison of THUMS male and female model. The female model was generated by integrating component models (head, torso and extremity models). The version v 4.02 5th percentile female model contains 2,514,045 elements and 878,461 nodes with a total mass of 49 kg. The head and neck models of the THUMS female model were validated by using the similar impact experiments used for male model validation [74].

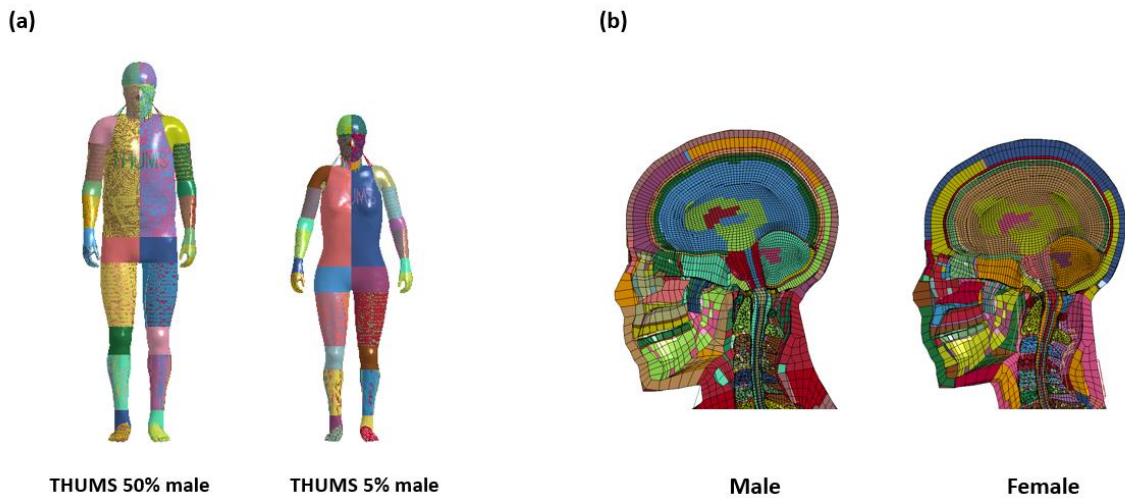


Figure 4-1 THUMS male and female model comparison.

4.2.2 Impact setting

Four typical sRPAS to head impact directions were simulated (Figure 4-2). A total of 17 simulations were conducted using the female model. The detailed setting is described Table 4-1. To ensure that the impact locations were the same for both average male and small female, a proportional method was used. A vertical line through head center of gravity was selected as reference and the impact locations were determined by the angles between vertical center line and sRPAS approaching directions. After simulations, linear accelerations of x, y and z directions were filtered with a low-pass CFC (channel frequency class) 1000Hz filter and then resultant acceleration was calculated based on the filtered x, y and z data. Rotational velocities were filtered with CFC 180 Hz filter. For injury metrics (HIC and BrIC), skull stress and CSDM, the previously developed methods and codes were used.

Table 4-1 sRPAS to female head setups

Case #	Impact Direction	Subject #	Impact Angle (Degree)	Sex	Impact Velocity (m/s - FPS)
1	Right	1	0	Female	16.8 - 55.1

2	Right	1	0	Female	18.3 - 60.1
3	Right	1	0	Female	21.1 - 69.2
4	Front	1	58	Female	17.5 - 57.3
5	Front	1	58	Female	18.0 - 59.2
6	Front	2	58	Female	18.3 - 59.9
7	Front	2	58	Female	21.4 - 70.1
8	Right	2	58	Female	18.7 - 61.2
9	Right	2	58	Female	21.9 - 71.9
10	Top	2	90	Female	16.8 - 55.2
11	Top	2	90	Female	19.5 - 63.9
12	Top	2	90	Female	21.5 - 70.5
13	Right	3	58	Female	18.6 - 60.9
14	Right	3	58	Female	21.9 - 72
15	Front	3	58	Female	21.9 - 71.8
16	Top	3	90	Female	19.7 - 64.5
17	Top	3	90	Female	21.5 - 70.5

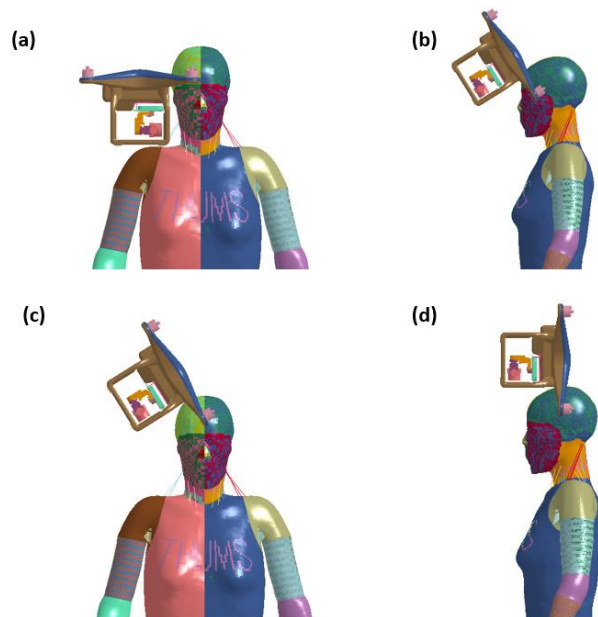


Figure 4-2 Typical impact directions.

4.2.3 Mass-based scaling method

There was no PMHS experiment conducted on female subjects. Therefore, the mass-based scaling law was applied to scale the existing male PMHS cadaveric data. In PMHS experiments conducted by the Ohio State University (OSU), only the masses of whole subjects were recorded. Thus, the whole body masses were applied to calculate the scaling factors. Table 4-2 summarizes the detailed information of subjects used in the OSU PMHS experiments, including subject age, standing height and body mass. From the literature, the 5th percentile small female has an average body weight of 108 lb [75].

Table 4-2 PMHS subjects

Subject #	Age	Standing Height (inch)	Body mass (lb)
1	60	70	170
2	73	66	163
3	67	71	143
4	67	72	193
5	74	74	195

The equations for calculating the mass-based scaling factor of head kinematics [72, 73] are shown below.

$$\text{Mass ratio: } \lambda_m = \frac{M_{male}}{M_{female}}$$

$$\text{Linear acceleration factor: } \lambda_a = (\lambda_m)^{-\frac{1}{3}}$$

$$\text{Angular velocity factor: } \lambda_\omega = (\lambda_m)^{-\frac{1}{3}}$$

$$\text{Time ratio (factor): } \lambda_T = (\lambda_m)^{\frac{1}{3}}$$

Where M_{male} and M_{female} represented for the body mass of male subject and female subject.

The equations of the predicted head kinematics are shown below.

$$\text{Linear acceleration of female: } \alpha_{female} = \frac{\alpha_{male}}{\lambda_a}$$

$$\text{Angular velocity of female: } \omega_{female} = \frac{\omega_{male}}{\lambda_\omega}$$

$$\text{Time of female: } T_{female} = \frac{T_{male}}{\lambda_T}$$

Where α_{male} and α_{female} represented for the linear acceleration of male and female; ω_{male} and ω_{female} represented for angular velocity of male and female; T_{male} and T_{female} represented for time history of male and female under impact.

4.3 Results

A total of 17 simulations were calculated using LS-DYNA. Each case took about 20 hours to solve 40-millisecond case using 2 CPUs.

4.3.1 Resultant head linear acceleration verification

In the lateral 0 degree impact cases (case 1, 2 and 3 in Figure 4-3), the durations of impact were approximately 2.4 milliseconds for all three cases, which were slightly longer than that of scaled PMHS results. For case 1 and 2, the peak linear accelerations were 27.5% and 23.5% higher than those of scaled PMHS experiments, respectively. For case 3, the simulated peak linear acceleration matched well with scaled experiments result.

In the frontal 58 degree impact cases (case 4, 5, 6, 7 shown in Figure 4-3), the time histories had 2 peaks with the impact duration of approximately 2.5 milliseconds. The patterns of curve matched well with scaled PMHS results, except for case 5. The peak values of case 4, 5 and 7 matched well with the scaled PMHS data. In case 6, the simulated peak linear acceleration was 35% over the scaled value.

In the lateral 58 degree cases (case 8, 9, 13 and 14 shown in Figure 4-3), generally, the peak linear accelerations were over-predicted, especially for case 13 in which the peak value was over-predicted by 41.5%. In case 14, the peak linear acceleration prediction

was 6% higher than scaled PHMS data. The simulated impact durations matched well with experimental data, which were in the range of 2 to 2.5 milliseconds.

Case 15 was a typical case in which the initial position of sRPAS was close to the coronal suture instead of the human face. Under the frontal 58 degree impact with initial sRPAS position being close to the frontal coronal suture (case 15 shown in Figure 4-3), the predicted curve matched well with the scaled PMHS curve. The impact duration was 2.7 milliseconds. The peak value of simulated and scaled results were 383 g's and 424.9 g's, respectively.

In the top 90 degree cases (10, 11, 12, 16 and 17 shown in Figure 4-3), the impact durations from simulations and scaled PMHS experiments were similar, which were approximately 2.5 milliseconds. However, the peak values from simulations were under-predicted. In case 10, 11 and 12, the peak values were 26.2%, 37.3% and 43.8% lower than scaled PMHS data, respectively. In case 16 and 17, the simulated peak values were similar to those of scaled experiments, which were only 12.2% and 2.6% lower than those of scaled PMHS data.

Overall, the average peak linear acceleration of simulations was 376.1 g, which matched well with scaled PMHS data of 367.42 g. Through root-mean-square deviation analysis, the peak value of female simulation was 116.9 g varying from that of scaled PMHS experiment with normalized root-mean-square deviation of 0.32.

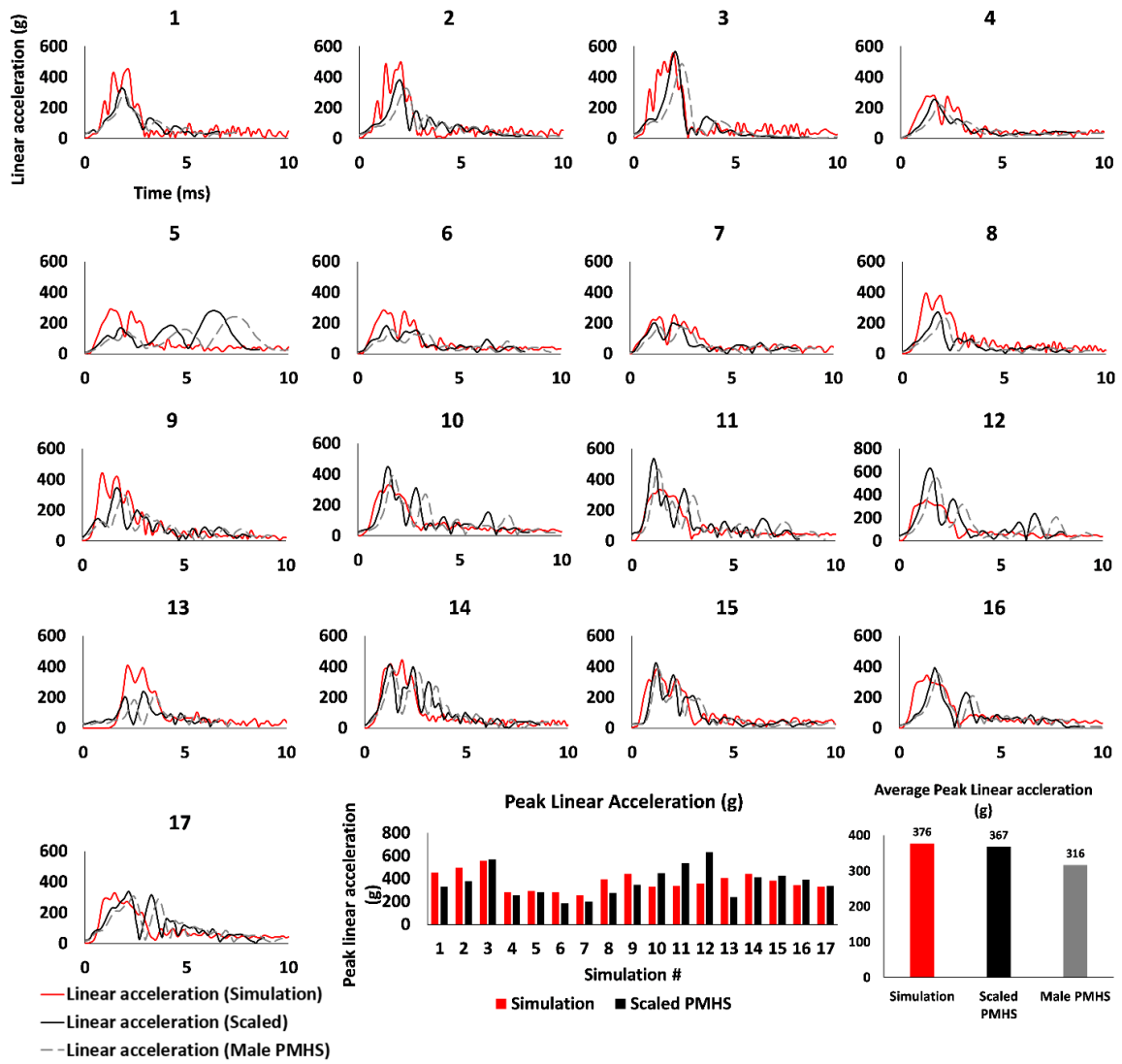


Figure 4-3 Head resultant linear acceleration of female. Experimental data were scaled digitized PMHS experiments data from ASSURE report.

4.3.2 Resultant head rotational velocity verification

In the lateral 0 degree cases (1, 2, and 3 shown in Figure 4-4), simulation-predicted rotational velocities matched well with scaled data in terms of patterns. However, for lower-velocity cases (case 1 and 2 which had initial velocities of 16.8 m/s – 55.1 FPS, 18.3m/s – 60.1 FPS, respectively), the peak value were over-predicted, which were 36.0% and 23.3% higher than those of scaled PMHS results, respectively. In case 3, both

curve shapes and peak values matched well with experiments. The model-predicted peak rotational velocity and scaled PHMS value were 2216.9 and 2212.9 deg/s, respectively.

In the frontal 58 degree impact cases (case 4, 5, 6 and 7 shown in Figure 4-4), the shapes of time histories perfectly matched with experimental curves. However, the peak value of case 4, 5 and 6 were under-predicted, which were 16.1%, 24.6% and 7.7% lower than scaled PHMS data. In case 7, the peak value was over-predicted by 39.4%.

In the lateral 58 degree impact cases (8, 9, 13 and 14 shown in Figure 4-4), the curve patterns matched. Generally, the simulations over-predicted the peak rotational velocity. In case 8 and 9, the peak rotational velocities were 33.9% and 19.3% higher than scaled PMHS values, respectively. In case 13 and 14, the peak values were 35.6% and 39.3% higher than those of scaled experiments, respectively.

Under the frontal 58 degree impact with the initial sRPAS position near the coronal suture (case 15 shown in Figure 4-4), the peak value of simulation happened at the end of simulation, which was different from the scaled PMHS curves, in which the peak value happened in the middle of impact duration. However, the simulated peak rotational velocity matched well with scaled PMHS result with 9% difference between them.

In the top 90 degree impact cases (case 10, 11, 12, 16 and 17 shown in Figure 4-4), the simulated curve shapes were similar to those of scaled PMHS experiments. However, the peak rotational velocities happened earlier than those of scaled curves showed. However, the peak rotational velocities matched well with experimental values, except for case 17, in which the peak value was under-predicted by 53.9%.

Overall, the simulation-predicted average rotational velocity was 1677.6 deg/s, which was 12.5% higher than the scaled PMHS average of 1466.9 deg/s. In root-mean-square error calculation, the peak value of female simulation was 538.6 deg/s different from that of scaled PMHS experiment with normalized root-mean-square value of 0.36.

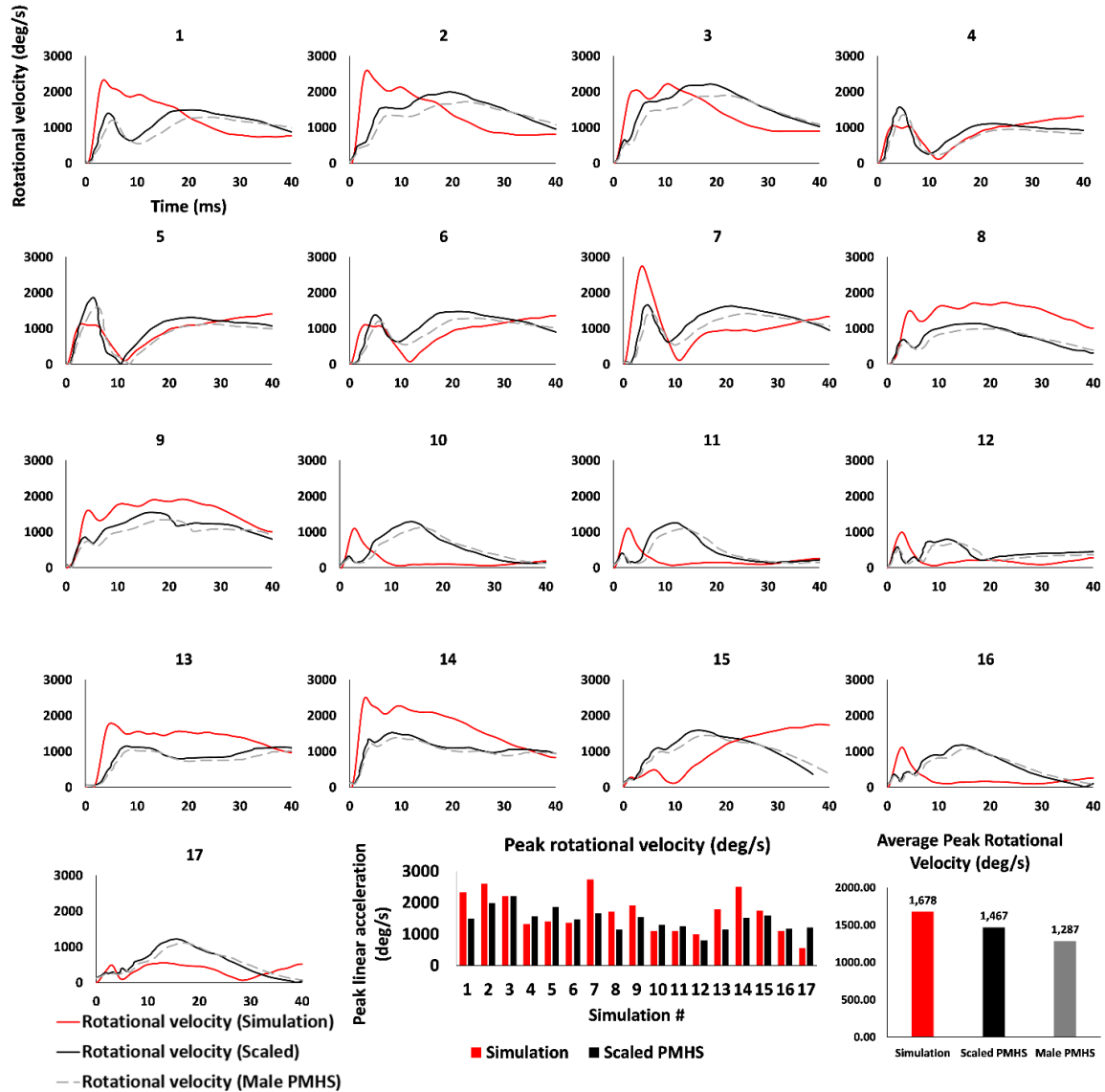


Figure 4-4 Head resultant rotational velocity of female. The experimental data were scaled digitized PMHS experiments data from ASSURE report.

4.3.3 Female vs. male head kinematics and injury metrics

Table 4-3 summarizes the results collected from the 17 small female cases, including peak linear acceleration, peak rotational velocity, HIC, BrIC, maximum skull stress, CSDM10 and CSDM15. For a comparison purpose, Table 4-4 summarizes the head kinematics, injury metrics and injury responses of 17 average male cases, which are also presented in Chapter 2.

Table 4-3 the summarized head kinematics, injury metrics, skull von Mises stress and brain strain value of female cases

Case #	Peak Linear acceleration (g)	Peak rotational velocity (deg/s)	HIC	BrIC	Maximum skull stress (MPa)	CSDM10	CSDM15
1	454	2328	3105	0.7341	67.3	0.8879	0.568
2	498	2599	3817	0.7988	69.3	0.9199	0.632
3	556	2216	5488	0.7235	79.8	0.9008	0.5907
4	282	1319	1459	0.4095	97	0.685	0.2076
5	291	1407	1611	0.437	97.6	0.7245	0.2657
6	284	1360	1538	0.4244	98.1	0.7121	0.2468
7	254	2742	1169	0.8485	65.7	0.9561	0.7568
8	395	1723	2961	0.6274	74.4	0.6599	0.1531
9	443	1912	3638	0.6795	99.8	0.734	0.244
10	331	1097	2053	0.3395	28.98	0.1135	0.0153
11	336	1101	2550	0.3418	28.88	0.12	0.0173
12	355	992	2989	0.3077	36.23	0.0917	0.0148
13	408	1784	2979	0.6437	47.79	0.7692	0.3077
14	443	2509	4057	0.7824	73.5	0.9127	0.6054
15	383	1755	3030	0.5443	71.3	0.5717	0.1161
16	344	1111	2502	0.3437	28	0.1245	0.0177
17	329	557	2301	0.176	28.678	0.0637	0.009

Table 4-4 the summarized head kinematics, injury metrics, skull von Mises stress and brain strain of male cases

Case #	Peak Linear acceleration (g)	Peak rotational velocity (deg/s)	HIC	BrIC	Maximum skull stress	CSDM10	CSDM15
1	284	1467	1311	0.4278	71.0	0.6377	0.2507
2	354	1581	1800	0.4636	77.6	0.6864	0.3296
3	391	1730	2380	0.4899	83.9	0.5714	0.1511

4	213	1017	690	0.3150	102.0	0.5038	0.0748
5	220	1075	757	0.3339	100.0	0.4867	0.0694
6	218	1067	749	0.3319	104.0	0.4580	0.0599
7	194	1393	543	0.4309	107.0	0.8245	0.4935
8	303	1398	1669	0.4074	62.3	0.2402	0.0149
9	364	1556	2074	0.4448	76.3	0.2307	0.0124
10	272	931	1138	0.2879	26.5	0.1437	0.0155
11	298	897	1481	0.2783	25.8	0.1327	0.0149
12	317	777	1957	0.2423	66.7	0.0646	0.00081
13	337	1473	1652	0.4046	72.6	0.5849	0.1905
14	371	1812	2233	0.5098	86.8	0.7284	0.3612
15	371	1409	2124	0.4388	127.0	0.2561	0.0287
16	295	865	1482	0.2681	25.6	0.1117	0.0132
17	321	780	1987	0.2423	65.8	0.0666	0.0083

4.3.4 Male vs. small female in terms average values

Figure 4-5 shows the average values of all 17 cases. Small female overall experienced 24.7% higher average peak linear acceleration and 81.5% higher HIC than male, respectively (Figure 4-5a & b). However, with higher linear acceleration and higher HIC, small female still experienced similar skull stress with average male (Figure 4-5c).

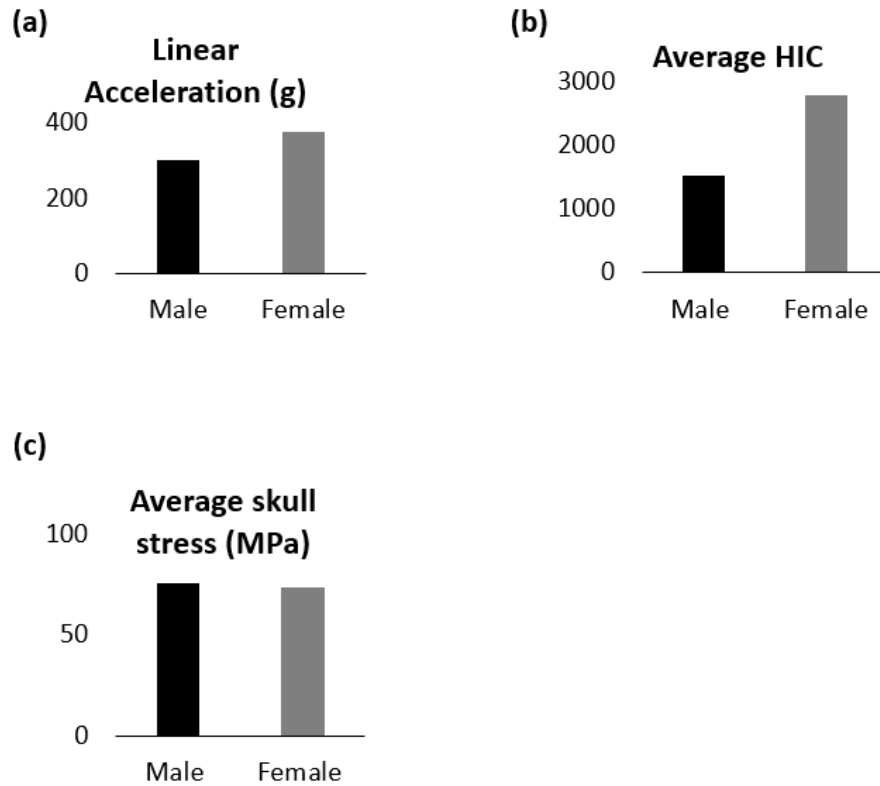


Figure 4-5 Average peak linear acceleration, HIC and skull stress comparisons of male and female model.

Generally, small female experienced 31% higher peak rotation velocity than average male did (Figure 4-6a). Small female experienced 41.7% higher BrIC than that of average male (Figure 4-6b). For CSDM, small female experienced 43% and 113.5% higher CSDM10 and CSDM15, respectively (Figure 4-6c & d).

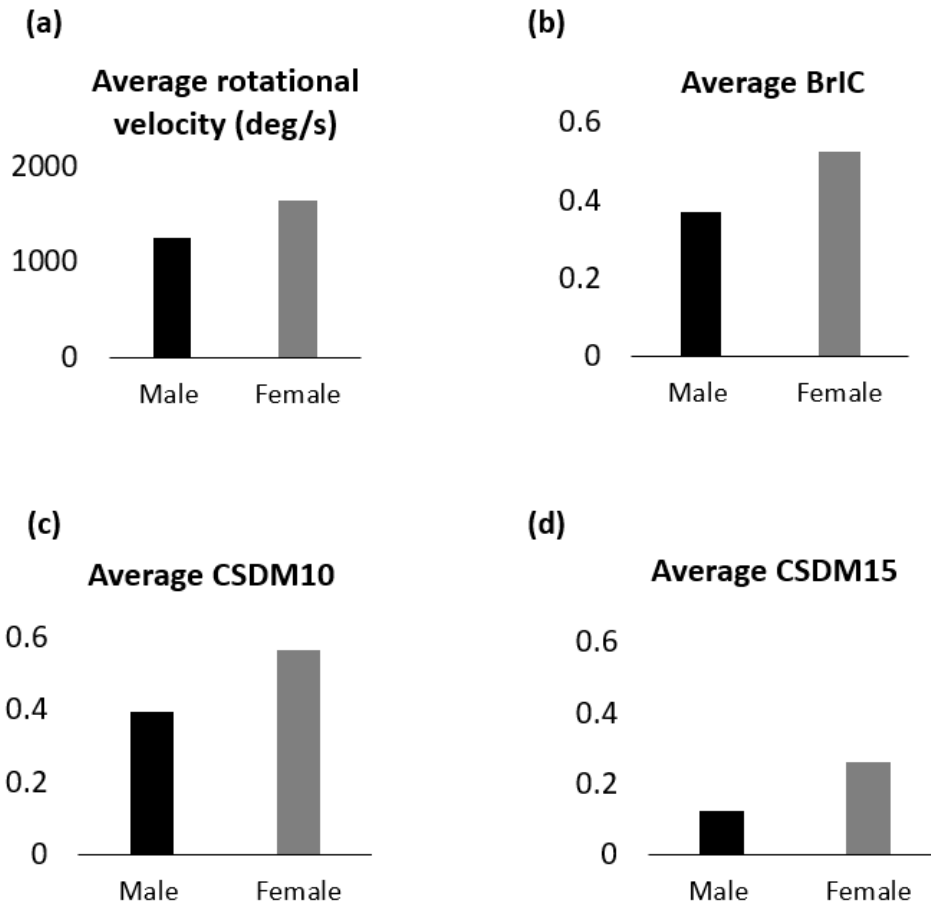


Figure 4-6 Average peak rotational velocity, BrIC and CSDM comparisons of male and female model.

4.4 Discussion

To investigate the risk that sRPAS posed to vulnerable population such as small female, we used a validated sRPAS FE model to investigate sRPAS to female head impacts. Due to the lack of female PMHS experiments, the model was verified with the head linear acceleration and rotational velocity data scaled from male PMHS experiments. Our studies served as the first study on sRAPS to small female impacts to provide data regarding brain strains and von Mises skull stresses. In general, results indicated that small female would have higher injury risks during sRPAS to head impacts, and hence need to be better protected.

Results demonstrated that small female experienced 24.7% higher linear acceleration than that of average male, which could be attributed to smaller head and weaker neck [63, 69]. The average HIC value of small female was 2779.2, which was much larger than that of average male. HIC was determined by the combination of linear acceleration and the impact duration. Normally, the impact duration of small female would be much shorter than that of male because of the lighter head mass [63]. However, under the shorter impact duration, the HIC value was still 81.5% larger than that of average male. Our data demonstrated that the small female suffered similar level skull von Mises stress with average male. It was considered that under the sRPAS to human head impact, although the HIC and peak linear acceleration of small female were larger than those of average male, the stress-related skull fracture risks seemed not to change much.

The 17 female impact cases showed that brain strains were generally at a low level, with most of brain strain under 0.15. However, in three lateral 0 degree (#1, #2 and #3), one frontal 58 degree (#7) and one lateral 58 degree (#14) cases, large brain strains were observed. Our data demonstrated that the investigation of brain injury risks could more focus on frontal and lateral impact rather than top impact. Small female also suffered 31% higher peak rotational velocity than that of average male, and 41.7% higher BrIC. The comparison of CSDM10 and CSDM15 between small female and average male demonstrated that small female experienced higher CSDM values, indicating higher brain injury risks.

4.5 Conclusions

The developed sRPAS FE model was applied to conduct a total of 17 sRPAS to small female impact simulations. The model-predicted linear acceleration and rotational velocity generally agreed well with scaled PMHS data. The higher peak linear acceleration and HIC values were observed for small female, though small female experienced similar level of skull von Mises stresses compared to average male. The strain analysis demonstrated that small female experienced higher CSDM10 and

CSDM15 compared to average male. Hence, the protection of the brain should be more focused on small female during sRPAS to head impacts

Chapter 5

5 Conclusions and future work

5.1 summary and conclusions

Due to the increasing usage of sRPAS, protecting human from sRPAS to head impact is needed. This thesis research was focused on understanding the sRPAS to head impacts to support safety regulation development.

The project started with the development of a representative quadcopter sRPAS FE model. Then, the sRPAS model was combined with the THUMS human body model. The contact conditions between sRPAS and human body model were determined through many trials comparing simulations to experiments. With invaluable PMHS experimental results in the ASSURE reports, the developed sRPAS FE model was finally adjusted to agree with the measurements of 17 cadaveric experiments.

Following with the sRPAS FE model development and validation, more simulations were conducted for systematically understanding the injury metrics and injury risks under sRPAS to head impact. By reasonably postulating that impact angle and location could be different from the desired settings, the sensitivity studies were conducted to help better understand head kinematics under slight changes of those initial parameters. The sensitivity study proved that even tiny changes of angle or location could greatly affect the head kinematics. The change rate (sensitivity) depended on the initial impact directions. For example, top 90 degree cases had highest sensitivity to angel changes. Lateral 58 degree had the highest sensitivity to the location changes.

Furthermore, a total of 68 cases were involved, including 6 different impact directions and 12 initial velocities. The peak head kinematics values, including peak linear acceleration and rotational velocity, were investigated. Moreover, several injury metrics including HIC and BrIC were calculated and assessed based on their correlations to head/brain responses such as maximum skull stress and CSDM. After excluding the abnormal cases, the HIC presented strong correlation with skull stress. The HIC was recommended for regulating the sRPAS safety.

After completing the work of previous chapters, we noticed that all the understanding of sRPAS to head impact was related to male population. However, there are other vulnerable populations such as small female. To develop and verify an sRPAS-to-small-female model, the impact settings similar to those of male were studied. Due to the lack of direct cadaveric data for small female, the scaling law was applied to the male PMHS results. Generally, the curve patterns and peak values of simulations agreed with the scaled results. The small female was found to experience similar level of skull stress as the averaged male did, even though small female had higher linear acceleration and HIC. Regarding brain strain, the small female experienced higher strain compared to the male during the same impact conditions.

5.2 Limitations

There are several limitations in this thesis. The first limitation was that the cadaveric data for the sRPAS to head impact is limited, partially because this is a novel and relatively new research direction. The lack of sRPAS to female cadaveric experiments limits the validation of sRPAS to small female modeling. In this thesis, the small female simulations were verified with the scaled data based on male PMHS experiments. For male models, although extensive validation on head kinematics has been conducted, there was no direct validation on head responses such as brain strain during sRPAS to head impacts. Nevertheless, the human model used in this study has been validated against brain-skull relative motion data and been extensively used in automotive and sports collision fields. In addition, the head model was justified to be appropriate for brain strain analysis as the strain level predicted in this thesis was in the range comparable to those automotive and sports-relevant head impacts.

The second limitation was that a no-fracture version of the human body model was used and hence the stress values predicted by the model should be referred as a comparative purpose as once fracture was allowed and happened and then the stresses would maintain or decrease.

The third limitation was that the representative sRPAS FE model did not show of the feature of falling camera during the impact. From the observation of PMHS video, the

failing cameras were observed in some cases, especially for the cases with camera assembly fixtures contacting with human head. The camera falling might affect the head/brain responses at a later stage of the impact.

The last limitation was that the developed sRPAS FE model did not have a complex battery model. The battery component was defined as a simplified block with an elastic material. For a physical battery, the material is much complex. Generally, Lithium-ion (Li-ion) battery was used to drive sRPAS. The Li-ion battery has several coating layers and polymer layer separators with different material model and properties assigned. The geometry and materials assigned can directly determine the overall mechanical properties and deformation situations during impact.

5.3 Future study

This thesis research delivers a novel approach to investigate head/brain injury risks under sRPAS to human head impact. Based on this study, there are several opportunities for future research of understanding the risks of sRPAS impact.

5.3.1 Injury metrics

Due to sRPAS structure variances, how and where the sRPAS interact with the head would greatly affect HIC values. The correlations between HIC and maximum skull stress was not that strong. However, when the correlation was investigated under each individual direction, the correlation level became stronger. From this point of view, simple blocks simulation was recommended as a method to eliminate the sRPAS structure effects and find the safety HIC value for sRPAS system. The simple block simulation could be done by using a similar weight of block instead of complex sRPAS to find out how HIC value changes under different impact directions. Further investigation on BrIC is needed. Especially, how BrIC, or a new injury metric could be better correlated to brain strain needs to be studied, which could help to mitigate brain strain related injuries. The current injury metrics used for evaluating the injury risk of sRPAS to human head impact were widely used for automotive safety in which the impactors were much heavier than sRPAS, and the impact durations of automotive were

much longer than that of sRPAS. Thus, the current injury metrics such as HIC and BrIC still need to be further evaluated and new injury metrics need to be found for impacts with lightweight sRPAS.

5.3.2 Vulnerable population

More research is much needed for small female to sRPAS impacts. Due to the limited time frame, current simulation cases can only simply compare the injury metrics and injury risks parameters between different sexes. More simulations are still needed for completely understanding the sRPAS to small female impact such as the impact from all possible directions. In addition, besides small females, the young child was also a vulnerable population in public. It is believed that the children can suffer more severe injuries compared to adults. They have lighter body and head mass, and their neck are not that stiff compared to adults. Therefore, combining the sRPAS FE model to some children models is needed for vulnerable population studies.

5.3.3 Protection method

The developed sRPAS to human head impact finite element system provides a feasible opportunity for sRPAS manufacturer to design some methods to protect human head from accidental sRPAS failing. For example, slightly reduce of sRPAS shell stiffness might help to reduce the head kinematics responses and reduce the injury risks. This could be easily done by adjusting the material properties of the sRPAS shell and comparing the injury metrics or injury responses. Besides, some novel protection methods could be investigated such as generating a soft padding foam on sRPAS body shell. Different from the dummy test or cadaveric test, the finite element method provides a direct insight of how skull stress and brain strain changes during the impact and the simulation cost was relatively lower.

5.4 Novelty, significance and impact of work

- 1) A representative quadcopter sRPAS FE model was developed and validated according to cadaveric experiments. It is expensive and time consuming to set up multiple experimental impacts with different impact angles, locations and

velocities. This study offers a new cost-effective and efficient approach to systematically investigate the sRPAS to human head impact.

- 2) This study developed a new way of analyzing the head/brain injury risks under sRPAS to human impacts. The human head FE model was numerically embedded with accelerometers which can accurately collect the time history of head kinematics. Additionally, new methods were developed to calculate HIC, BrIC, maximum skull stress and CSDM. Those analysis methods could be directly applied to further head impact investigations in the future.
- 3) The study reported sRPAS short impact durations, usually under 3 milliseconds. It was found that for such short duration impacts, the HIC15 would be sufficient to capture maximum HIC values. With short durations, the traditional 80g, 3 milliseconds clip used in automotive safety field would not fit for sRPAS to head impact.
- 4) Compared to other head impact studies, the BrIC and rotational velocity did not have a strong correlation with CSDM10 and CSDM15 in sRPAS to head impacts. The shape of rotational velocities had huge effect on brain strains and affected the strength of correlation. This study suggests an improved brain injury metric is needed.
- 5) The differences between average male and small female were investigated. From this study, the similar skull stress level but higher brain strain level were observed in the small female. The data emphasized the importance of vulnerable population studies, especially for the study of strain-related injuries.
- 6) Overall, this study provided unique understanding of the head kinematics, injury metrics, and injury mechanism under sRPAS to head impact.

References

- [1] L. K. Chung, Y. Cheung, C. Lagman, N. A. Yong, D. Q. McBride, and I. Yang, "Skull fracture with effacement of the superior sagittal sinus following drone impact: a case report," *Child's nervous system*, vol. 33, no. 9, pp. 1609-1611, 2017.
- [2] D. M. Atwater, "The Commercial Global Drone Market," *Graziadio Business Review*, vol. 18, no. 2, 2015.
- [3] C. H. Koh *et al.*, "Weight threshold estimation of falling UAVs (Unmanned Aerial Vehicles) based on impact energy," *Transportation Research Part C: Emerging Technologies*, vol. 93, pp. 228-255, 2018.
- [4] G. Olivares, J. Bolte, R. Prabhu, and S. Duma, "Task A14: UAS Ground Collision Severity Evaluation," 2017-2019.
- [5] H. Mao, "Modeling the head for impact scenarios," in *Basic Finite Element Method as Applied to Injury Biomechanics*: Elsevier, 2018, pp. 469-502.
- [6] S. Mansour, J. Magnan, H. H. Ahmad, K. Nicolas, and S. Louryan, *Comprehensive and clinical anatomy of the middle ear*. Springer, 2019.
- [7] O. Oliva-Perez, "Evaluation of the FAA Hybrid III 50th percentile anthropometric test dummy under the FAR 23.562 and 25.562 emergency landing conditions for the combined horizontal-vertical dynamic loading," Wichita State University, 2010.
- [8] T. Green and T. Barth, "Injury evaluation and comparison of lateral impacts when using conventional and inflatable restraints," *Creswell, OR: SAFE Association*, 2006.
- [9] M. Anghileri, L. M. L. Castelletti, and E. Fracasso, "Numerical models of anthropomorphic test devices to investigate human related impact events," 2005.
- [10] H. Chen, D. Poulard, J. Forman, J. Crandall, and M. B. Panzer, "Evaluation of geometrically personalized THUMS pedestrian model response against sedan-pedestrian PMHS impact test data," *Traffic injury prevention*, vol. 19, no. 5, pp. 542-548, 2018.
- [11] D. Sahoo, C. Deck, N. Yoganandan, and R. Willinger, "Anisotropic composite human skull model and skull fracture validation against temporo-parietal skull fracture," *Journal of the mechanical behavior of biomedical materials*, vol. 28, pp. 340-353, 2013.
- [12] M. Vander Vorst, J. Stuhmiller, K. Ho, N. Yoganandan, and F. Pintar, "Statistically and biomechanically based criterion for impact-induced skull fracture," in *Annual Proceedings/Association for the Advancement of Automotive Medicine*, 2003, vol. 47: Association for the Advancement of Automotive Medicine, p. 363.
- [13] P. Chan *et al.*, "Development of generalized linear skull fracture criterion," in *20th International Technical Conference on the Enhanced Safety of Vehicles, Lyon, France*, 2007.
- [14] J. R. Kerrigan, D. B. Murphy, D. C. Drinkwater, C. Y. Kam, D. Bose, and J. R. Crandall, "Kinematic corridors for PMHS tested in full-scale pedestrian impact tests," in *Experimental Safety Vehicles Conference*, 2005.
- [15] J. Kerrigan *et al.*, "Kinematic comparison of the Polar-II and PMHS in pedestrian impact tests with a sport-utility vehicle," *Proceedings of the 2005 International Research Council on the Biomechanics of Impact (IRCOBI), Prague, Czech Republic*, 2005.
- [16] L. Voo, S. Kumaresan, F. A. Pintar, N. Yoganandan, and A. Sances, "Finite-element models of the human head," *Medical and Biological Engineering and Computing*, vol. 34, no. 5, pp. 375-381, 1996.

- [17] K. M. Tse, S. P. Lim, V. B. C. Tan, and H. P. Lee, "A review of head injury and finite element head models," *Am. J. Eng. Technol. Soc.*, vol. 1, no. 5, pp. 28-52, 2014.
- [18] A. N. Smith, *Finite Element Analysis of Traumatic Brain Injury due to Small Unmanned Aircraft System (sUAS) Impacts on the Human Head*. Mississippi State University, 2018.
- [19] A. F. Dori, "Computational Modeling of Thoracic Injury Response due to Impact of a Small Unmanned Aerial System (SUAS)," 2017.
- [20] B. Yang *et al.*, "Development of a finite element head model for the study of impact head injury," *BioMed research international*, vol. 2014, 2014.
- [21] J. S. Ruan, T. B. Khalil, and A. I. King, "Finite element modeling of direct head impact," SAE Technical Paper, 0148-7191, 1993.
- [22] C. Zhou, T. B. Khalil, and A. I. King, "A new model comparing impact responses of the homogeneous and inhomogeneous human brain," *SAE transactions*, pp. 2999-3015, 1995.
- [23] P. Dixit and G. Liu, "A review on recent development of finite element models for head injury simulations," *Archives of Computational Methods in Engineering*, vol. 24, no. 4, pp. 979-1031, 2017.
- [24] H. Mao *et al.*, "Development of a finite element human head model partially validated with thirty five experimental cases," *Journal of biomechanical engineering*, vol. 135, no. 11, 2013.
- [25] H. Mao, H. Gao, L. Cao, V. V. Genthikatti, and K. H. Yang, "Development of high-quality hexahedral human brain meshes using feature-based multi-block approach," *Computer methods in biomechanics and biomedical engineering*, vol. 16, no. 3, pp. 271-279, 2013.
- [26] S. Kleiven and H. von Holst, "Consequences of head size following trauma to the human head," *Journal of biomechanics*, vol. 35, no. 2, pp. 153-160, 2002.
- [27] T. J. Horgan and M. D. Gilchrist, "The creation of three-dimensional finite element models for simulating head impact biomechanics," *International Journal of Crashworthiness*, vol. 8, no. 4, pp. 353-366, 2003.
- [28] E. G. Takhounts, R. H. Eppinger, J. Q. Campbell, R. E. Tannous, E. D. Power, and L. S. Shook, "On the development of the SIMon finite element head model," SAE Technical Paper, 2003.
- [29] J.-S. Raul, D. Baumgartner, R. Willinger, and B. Ludes, "Finite element modelling of human head injuries caused by a fall," *International Journal of Legal Medicine*, vol. 120, no. 4, pp. 212-218, 2006.
- [30] S. Ji, W. Zhao, Z. Li, and T. W. McAllister, "Head impact accelerations for brain strain-related responses in contact sports: a model-based investigation," *Biomechanics and modeling in mechanobiology*, vol. 13, no. 5, pp. 1121-1136, 2014.
- [31] X. Du, A. Dori, E. Divo, V. Huayamave, and F. Zhu, "Modeling the motion of small unmanned aerial system (sUAS) due to ground collision," *Proceedings of the Institution of Mechanical Engineers, Part G: Journal of Aerospace Engineering*, vol. 232, no. 10, pp. 1961-1970, 2018.
- [32] C. A. S. Authority, "Human injury model for small unmanned aircraft impacts," *Monash University: Melbourne, Australia*, 2013.
- [33] L. XIN, "MATHEMATICAL MODELLING OF HUMAN INJURY LEVELS DUE TO UNMANNED AERIAL VEHICLE (UAV) IMPACT."
- [34] T. Magister, "The small unmanned aircraft blunt criterion based injury potential estimation," *Safety Science*, vol. 48, no. 10, pp. 1313-1320, 2010.
- [35] D. B. Stark *et al.*, "Human Response and Injury Resulting from Head Impacts with Unmanned Aircraft Systems," *Stapp car crash journal*, vol. 63, pp. 29-64, Nov 2019.

- [36] C. Giordano, X. Li, and S. Kleiven, "Performances of the PIPER scalable child human body model in accident reconstruction," *PloS one*, vol. 12, no. 11, p. e0187916, 2017.
- [37] Z. Li, W. Liu, J. Zhang, and J. Hu, "Prediction of skull fracture risk for children 0–9 months old through validated parametric finite element model and cadaver test reconstruction," *International journal of legal medicine*, vol. 129, no. 5, pp. 1055-1066, 2015.
- [38] W. N. Hardy, C. D. Foster, M. J. Mason, K. H. Yang, A. I. King, and S. Tashman, "Investigation of Head Injury Mechanisms using Neutral Density Technology and High-Speed Biplanar X-Ray," *Stapp car crash journal*, vol. 45, pp. 337-368, 2001.
- [39] W. N. Hardy *et al.*, "A study of the response of the human cadaver head to impact," (in eng), *Stapp car crash journal*, vol. 51, pp. 17-80, Oct 2007, doi: 2007-22-0002 [pii].
- [40] A. Alshareef *et al.*, "Biomechanics of the Human Brain during Dynamic Rotation of the Head," *Journal of neurotrauma*, vol. 37, no. 13, pp. 1546-1555, Jul 1 2020, doi: 10.1089/neu.2019.6847.
- [41] J. B. Barker and D. Cronin, "Multi-level Validation of a Male Neck Finite Element Model with Active Musculature," *Journal of biomechanical engineering*, Jul 22 2020, doi: 10.1115/1.4047866.
- [42] H. Mao *et al.*, "Development of a finite element human head model partially validated with thirty five experimental cases," *Journal of biomechanical engineering*, vol. 135, no. 11, pp. 111002-15, Nov 1 2013, doi: 10.1115/1.4025101.
- [43] T. M. Corporation, "Documentation: Total Human Model for Safety (THUMS) AM50 pedestrian/occupant model academic version 4.02_ 20181226," ed, 2018.
- [44] L. Shi, Y. Han, H. Huang, J. Davidsson, and R. Thomson, "Evaluation of injury thresholds for predicting severe head injuries in vulnerable road users resulting from ground impact via detailed accident reconstructions," *Biomechanics and modeling in mechanobiology*, vol. 19, no. 5, pp. 1845-1863, 2020.
- [45] N. Atsumi, Y. Nakahira, and M. Iwamoto, "Development and validation of a head/brain FE model and investigation of influential factor on the brain response during head impact," *International journal of vehicle safety*, vol. 9, no. 1, pp. 1-23, 2016.
- [46] M. Fahlstedt *et al.*, "Ranking and rating bicycle helmet safety performance in oblique impacts using eight different brain injury models," *Annals of biomedical engineering*, pp. 1-13, 2021.
- [47] D. Sahoo, F. Coulangeat, F. Fuerst, and G. Marini, "Comparison of Head Injury Criteria Based on Real-World Accident Simulations under Visual Performance Solution (VPS)."
- [48] Y. Miyazaki *et al.*, "Development of a Rotational Brain Injury Criterion with Consideration of the Direction and Duration of Head Rotational Motion."
- [49] S. Roth, J. Vappou, J.-S. Raul, and R. Willinger, "Child head injury criteria investigation through numerical simulation of real world trauma," *Computer methods and programs in biomedicine*, vol. 93, no. 1, pp. 32-45, 2009.
- [50] J. S. Ruan, R. El-Jawahri, S. Barbat, S. W. Rouhana, and P. Prasad, "Impact response and biomechanical analysis of the knee-thigh-hip complex in frontal impacts with a full human body finite element model," SAE Technical Paper, 2008.
- [51] J. Marcicki *et al.*, "A simulation framework for battery cell impact safety modeling using LS-DYNA," *Journal of The Electrochemical Society*, vol. 164, no. 1, p. A6440, 2017.
- [52] N. H. T. S. Administration, "Occupant crash protection—head injury criterion," *Washington, DC: NHTSA.(S6. 2 of FMVSS 571.208)*, 1972.
- [53] N. H. T. S. Administration, "Final Economic Assessment, FMVSS No. 201, Upper Interior Head Protection," *Office of Regulatory Analysis, Plans and Policy. Washington DC*, 1995.

- [54] T. A. Gennarelli, L. E. Thibault, J. H. Adams, D. I. Graham, C. J. Thompson, and R. P. Marcincin, "Diffuse axonal injury and traumatic coma in the primate," *Annals of Neurology: Official Journal of the American Neurological Association and the Child Neurology Society*, vol. 12, no. 6, pp. 564-574, 1982.
- [55] A. K. Ommaya and T. Gennarelli, "Cerebral concussion and traumatic unconsciousness: correlation of experimental and clinical observations on blunt head injuries," *Brain*, vol. 97, no. 4, pp. 633-654, 1974.
- [56] S. S. Margulies and L. E. Thibault, "A proposed tolerance criterion for diffuse axonal injury in man," *Journal of biomechanics*, vol. 25, no. 8, pp. 917-923, 1992.
- [57] E. G. Takhounts, M. J. Craig, K. Moorhouse, J. McFadden, and V. Hasija, "Development of brain injury criteria (BrIC)," *Stapp car crash journal*, vol. 57, pp. 243-66, Nov 2013.
- [58] L. E. Thibault, T. A. Gennarelli, S. S. Margulies, J. Marcus, and R. Eppinger, "The strain dependent pathophysiological consequences of inertial loading on central nervous system tissue," in *International conference on the biomechanics of impacts*, Bron, 1990.
- [59] A. C. Bain and D. F. Meaney, "Tissue-level thresholds for axonal damage in an experimental model of central nervous system white matter injury," *Journal of biomechanical engineering*, vol. 122, no. 6, pp. 615-622, 2000.
- [60] K. Taylor, A. Post, T. B. Hoshizaki, and M. D. Gilchrist, "The effect of a novel impact management strategy on maximum principal strain for reconstructions of American football concussive events," *Proceedings of the Institution of Mechanical Engineers, Part P: Journal of sports engineering and technology*, vol. 233, no. 4, pp. 503-513, 2019.
- [61] K. Bian and H. Mao, "Mechanisms and variances of rotation-induced brain injury: a parametric investigation between head kinematics and brain strain," *Biomechanics and modeling in mechanobiology*, vol. 19, pp. 2323-2341, 2020.
- [62] Y. Levy, "Computational Modeling of the Human Brain for mTBI Prediction and Diagnosis," 2020.
- [63] J. T. Eckner, K. L. O'Connor, S. P. Broglio, and J. A. Ashton-Miller, "Comparison of head impact exposure between male and female high school ice hockey athletes," *The American journal of sports medicine*, vol. 46, no. 9, pp. 2253-2262, 2018.
- [64] C. C. Giza *et al.*, "Summary of evidence-based guideline update: evaluation and management of concussion in sports: report of the Guideline Development Subcommittee of the American Academy of Neurology," *Neurology*, vol. 80, no. 24, pp. 2250-2257, 2013.
- [65] K. G. Harmon *et al.*, "American Medical Society for Sports Medicine position statement: concussion in sport," *Clinical Journal of Sport Medicine*, vol. 23, no. 1, pp. 1-18, 2013.
- [66] T. Covassin, R. Moran, and R. Elbin, "Sex differences in reported concussion injury rates and time loss from participation: an update of the National Collegiate Athletic Association Injury Surveillance Program from 2004–2005 through 2008–2009," *Journal of athletic training*, vol. 51, no. 3, pp. 189-194, 2016.
- [67] J. M. Hootman, R. Dick, and J. Agel, "Epidemiology of collegiate injuries for 15 sports: summary and recommendations for injury prevention initiatives," *Journal of athletic training*, vol. 42, no. 2, p. 311, 2007.
- [68] Z. Y. Kerr *et al.*, "Epidemiologic measures for quantifying the incidence of concussion in national collegiate athletic association sports," *Journal of athletic training*, vol. 52, no. 3, pp. 167-174, 2017.
- [69] G. L. Garces, D. Medina, L. Milutinovic, P. Garavote, and E. Guerado, "Normative database of isometric cervical strength in a healthy population," *Medicine and science in sports and exercise*, vol. 34, no. 3, pp. 464-470, 2002.

- [70] H.-W. Staudte and N. Dühr, "Age-and sex-dependent force-related function of the cervical spine," *European Spine Journal*, vol. 3, no. 3, pp. 155-161, 1994.
- [71] S. Rowson and S. M. Duma, "Brain injury prediction: assessing the combined probability of concussion using linear and rotational head acceleration," *Annals of biomedical engineering*, vol. 41, no. 5, pp. 873-882, 2013.
- [72] N. Yoganandan and F. A. Pintar, "Deflection, acceleration, and force corridors for small females in side impacts," *Traffic injury prevention*, vol. 6, no. 4, pp. 379-386, 2005.
- [73] T. Wu, J. Antona-Makoshi, A. Alshareef, J. S. Giudice, and M. B. Panzer, "Investigation of cross-species scaling methods for traumatic brain injury using finite element analysis," *Journal of neurotrauma*, vol. 37, no. 2, pp. 410-422, 2020.
- [74] T. M. Corporation, "Documentation: Total Human Model for Safety (THUMS) AF05 pedestrian/occupant model academic version 4.02_20181226," ed, 2018.
- [75] M. L. Davis, "Development and Full Body Validation of a 5 th Percentile Female Finite Element Model," Wake Forest University, 2017.

Curriculum Vitae

Name: Yuhu Weng

Post-secondary Education and Degrees: Western University
London, Ontario, Canada
2016-2020 BSc.

Western University
London, Ontario, Canada
2020-2021 M.E.Sc

Honours and Awards: Dean’s Honor List
2017-2020

Related Work Experience Summer Research Assistant
Western University
2019

Teaching Assistant
Western University
2020-2021

Publications:

1. Weng Y, Bian K, Gunasekaran K, Gholipour J, Vidal C and Mao H. 2021. Small Remotely Piloted Aircraft System to Head Impact – Computational Model Development and Head Response Analysis. Journal of Biomechanics. BM-D-21-00435. Under review.
2. Weng Y, Gunasekaran K, Bian, Ruella C, Spanos M, Vidal C and Mao H. 2020. Investigating Head Injury Criteria and Gender Difference During Small Unmanned Aircraft to Human Collision. 2020. Biomedical Engineering Society. Online poster presentation.